UNIVERSITY OF CALIFORNIA SAN DIEGO

Unveiling the photochemistry and photophysics of organic molecules in optical cavities

A dissertation submitted in partial satisfaction of the
requirements for the degree
Doctor of Philosophy

in

Chemistry

by

Juan Bernardo Pérez Sánchez

Committee in charge:

Professor Joel Yuen-Zhou, Chair
Professor Leonid Butov
Professor Michael Galperin
Professor James Andrew McCammon
Professor Michael Tauber

2024

The dissertation of Juan Bernardo Pérez Sánchez is approved, and it is acceptable in quality and form for publication on microfilm and electronically.

University of California San Diego

2024

DEDICATION

First and foremost, I would like to express my deepest gratitude to my mother Ana Rosaura Sánchez, my father Juan Bernardo Pérez, and my brothers Joaquín Andrés Pérez Sánchez and Julián Alberto Pérez Sánchez. Although they have supported me from a distance, their unwavering belief in me has been a constant source of strength and motivation. Their encouragement and love have been instrumental in helping me navigate through this challenge.

I am also immensely grateful to my colleagues and friends from the Yuen-Zhou group Sindhana S. Pannir-Sivajothi, Kai Schwennicke, Jorge Campos Gonzalez Angulo, Luis Angel Martinez Martinez, Matthew Du, Raphael Ribeiro, Arghadip Koner, Federico Mellini, Yong Rui Poh, and Sricharan R.C., who have provided not only professional support but also enduring friendship. Without their collaboration, enthusiasm, insightful discussions, and camaraderie, achieving my academic goals would have been impossible. They have also been there to celebrate the successes and offer support during the difficult times.

I would also like to express my gratitude to my friends Julian Alberto Castro, Christian Daniel Navia, David Alejandro Gutierrez, Andrey Joaqui Joaqui, Laura Danelly Salas, Clark Gold Wang, and Christian Seitz. Their companionship has been a constant source of inspiration and joy.

A special thanks to my Principal Investigator, Joel. Your patience, guidance, confidence, and expertise have been invaluable in my growth as a researcher. You have taught me not just the intricacies of our field, but also the perseverance and dedication required to pursue a PhD and to become a successful scientist. Your support and mentorship have been crucial in shaping my academic career, and for that, I am profoundly thankful.

I dedicate this thesis to Kevin, Juliana, and Saray.

TABLE OF CONTENTS

ACKNOWLEDGEMENTS

Chapter 2, in full, is a reprint of the material as it appears in The Journal of Physical Chemistry Letters. Pérez-Sánchez, Juan B.; Yuen-Zhou, Joel. 11, 152-159, 2019. The dissertation author was the primary investigator and author of this paper.

Chapter 3, in full, is a reprint of the material as it appears in Proceedings of the National Academy of Sciences (PNAS). Pérez-Sánchez, Juan B.; Koner, Arghadip; Stern, Nathaniel P.; Yuen-Zhou, Joel. 120, 15, e2219223120, 2023. The dissertation author was the primary investigator and author of this paper.

Chapter 4, in full, is a reprint of the material as it appears in Physical Review Research. Pérez-Sánchez, Juan B.; Mellini, Federico; Giebink, Noel C.; Yuen-Zhou, Joel. PRR, 6, 013222, 2024. The dissertation author was the primary investigator and author of this paper.

Chapter 5 is part of a review in preparation for publication whose authors are Kai Schwennicke, Arghadip Koner, Juan B. Pérez-Sánchez, Wei Xiong, Noel C. Giebink, Marissa L. Weichman and Joel Yuen-Zhou. The dissertation author was a co-author of this paper.

Chapter 6, in full, is a reprint of the material in preparation for publication whose authors are Juan B. Pérez-Sánchez and Joel Yuen-Zhou. The dissertation author was the primary investigator and author of this paper.

VITA

2010-2015	Bachelor in sciences Chemistry, Universidad del Valle, Cali, Valle del Cauca, Colombia.
2015-2017	Master of sciences Chemistry, Universidad del Valle, Cali, Valle del Cauca, Colombia.
2018-2024	PhD in Chemistry, University of California San Diego, La Jolla, California, United States.

PUBLICATIONS

Juan B. Pérez-Sánchez, and Joel Yuen-Zhou. "Radiative pumping vs vibrational relaxation of molecular polaritons: a bosonic mapping approach", ArXiv, https://arxiv.org/abs/2407.20594, 2024.

Kai Schwennicke, Arghadip Koner, Juan B. Pérez-Sánchez, Noel C. Giebink, Marissa L. Weichman, and Joel Yuen-Zhou. "Linear optics and optical filtering effects in molecular polaritonics", In preparation, 2024.

Tomohiro Ishii, Juan B. Pérez-Sánchez, Joel Yuen-Zhou, Chihaya Adachi, Takuji Hatakeyama, and Stéphane Kéna-Cohen. "Modified Prompt and Delayed Kinetics in a Strongly-Coupled Organic Microcavity Containing a Multi-Resonance TADF Emitter", ACS Photonics, In print, 2024.

Juan B. Pérez-Sánchez, Federico Mellini, Noel C. Giebink, and Joel Yuen-Zhou. "Collective polaritonic effects on chemical dynamics suppressed by disorder", PRR, 6, 013222, 2024.

Hongfei Zeng, Juan B. Pérez-Sánchez, Christopher Eckdahl, Pufan Liu, Woo Je Chang, Emily Weiss, Julia Kalow, Nathaniel Stern, and Joel Yuen-Zhou. "Control of photoswitching kinetics with strong light-matter coupling in a cavity", JACS, 145, 36, 19655-19661, 2023.

Christophe H Valahu, Vanessa C Olaya-Agudelo, Ryan J MacDonell, Tomas Navickas, Arjun D Rao, Maverick J Millican, Juan B. Pérez-Sánchez, Joel Yuen-Zhou, Michael J Biercuk, Cornelius Hempel, Ting Rei Tan, and Ivan Kassal. "Direct observation of geometric phase in dynamics around a conical intersection", Nature Chem. 15, 1503-1508, 2023.

Juan B. Pérez-Sánchez, Arghadip Koner, Nathaniel P. Stern, and Joel Yuen-Zhou. "Simulating molecular polaritons in the collective regime using few-molecule models", PNAS. 120, 15, e2219223120, 2023.

Robert Collison*, Juan B. Pérez-Sánchez*, Matthew Du, Jacob Trevino, Joel Yuen-Zhou, Stephen O'Brien, and Vinod M. Menon, "Purcell Effect of Plasmonic Surface Lattice Resonances and Its Influence on Energy Transfer", ACS Photonics. vol. 8, 2211-2219, 2021.

J. Yuen-Zhou, L. A. Martínez-Martínez, and Juan B. Pérez-Sánchez, "Polariton chemistry: controlling organic photophysical processes with strong light-matter coupling", Proceedings Volume 11464, Physical Chemistry of Semiconductor Materials and Interfaces XIX. vol. 11464, 31-42, 2020.

Juan B. Pérez-Sánchez, and J. Yuen-Zhou, "Polariton assisted down-conversion of photons via nonadiabatic molecular dynamics: A molecular dynamical Casimir effect", J. Phys. Chem. Lett. vol. 11, 152-159, 2019.

ABSTRACT OF THE DISSERTATION

Unveiling the photochemistry and photophysics of organic molecules in optical cavities

by

Juan Bernardo Pérez Sánchez
Doctor of Philosophy in Chemistry

University of California San Diego 2024

Professor Joel Yuen-Zhou, Chair

Molecular polaritons offer a promising avenue for manipulating light and matter properties through both single-molecule and collective strong light-matter coupling within optical cavities. Over the past decade, numerous theoretical and experimental studies have reported changes in optical and chemical properties as a result of this strong interaction. However, the field is fraught with inconsistent findings. Some experimental results cannot be reproduced or are later given non-polaritonic explanations, while theoretical models often fail to account for observed changes and make correct predictions. This disconnect between theory and experiment arises from the use of overly simplistic models to explain the highly complex nature of polaritonic systems in general, and organic molecules in particular.

In the field of polariton chemistry, which aims to exploit collective strong coupling to modify chemical reactivity, there has been a tendency to interpret experiments conducted in the collective regime using single-molecule strong coupling models. In such models, the excited states of individual molecules hybridize with cavity modes to create vibronic-polariton states, altering the energy levels of the molecules and hence reactivity. In contrast, in the collective regime, polaritons are excitations delocalized over the entire ensemble of molecules, and it is unclear how

they influence the local vibronic dynamics of individual molecules.

This thesis presents our efforts to unveil the novel photochemical and photophysical phenomena in organic exciton polaritons. Our findings can be summarized as follows: while collective strong light-matter coupling can significantly alter optical properties, such as the photonic density of states, it has negligible direct effects on the internal degrees of freedom involved in chemical reactivity of individual molecules. Nevertheless, we conclude that polaritonic modifications to optical properties can influence molecular processes in a weak coupling manner, leading to long-range resonance energy transfer, and changes in absorption, emission, and Raman scattering rates that are enhanced inside the cavity. Further advancements require identifying the missing elements in our theories. Effects such as temperature and the multimode nature of optical microcavities may be crucial for understanding the experimental observations that remain unexplained to this day, and for definitively determining novel applications of collective strong light-matter coupling with organic molecules.

Chapter 1

Introduction

Controlling chemical dynamics using coherent optical sources has been a long-standing goal since the invention of the laser. One of the pioneering approaches in this field is mode-selective chemistry, where lasers are used to selectively excite specific vibrational or rotational modes of molecules, thereby directing the course of chemical reactions with unprecedented specificity [1]. However, energy deposited into a specific mode rapidly redistributes among other modes within the molecule, drastically reducing the effectiveness of this approach. To deal with this fundamental problem, Brumer and Shapiro described a scheme that exploits the relative phase of two lasers as a control knob to induce destructive and constructive interferences between the two different reaction pathways [2]. Similarly, Tannor and Rice [3] exploit the delay time between two ultrashort lasers as a control knob to deexcite the molecules once it has reached the desired nuclear configuration. Subsequently, multi-parameters control schemes assisted by learning algorithms were proposed to optimize the laser pulses based on on-site experimental feedback [4]. Ultimately, control schemes make use of highly intense lasers to induce several multiphotonic processes in a timescale faster than the motion. This highly nonlinear regime is more easily understood with the concept of light-induced potentials (LIPs), which gave rise to the idea of "shaping" the potential energy surface (PES) using tailored laser fields [5] or using highly intense periodic fields (Floquet engineering) [6]. Besides control of reactivity, complementary techniques have been designed to probe wavepacket dynamics in femtosecond timescales based

on the same general principles [7].

Photonic devices such as optical microcavities [8] or plasmonic nanocavities [9] can support highly confined electromagnetic fields. Light-matter interaction in these infrastructures is comparable with molecular and cavity linewidths, so that light must be considered beyond a perturbative treatment [10–21]. In this SC regime, new hybrid light-matter states called polaritons emerge. Contrary to the aforementioned laser control strategies, this regime does not necessarily require high intensity lasers, but occur despite the cavity modes being in their vacua or low-lying excitations.

While single molecules can strongly couple to confined fields of plasmonic nanocavities [22], a more common scenario requires an ensemble of matter excitations collectively coupled to optical modes in microcavities. In this collective regime, polariton states are accompanied by a dense manifold of so-called dark states. Organic exciton polaritons are particularly interesting systems since SC between electronic and vibrational degrees of freedom (DoF) gives rise to intricate relaxation processes that allow for population transfer between dark and polariton states, a feature that plays a central role in modification of chemical reactivity [16, 23–42], polariton-assisted remote energy transfer [43–45], polariton transport [46–52], and polariton condensation [53–61].

Despite recent advancements, the field features contradictory findings: some studies report no changes due to formation of polaritons, or provide alternative, non-polaritonic explanations for the observed modifications. A crucial step towards solving these inconsistencies is to have a tractable theoretical and computational framework that can describe the myriads of molecules in the ensemble, and the complex internal vibrational structure of each molecule. Indeed, theoretical methods that can incorporate effects of intermolecular interactions [62–64], multiple optical cavity modes [65–67], complex vibrational and electronic structure [42,68–75], and molecular disorder [67, 76–85], while considering a large number of molecules, are in much need to explain experimental observations.

This thesis is structured as a series of papers, each representing a step towards understanding how strong light-matter interaction with organic molecules

can affect their local excited state dynamics. In the second chapter, we demonstrate that nonlinear optical phenomena can arise under single-molecule strong coupling, which can be exploited to achieve photon downconversion [86]. However, we show that this phenomenon vanishes quickly when the strong coupling is achieved with more than one molecule. This highlights the need for a formalism in the collective regime, which is the focus of the following chapters. In the third chapter, we develop a numerically exact formalism for the collective regime exploiting a permutationally symmetric representation of the many-body wavefunction [87]. We call this method Collective dynamics Using Truncated Equations (CUT-E), and it is based on a separation of the light-matter interaction into its collective and single-molecule components. CUT-E expresses the system's equations of motion as a $1/N$ expansion, which makess the system easily solvable in the $N \to \infty$ limit. This formalism is intuitive, reproduces well known results of polariton relaxation rates, and explains mechanisms for donor-acceptor energy transfer assisted by polaritons. In the fourth chapter, we generalize our formalism to incorporate molecular disorder and large number of excitations [88]. We reveal that changes in excited state dynamics are only possible while molecules retain inter-exciton coherence, which vanishes in femtosecond timescales (specially in highly disordered ensembles). This implies that modifications of Potential Energy Surfaces (PES) under collective light-matter coupling are unfeasible, and polaritons only assist in the creation of initial states that evolve under the bare molecular Hamiltonian. This challenged the prevailing paradigm of the field. In the fifth chapter, we use our method to numerically confirm that, in the $N \to \infty$ limit, initial state preparation assisted by polaritons can be done using a laser operating in the weak coupling regime [89]. In other words, polaritons merely act as optical filters, and non-trivial polaritonic effects rely on single-molecule light-matter coupling terms ($1/N$ effects). In chapter 6, we focus on the best known $1/N$ effects in molecular polaritonics: relaxation from dark to polariton states. To do so, we derive a bosonic picture of molecular polaritons that generalizes our CUT-E formalism to account for an arbitrary number of excitations [90]. This second quantization picture enforces permutational symmetries directly on the Hamiltonian. We use

our method to rigorously derive the vibrational relaxation and radiative pumping relaxation mechanisms, calculate the corresponding relaxation rates, and relate them to photophysical processes such as fluorescence, photon recycling, and Raman scattering. Finally, in chapter seven we summarize our findings and provide future directions.

Chapter 2

Polariton assisted down-conversion of photons via nonadiabatic molecular dynamics

Quantum dynamics of the photoisomerization of a single 3,3'-diethyl-2,2'-thiacynine iodide molecule embedded in an optical microcavity was theoretically studied. The molecular model consisting of two electronic states and the reaction coordinate was coupled to a single cavity mode via the quantum Rabi Hamiltonian, and the corresponding time-dependent Schrödinger equation starting with a purely molecular excitation was solved using the Multiconfigurational Time-Dependent Hartree Method (MCTDH). We show that, for single-molecule SC with the photon mode, nonadiabatic molecular dynamics produces mixing of polariton manifolds with differing number of excitations, without the need of counter-rotating light-matter coupling terms. Therefore, an electronic excitation of the molecule at *cis* configuration is followed by the generation of two photons in the *trans* configuration upon isomerization. Conditions for this phenomenon to be operating in the collective strong light-matter coupling regime are discussed and found to be unfeasible for the present system, based on simulations of two molecules inside the microcavity. Yet, our finding suggests a new mechanism that, without ultrastrong coupling (USC), achieves photon down-conversion by exploiting the emergent molecular dynamics arising in polaritonic architectures.

2.1 Introduction

Single molecules strongly interacting with confined electromagnetic fields are commonly described by the Rabi model [12, 22, 91] where the matter part is taken to be a two-level system with no internal structure. This description is insufficient to study molecular processes where nuclear dynamics plays a major role [92]. Theories that take into account the correlated nuclear-electronic-photonic dynamics have been recently developed to account for the rovibrational structure of molecules [93–95]. In these new frameworks, molecular-photonic dynamics are described in dressed or polaritonic potential energy surfaces (PESs), and are governed by novel features such as light-induced avoided crossings (LIACs) and light-induced conical intersections (LICIs) [40, 96–98].

Most recent works focus on using strong light-matter coupling to change molecular processes such as photodissociation [99–101], photoisomerization [33, 94, 102–105], and charge and energy transfer [104, 106]. In this chapter we focus on a less addressed complementary question: can the emergent molecular dynamics under SC be harnessed for photonic applications? Previous studies on atomic systems have shown that nonlinear optical effects can arise from the interplay of translational or vibrational motion and the coupling to a confined radiation field [107, 108]; however, as far as we are aware, no molecular analogues of these phenomena have been previously reported. By theoretically studying the photoisomerization of a single 3,3'-diethyl-2,2'-thiacynine iodide molecule that strongly interacts with a cavity, we find that for specific cavity frequencies and sufficiently strong couplings, molecular photoexcitation into an electronic excited state can be followed by the spontaneous emission of two photons of a lower frequency via the cavity after isomerization, thus offering a new mechanism for photonic down-conversion using molecular polaritons. This phenomenon provides a molecular version of the dynamical Casimir (DC) effect, where photon pair creation arises from nonadiabatic modulation of the electromagnetic vacuum. As we shall show, molecular nonadiabatic effects mix states with different excitation numbers, without the need of the usually invoked counter-rotating light-matter coupling terms which are relevant in the standard realizations of the DC effect, which operate

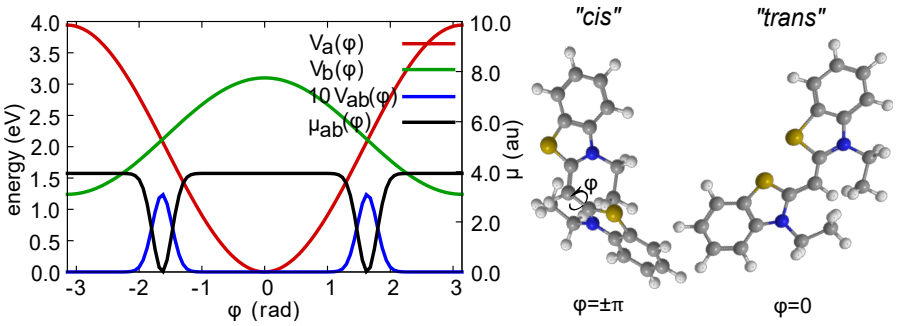

Figure 2.1: Potential energy surfaces $V_a(\phi)$ and $V_b(\phi)$, diabatic coupling $V_{ab}(\phi)$, and transition dipole moment $\mu_{ab}(\phi)$ for 3,3'-diethyl-2,2'-thiacynine iodide; parameters from ref. [111]. *cis* and *trans* configurations are located around $\phi = \pm\pi$ and $\phi = 0$ respectively. Diabatic coupling $V_{ab}(\phi)$ generates molecular avoided crossings near $\phi = \pm 1.63$ rad.

under USC conditions [12, 109, 110].

2.2 Model

To begin with, the bare molecular Hamiltonian is given by ($\hbar = 1$) $\hat{H}_{mol} = \hat{T}_N + \hat{H}_{el}(\phi)$, where $\hat{T}_N = -\frac{1}{2m}\frac{\partial^2}{\partial\phi^2}$,

$$\hat{H}_{el}(\phi) = \begin{pmatrix} V_a(\phi) & V_{ab}(\phi) \\ V_{ab}(\phi) & V_b(\phi) \end{pmatrix}, \tag{2.1}$$

ϕ is the torsional angle of the molecule (reaction coordinate), $V_a(\phi)$ and $V_b(\phi)$ are *diabatic* PESs, and $V_{ab}(\phi)$ is the diabatic coupling, responsible to produce transitions between the electronic states $|a\rangle$ and $|b\rangle$. Diagonalization of $\hat{H}_{el}$ as a function of ϕ produces adiabatic states of low energy $|g\rangle$ and high energy $|e\rangle$. These purely molecular quantities can be determined by quantum chemistry calculations and spectroscopic measurements. In this chapter, we take these properties from a previous model parametrized by Hoki and Brumer (see Figure 2.1) [111].

On the other hand, the Hamiltonian of the cavity mode is given by

$$\hat{H}_{cav} = \omega_c(\hat{a}^\dagger\hat{a} + 1/2), \tag{2.2}$$

where ω_c is the cavity frequency, and $\hat{a}$ is the photon annihilation operator. The

Hamiltonian of the cavity-molecule system is the sum of those corresponding to the molecule, the cavity mode, and the interaction between them:

$$\hat{H} = \hat{H}_{mol} + \hat{H}_{cav} + \hat{H}_I. \tag{2.3}$$

In this chapter, the cavity-molecule coupling is modeled as described in ref. [40], where the photon is coupled to the electronic transition through the molecular transition dipole moment $\mu_{ab}(\phi)$ (see Figure 2.1). Equation 2.3 can then be re-expressed as $\hat{H} = \hat{T}_N + \hat{H}_{e-p}(\phi)$, with the adiabatic polaritonic BO Hamiltonian given by

$$\hat{H}_{e-p}(\phi) = \hat{H}_{el} + \omega_c(\hat{a}^\dagger\hat{a} + 1/2) + g(\phi)(\hat{a}^\dagger + \hat{a})\hat{\sigma}_x. \tag{2.4}$$

Here, $g(\phi) = \epsilon\omega_c\mu_{ab}(\phi)$ and $\epsilon = 1/\sqrt{2V\omega_c\epsilon_0}$.

By conveniently using the Fock state basis for the cavity mode, $\hat{H}_{e-p}$ can be diagonalized to obtain adiabatic polaritonic PESs. These are shown in Figure 2.2 for specific values of cavity frequency and light-matter coupling. To establish a reference, the electronic energy gap at the *cis* configuration of the molecule is labeled as $\omega_{ab} \equiv V_a(\phi = -\pi) - V_b(\phi = -\pi) = 2.70$ eV. An experimental realization of single-molecule SC was recently carried out by Chikkaraddy and collaborators using a plasmonic nanocavity ($V < 40$ nm^3) and an electronic transition of the methyl blue molecule [22]. The coupling strength at the single molecule level was $g \approx 0.09$ eV with the transition dipole moment of the molecule being 3.8 D. For the present model, the transition dipole moment is 10 D, so we believe it is reasonable to consider $g = 0.21$ eV as the highest single-molecule coupling strength. Following that restriction, we varied ω_c from 25% to 100% of ω_{ab}, as well as the light-matter scaling parameter ϵ from 0.01 au to 0.04 au. This corresponds to a light-matter coupling ranging from 4% to 16% of ω_c. As an illustration, a coupling constant $g = 0.21$ eV in our model corresponds to a single-photon electric field amplitude inside the optical microcavity of 1×10^9 $\frac{V}{m}$, corresponding to the free space electric field amplitude of a wave laser at the same frequency, but with an intensity $I = 1.4 \times 10^{11}$ $\frac{W}{cm^2}$.

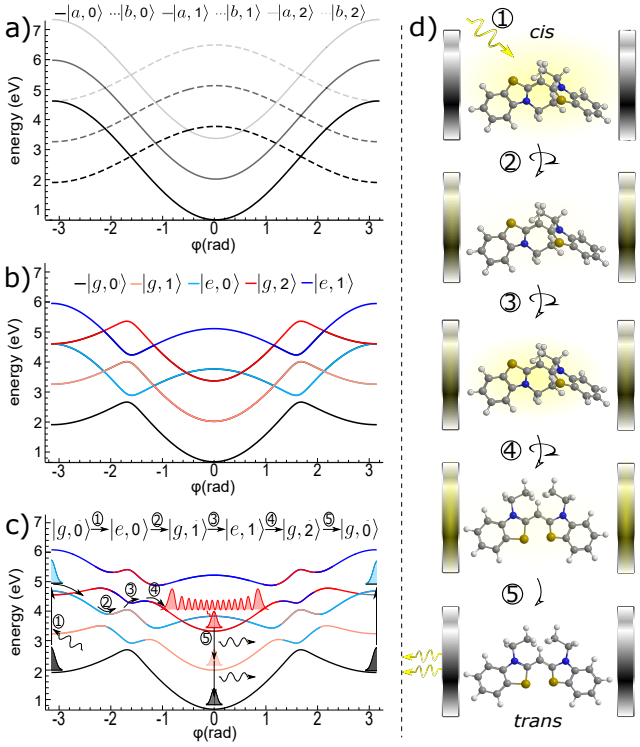

Figure 2.2: Polaritonic PESs for $\omega_c = 0.5\omega_{ab}$. a) Ignoring both light-matter and diabatic couplings. b) Turning on diabatic coupling, generating adiabatic states $|g\rangle$ and $|e\rangle$. c) Turning on both light-matter and diabatic couplings ($\epsilon = 0.04$ au $\rightarrow g \approx 0.21$ eV). d) Mechanism of photon down-conversion is shown as a sequence of five steps. Light red: one photon $|g,1\rangle$. Dark red: two photons $|g,2\rangle$. Light blue: one exciton $|e,0\rangle$. Dark blue: one exciton with one photon $|e,1\rangle$. d) Diagrammatic representation of mechanism in c).

Notice that polaritonic PESs (Figure 2.2c) at the *cis* and *trans* configurations resemble their counterparts in the absence of light-matter coupling (Figure 2.2b); this effect is a consequence of the cavity and the molecule being highly off-resonance at those configurations. However, as the torsional angle ϕ changes, so does the electronic energy gap, leading to resonances at $\phi = \pm 1.16, \pm 2.14$ rad. Light-matter coupling about these resonances generates LIACs. In this adiabatic polaritonic basis, the kinetic energy operator is not longer diagonal, and it generates nonadiabatic couplings among different polaritonic PES. By analogy with atomic systems or synthetic qubit systems, where different polariton manifolds can be couple through counter-rotating terms [12, 109, 110, 112], coexistence of nonadiabatic and light-matter couplings is enough to mix polaritons with different

number of excitations, with the difference that parity in excitation number need not be conserved. Figures 2.2c and 2.2d summarize our proposal to achieve photon down-conversion using molecular polaritons:

1. Resonant optical excitation of the molecule from state $|g,0\rangle$ to state $|e,0\rangle$. This transition occurs via direct interaction between the molecular dipole and a high frequency photon that is transparent (non-resonant) with respect to the cavity.

2. Adiabatic dynamics across a LIAC converts electronic excitation into a cavity photon ($|e,0\rangle \rightarrow |g,1\rangle$).

3. Nonadiabatic wavepacket dynamics across a molecular avoided crossing converts vibrational energy into electronic energy ($|g,1\rangle \rightarrow |e,1\rangle$).

4. Adiabatic dynamics across a second LIAC converts electronic excitation into a second cavity photon ($|e,1\rangle \rightarrow |g,2\rangle$).

5. Photons are spontaneously emitted into the electromagnetic bath through the cavity ($|g,2\rangle \rightarrow |g,0\rangle$).

We emphasize that steps 2 and 4 are possible only if light-matter coupling is strong enough to create a sizable LIAC that favors adiabatic nuclear dynamics. In other words, energy exchange between cavity photon and molecule must be fast compared to the instantaneous nuclear motion at the vicinity of the LIAC. Interestingly, steps 3 and 4 resemble a mechanism previously studied by Dobrovsky and Levine, who explored the possibility of light emission starting with a high-energy collision and subsequent nonadiabatic molecular dynamics [113]. Notice that our mechanism does no rely on counter-rotating light-matter coupling terms in any of its steps. Even though we gained much conceptual insight by appealing to a Fock basis for the cavity mode, we will numerically deal with the latter in quadrature coordinates [114],

$$\hat{a} = \sqrt{\frac{\omega_c}{2}} \left(\hat{x} + \frac{i}{\omega} \hat{p} \right), \tag{2.5}$$

where $\hat{p} = -i\frac{\partial}{\partial x}$. With these identifications, Eq. 2 can be rewritten as

$$\hat{H} = \hat{T}_N + \frac{\hat{p}^2}{2} + \begin{pmatrix} V_a(\phi) + \frac{1}{2}\omega_c^2 x^2 & V_{ab}(\phi) + g(\phi)x \\ V_{ab}(\phi) + g(\phi)x & V_b(\phi) + \frac{1}{2}\omega_c^2 x^2 \end{pmatrix}, \tag{2.6}$$

where the cavity mode appears as an additional "vibrational" coordinate, whose numerical implementation is straightforward [40]. The wave function is expanded as a linear combination of diabatic electronic states $|k\rangle$:

$$\langle x, \phi | \Psi(t) \rangle = \sum_k \psi_k(x, \phi, t) |k\rangle, \quad \text{for } k = a, b, \tag{2.7}$$

and the initial state is chosen to represent an impulsive Franck-Condon excitation of the molecule (directly via a high-energy photon that is transparent to the cavity), namely, a product state of the molecular ground state on top of the excited electronic state $|a\rangle$ at the *cis* configuration $\varphi_b(\phi)$, accompanied by the vacuum state of the cavity mode $\chi(x)$:

$$\langle x, \phi | \Psi(0) \rangle = \varphi_b(\phi)\chi(x)|a\rangle. \tag{2.8}$$

To analyze the computational results, we calculate adiabatic populations of electronic and photonic states as a function of time:

$$P_{\kappa,n}(t) = \langle \Psi(t) | \kappa, n \rangle \langle \kappa, n | \Psi(t) \rangle, \quad \text{for } \kappa = g, e, \text{and } n = 0, 1, 2, ... \tag{2.9}$$

In this expression, the torsional degree of freedom ϕ is traced out.

2.3 Results

2.3.1 Computational Details and Convergence Analysis

For the numerical integration of the TDSE, we employ the Multi-configurational Time Dependent Hartree (MCTDH) algorithm implemented in the Heidelberg package [115, 116]. In the multi-set formulation, The wavefunction is expanded in a set of electronic states ($k = a, b$):

$$\langle x, \phi | \Psi(t) \rangle = \sum_{(k=a)}^{b} \psi^{(k)}(x, \phi, t) | k \rangle, \tag{2.10}$$

where the wavefunction $\psi^{(k)}(x, \phi, t)$ is represented as a linear combination of Hartree products, each one of them consisting of a product of so-called single-particle functions (SPFs), namely

$$\psi^{(k)}(x, \phi, t) = \sum_{j_x=1}^{n_x} \sum_{j_\phi=1}^{n_\phi} A^{(k)}_{j_x j_\phi}(t) \varphi^{(k)}_{j_x}(x, t) \times \varphi^{(k)}_{j_\phi}(\phi, t), \tag{2.11}$$

where n_x and n_ϕ are the number of SPFs for the cavity and nuclear degrees of freedom respectively. For each SPF, in turn, a discrete variable representation (DVR) is used.

For an accurate representation of the wavefunction, convergence of the dynamics with respect to the number of SPFs and number of DVR points for each degree of freedom must be ensured. We used $n_x = n_\phi = 4$, and 199 and 150 grid points for the nuclear and photonic degrees of freedom respectively.

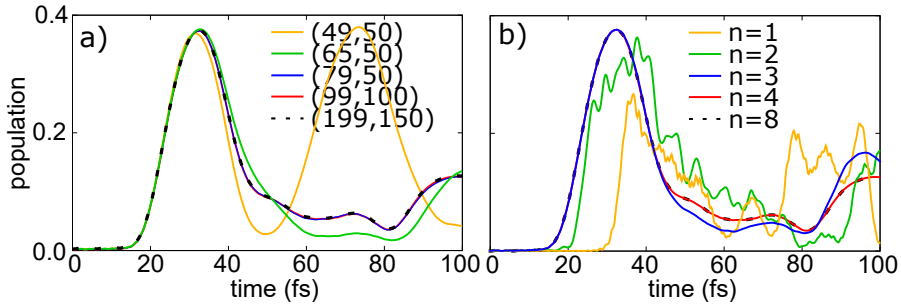

Figure 2.3: Convergence of simulations for 2-photon population for $\omega_c/\omega_{ab} = 0.5$ and $\epsilon = 0.04$. a) With respect to the number of grid points. b) With respect to the number of Single Particle Functions (SPFs).

In general, the dipole self-energy term $\frac{g(\phi)^2}{\omega_c}$ should be included in the Hamiltonian (Eq. 4) in order to ensure a bounded ground state of the polaritonic system [117]. In Figure S2, we compare the results of the quantum dynamics simulations with and without such term in the Hamiltonian.

It is evident that such term has almost no influence in the dynamics. This is because our model has no permanent dipole, light-matter coupling is not large

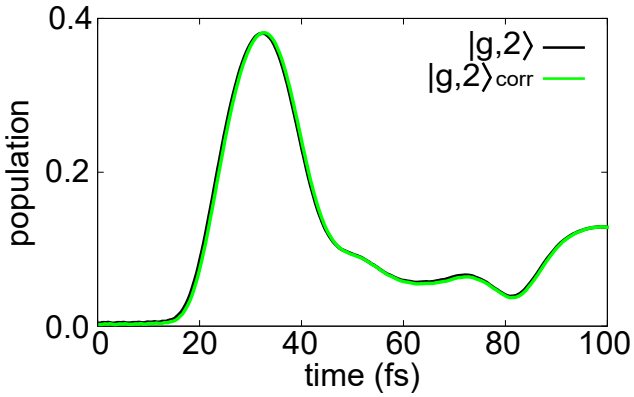

Figure 2.4: 2-photon population for $\omega_c/\omega_{ab} = 0.5$ and $\epsilon = 0.04$ with (green) and without (black) the correction dipole self-energy term.

enough, and the transition dipole moment is constant for most values of ϕ (see Figure 1).

2.3.2 Quantum Dynamics and Polaritonic Potential Energy Surfaces

In Figure 2.5a we present the adiabatic populations as a function of time. At short time, we can observe low amplitude and fast oscillations corresponding to off-resonance population transfer between $|e,0\rangle$ and $|g,1\rangle$ due to light-matter coupling. However, as the dynamics proceeds, those two states become resonant, and there is a fast decay of the initial state $|e,0\rangle$ first into $|g,1\rangle$, then into $|e,1\rangle$, and finally into $|g,0\rangle$ and $|g,2\rangle$ by the end of the isomerization. The population of $|g,2\rangle$ at 30 fs evidences the photon pair generation. In Figure 2.5b we see that if ω_c is too low or too large compared to ω_{ab}, the state with two photons is not significantly populated. In the first case, the LIAC lies near the region in which the transition dipole moment is drastically reduced, suppressing light-matter coupling. In addition, the polaritonic PES near the LIAC is too steep, implying nuclear dynamics that are too fast to be affected by the electronic-photonic coupling. In the second case, although light-matter coupling is not suppressed, the initial energy is not high enough to produce a nonadiabatic transition that would generate the second photon (see supporting information of Fig. [86], Figure S3). Those

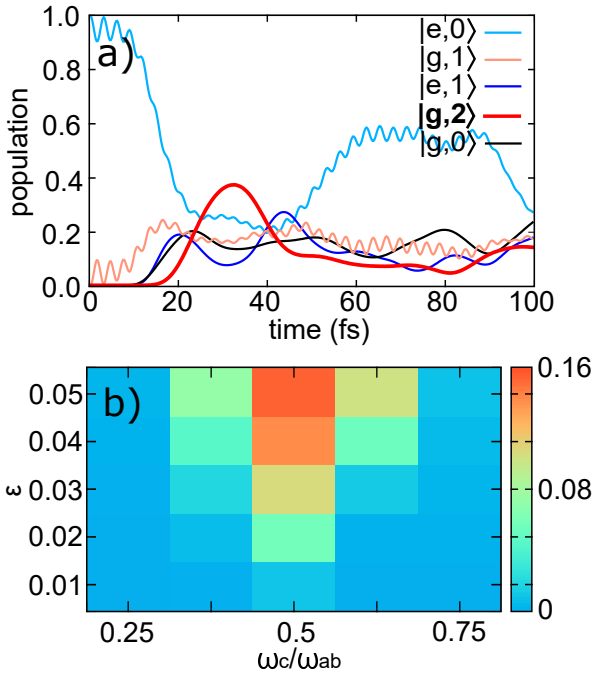

Figure 2.5: a) Time-dependent adiabatic populations of photonic - electronic states for $\epsilon = 0.04$ au ($g = 0.21$ eV) and $\omega_c/\omega_{ab} = 0.5$. b) Time average of two-photon population $\overline{P_{g,2}} = \frac{1}{T}\int_0^T P_{g,2}(t)dt$ ($T = 50$ fs) for different values of coupling strength ϵ and cavity frequency ω_c.

inconveniences are overcome if ω_c is near half of ω_{ab} and the light-matter coupling is sufficiently strong so that a large population of the state $|g, 2\rangle$ is produced. It should also be noticed that the cavity frequency does not have to be exactly half of the exciton frequency, as vibrations can account for the remaining energy to form the two photons. For a better understanding of the mechanism, we calculate the time dependent probability density for each adiabatic state:

$$\rho_\kappa(x, \phi, t) = \langle \Psi(t)|x, \phi, \kappa\rangle\langle x, \phi, \kappa|\Psi(t)\rangle, \ \kappa = g, e. \tag{2.12}$$

Numerical simulations shown in Figure 2.6 support the mechanism proposed: at 0 fs the wavepacket corresponds to the Franck-Condon excitation of the *cis* molecular configuration with the cavity in the vacuum state $|e, 0\rangle$. At 10 fs there is population of the state $|g, 1\rangle$ due to strong light-matter coupling. Subsequently, population at the state $|e, 1\rangle$ is created at 20 fs, indicating that nonadiabatic molecular dynamics has occurred. Finally, at 30 fs we clearly notice formation of a wavepacket in the lower adiabatic state with two photons $|g, 2\rangle$,

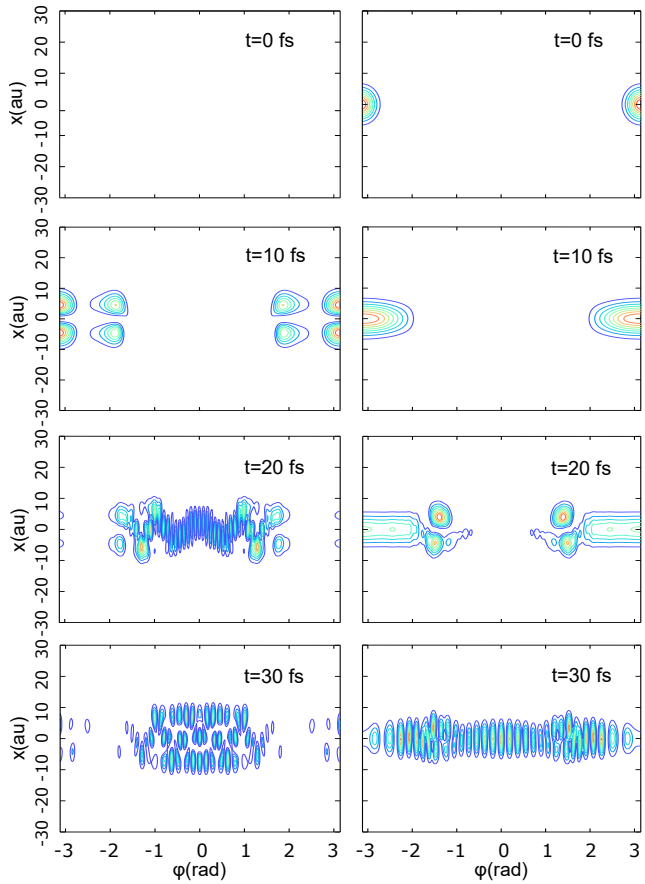

Figure 2.6: Time dependent probability density along cavity (x) and nuclear (ϕ) degrees of freedom for adiabatic electronic states $|g\rangle$ (left) and $|e\rangle$ (right). The largest number of photons in the wave function is given by the number of nodes along x coordinate.

in the *trans* configuration. Consistently, 30 fs is the time when the population of the $|g, 2\rangle$ state reaches its maximum value (see Figure 2.5a). Other mechanisms that can be observed proceed as $|e, 0\rangle \rightarrow |g, 1\rangle \rightarrow |e, 0\rangle$ (purely adiabatic dynamics and no photon down-conversion), $|e, 0\rangle \rightarrow |g, 1\rangle$ (adiabatic dynamics across one LIAC and no photon down-conversion), and $|e, 0\rangle \rightarrow |g, 0\rangle$ (purely nonadiabatic dynamics and no photon down-conversion). It is also worth noticing that states with more than two excitations (e.g. $|e, 2\rangle$, $|g, 3\rangle$) are not appreciably populated during the dynamics at any time, confirming that counter-rotating terms do not play a significant role in this phenomenon.

We shall briefly discuss the effects of various types of dissipation in our down-conversion mechanism. It is clear that any dissipative effect that operates

within the time scale of the photon down-conversion mechanism above ($\sim$ 30 fs) would be detrimental. In particular, one may think that cavity leakage could play a significant constraint in the realization of our mechanism: single-molecule strong light-matter coupling utilizes plasmonic nanocavities with a very low quality factor ($Q \approx 12$) [22], leading to photon leakage times less than 10 fs. However, we believe this time scale should not limit our mechanism, as it relies on the upper polariton being mostly molecular due to the large detuning between the cavity and the molecular transition at the Franck-Condon region. Hence, the dominant dissipative effects must be molecular, and they operate within a time scale of 40 fs, according to the study in ref. [111]. Importantly, this molecular dissipation timescale is chemical specific, and we suspect that some molecules will suffer important sources of down-conversion efficiency reduction due to nonadiabatic effects (e.g., nonradiative decay through conical intersections [118]) from additional intramolecular vibrational modes that require explicit description. A more detailed account of such processes is beyond the scope of our work, but should be an important direction in future studies.

A complementary interpretation of the down-conversion mechanism can be provided from a time-independent perspective: for the molecule at the *cis* configuration, the upper polariton is mostly excitonic and accessible by means of a high-frequency photon. However, due to nonadiabatic couplings, the upper polariton is mixed with the lower polariton of the second excitation manifold at the *trans* configuration, which is accompanied by two photons.

2.3.3 Photon Downconversion in the Collective Regime

Experiments involving a single emitter strongly coupled to a confined electromagnetic field have been recently carried out by placing molecules on plasmonic nanocavities [22,91,119–122] and Fabry-Pérot microcavities [123]. However, one of the most common setups to achieve SC involves the use of a macroscopic amount of molecules. The electromagnetic field interacts with an ensemble of N molecules to form 2 (upper and lower) polariton states, and $N-1$ mostly molecular (dark) states that mix weakly with light either due to disorder or vibrational motion [27, 94].

Under these conditions, collective light-matter coupling scales as $\sim \sqrt{N}\epsilon$, where ϵ is the individual light-matter coupling and N is the number of particles in the microcavity.

To investigate the feasibility of achieving down-conversion using collective light-matter coupling, we performed calculations of two molecules embedded in an optical microcavity. We assume that molecules interact identically with the cavity mode and have no direct electrostatic interaction between them. The Hamiltonian is a generalization of the Dicke model [124] that includes the nuclear degrees of freedom:

$$\hat{H} = \sum_{i=1}^{N} \left(\hat{T}_{N,i} + \hat{H}_{el,i} \right) + \omega_c (\hat{a}^\dagger \hat{a} + 1/2) + \sum_{i=1}^{N} g(\phi_i)(\hat{a}^\dagger + \hat{a})\hat{\sigma}_{x,i}. \tag{2.13}$$

We study the two-photon generation at constant collective light-matter coupling for $N = 1, 2$ molecules (thus setting the individual light-matter coupling in each case at $\epsilon = 0.04/\sqrt{N}$ au). We first assume that only molecule 1 is initially excited, and calculate electronic state populations of each molecule at the *cis* ($|g_C\rangle$, $|e_C\rangle$) and *trans* ($|g_T\rangle$, $|e_T\rangle$) configurations using the projection operators

$$\hat{P}^i_{\kappa,C} = \int d\phi_i |[\Theta(\phi_i - 1.63) + \Theta(-\phi_i - 1.63)]|\kappa_i, \phi_i\rangle\langle\kappa_i, \phi_i| \tag{2.14}$$

and

$$\hat{P}^i_{\kappa_i,T} = 1 - \hat{P}^i_{\kappa_i,C}, \tag{2.15}$$

where $\hat{P}^i_{\kappa_i,C}$ is the projector of the i-th molecule over the *cis* configuration and electronic state κ_i, and $\Theta(\phi)$ is the Heaviside step function. For instance, the probability of both molecules to be at the *cis* configuration in the ground state, i.e. state $|g_C g_C\rangle$, is given by $\langle \hat{P}^1_{g,C} \hat{P}^2_{g,C} \rangle$. Furthermore, we calculate the population of two photon states as the expectation value of the projection operator $|2\rangle\langle 2|$. Finally, we repeat the same analysis for an initial electronic state given by $\frac{1}{\sqrt{2}}(|ge\rangle + |eg\rangle)$.

As can be observed in Figure 2.7a, most dynamics during the first 100 fs involves the isomerization of the initially excited molecule, while the second molecule remains at the *cis* configuration in the ground state. This path resembles that of the single-molecule scenario, in which the excited molecule isomerizes in

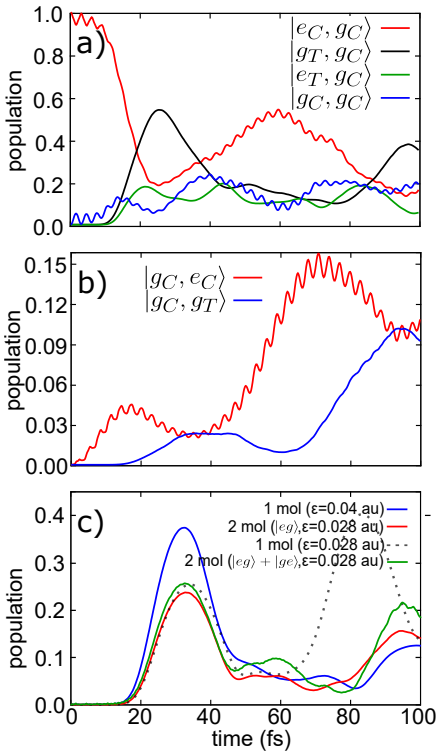

Figure 2.7: Population dynamics for $\omega_c/\omega_{ab} = 0.5$ and $\epsilon = 0.03$ au, if only molecule 1 is initially excited. a) States with significant population during the first 100 fs. b) Population of states in which molecule 2 undergoes isomerization reaction. Notice the difference in vertical scale. c) Comparison between populations of two-photon states for one and two molecules with the same *collective* light-matter coupling (blue *vs* red and green), and for two and one molecules with the same *individual* light-matter coupling (red and green *vs* dashed black).

around 30 fs, ending at the *trans* configuration in both the molecular ground and the excited state (see Figure 2.6). After 40 fs, the second molecule gets excited and also undergoes isomerization. However, this process seems to occur only if the first molecule is in its ground state at the *cis* configuration (Figure 2.7b). This can be understood by noticing that the molecules at the *cis* configuration are closer to resonance with the cavity mode. The individual coupling of each molecule with the cavity mode produces an effective coupling between them, causing the excitation of one molecule to be transferred to the other one (i.e $|e_C g_C\rangle \rightarrow |g_C e_C\rangle$), as has been reported in previous works [102,125]. Evidently, this process is not very likely in our setup, and should not be observed in the limit where the single-molecule coupling is weak.

The mechanism involving two molecules can thus be summarized as follows:

1. Optical excitation of the first molecule ($|g_C, g_C\rangle \rightarrow |e_C, g_C\rangle$).

2. Isomerization of the first molecule. ($|e_C, g_C\rangle \rightarrow |e_T, g_C\rangle$ and $|e_C, g_C\rangle \rightarrow |g_T, g_C\rangle$). As in the single molecule scenario, this can produce zero, one or two photons.

3. Cavity-mediated energy transfer from the first to the second molecule at the *cis* configuration ($|e_C g_C\rangle \rightarrow |g_C e_C\rangle$).

4. Isomerization of the second molecule ($|g_C, e_C\rangle \rightarrow |g_C, e_T\rangle$ and $|g_C, e_C\rangle \rightarrow |g_C, g_T\rangle$), producing zero, one, or two photons.

As one would expect based on the mechanism above, Figure 2.7c shows that having two molecules instead of one does not increase the likelihood of generation of two photons (see blue and red curves), so long as the *collective* light-matter coupling $\sqrt{N}\epsilon = 0.04$ au remains the same. To reinforce the observation that the observed effect is essentially a single-molecule one, we notice that for fixed *individual* light-matter coupling $\epsilon = 0.028$ au, the two-photon state populations for two and one molecules (see red and black dashed curves) is very similar at short times. The reason we do not observe significant collective effects is that the molecules at the initial configuration are not in resonance with the cavity, but become resonant as the isomerization proceeds. As a consequence, initial excitation of one molecule can lead to efficient energy exchange with the cavity only after sufficient nuclear dynamics ensues, while the other molecule remains off resonant. This was observed to be true even if the initial excitation is shared by all molecules in superposition. In other words, the Rabi splittings for the relevant LIACs relevant for this process mainly depend on the single-molecule coupling even if many molecules are present.

We believe that the fact that the cavity and the molecule are off-resonance at the initial configuration is not a vital characteristic of the down-conversion mechanism proposed here. If the molecules are resonant with the cavity at the Franck-Condon region, an excitation of the upper-polariton can still produce a molecular nonadiabatic transition that would generate a second excitation, which

can afterward become a second photon. The Rabi splitting in that case would be of a collective nature, and the two-photon generation would be possible if the isomerization is faster than the decay from the upper-polariton to the dark states [118]. However, deleterious effects arising solely from collective coupling [126] may also complicate the down-conversion mechanism. The nonadiabatic molecular dynamics associated with molecules which are resonant at the Franck-Condon configuration could not be observed for the molecule studied here. Hence, the effectiveness of our down-conversion scheme in the collective regime is molecule-specific and will require additional investigations.

2.4 Summary

We have shown that strong light-matter coupling in conjunction with nonadiabatic molecular dynamics can lead to emerging nonlinear optical phenomena such as photon down-conversion. While much attention has been recently placed into the study novel chemical dynamics afforded by molecular polaritons, we wish to emphasize a complementary aspect of the problem that is equally rich and relevant: the use of molecular dynamics to generate new photonic phenomena. The elucidated effect operates at the single molecule SC regime, but we have provided plausible arguments that would allow to extend it to the collective regime, where many experiments are being currently performed.

2.5 Acknowledgments

Chapter 2, in full, is a reprint of the material as it appears in The Journal of Physical Chemistry Letters. Pérez-Sánchez, Juan B.; Yuen-Zhou, Joel. 11, 152-159, 2019. The dissertation author was the primary investigator and author of this paper. J.B.P.S. and J.Y.Z. were funded with the NSF EAGER Award CHE 1836599.

Chapter 3

Simulating molecular polaritons in the collective regime using few-molecule models

The study of molecular polaritons beyond simple quantum emitter ensemble models (e.g., Tavis-Cummings) is challenging due to the large dimensionality of these systems and the complex interplay of molecular electronic and nuclear degrees of freedom. This complexity constrains existing models to either coarse-grain the rich physics and chemistry of the molecular degrees of freedom or artificially limit the description to a small number of molecules. In this chapter we exploit permutational symmetries to drastically reduce the computational cost of *ab-initio* quantum dynamics simulations for large N. Furthermore, we discover an emergent hierarchy of timescales present in these systems, that justifies the use of an *effective* single molecule to approximately capture the dynamics of the entire ensemble, an approximation that becomes exact as $N \to \infty$. We also systematically derive finite N corrections to the dynamics, and show that addition of k extra effective molecules is enough to account for phenomena whose rates scale as $\mathcal{O}(N^{-k})$. Based on this result, we discuss how to seamlessly modify existing single-molecule SC models to describe the dynamics of the corresponding ensemble. We call this approach Collective dynamics Using Truncated Equations (CUT-E), benchmark it against well-known results of polariton relaxation rates, and apply it to describe a

universal cavity-assisted energy funneling mechanism between different molecular species. Beyond being a computationally efficient tool, this formalism provides an intuitive picture for understanding the role of bright and dark states in chemical reactivity, necessary to generate robust strategies for polariton chemistry.

3.1 Introduction

Theoretical work aimed at explaining experimental results or predicting new phenomena emerging in polaritonic architectures face the formidable challenge of properly modeling the molecular (local) degrees of freedom of each molecule while describing the super-radiant interaction of the molecular ensemble with the field (collective). The dynamics arising from the complex interplay of vibrational and electronic degrees of freedom in molecules renders simple quantum optics models (such as the original Tavis-Cummings Hamiltonian [127]), limited in their applicability to molecular polaritons. Thus, molecular polaritons face unique challenges and opportunities that are not encountered in more traditional polariton systems [128], such as atomic or artificial qubit ensembles [129], or cryogenic inorganic semiconductors [130]. Most of the reported simulations of molecular polaritons can only deal with one of two aforementioned challenges at a time. On the one hand, theoretical studies that acknowledge the collective nature of the light-matter coupling are typically limited to a few dozen molecules at a time and involve sophisticated numerical treatments [131], simplifications such as single vibrational mode descriptions [132], or semiclassical trajectories [42, 133]. On the other hand, models that implement *ab initio* treatments are often restricted to a single or few molecules in a cavity [73, 134, 135]. Regardless, from a computational standpoint, it seems suspicious that it is necessary to explicitly simulate the dynamics of N molecules, especially if they are identical to each other. Indeed, there are numerous symmetries in the system that should significantly reduce the computational cost of these simulations [62, 63, 136–144].

In this chapter, we outline a wavefunction-based formalism that makes use of such symmetries to significantly reduce the complexity of quantum dynamics

simulations of the single-excitation manifold of molecular polaritons. Moreover, this formalism naturally provides a hierarchy of approximations to further simplify the problem in a way that, in the $N \to \infty$ limit, polaritonic properties can be calculated using a modified *effective* single molecule coupled to a cavity with the collective coupling. This provides grounds for some single-molecule SC phenomena to appear in the collective regime, consistent with previous work where linear optical properties can be calculated from effective single-molecule models in the thermodynamic limit [145, 146]. Moreover, we show that a system of two effective molecules can describe all the effects with rates that scale as $1/N$. In general, we show that processes with $\mathcal{O}(N^{-k})$ rates are described by $k+1$ effective molecules strongly coupled to the cavity. This implies that, for a large ensemble of molecules, it is enough to consider only a few effective molecules to solve for the dynamics of the original polariton system (see Figure 3.1). The model can be applied to study disordered ensembles (e.g., a mixture with two chemical species) without a significant increase in the computational cost.

The article is organized as follows: in Section 3.2 we present the Hamiltonian and the multiconfigurational representation of the total wavefunction of the system, in which permutational symmetries become evident. Then, we uncover a convenient mathematical structure of the Equations of Motion (EoM) where approximate symmetries emerge, and which become useful for large N, while keeping the collective light-matter coupling $\sqrt{N}g$ finite, with g being the single-molecule coupling (this is the physical condition of interest in experiments, and which concerns us hereafter). This structure allows us to derive the simple effective Hamiltonians involving only a few molecules, that solve for the dynamics of the entire ensemble. In Section 3.3.5 we make use of the effective single-molecule model to demonstrate how both optical and material properties in the original system can be computed using the effective single-molecule simulation. In Section 3.3.6 we benchmark our formalism against a well known result: the non-radiative relaxation of polariton and dark states. In Section 3.3.8 we present a pedagogical and intriguing application that reveals the power of our formalism, describing how to exploit polariton dynamics to obtain nonstatistical outcomes in photoproducts.

Finally we summarize the work in Section 3.4.

3.2 Model

Consider a system of N molecules collectively coupled to a single cavity mode. The Tavis-Cummings Hamiltonian, extended to include vibrational degrees of freedom missing from original models, can be written as (hereafter $\hbar = 1$)

$$\hat{H} = \sum_{i}^{N} \left(\hat{H}_m^{(i)} + \hat{H}_I^{(i)} \right) + \hat{H}_{cav}, \tag{3.1}$$

where

$$\hat{H}_m^{(i)} = -\frac{1}{2\mu}\frac{\partial^2}{\partial q_i^2} + V_g(q_i)|g_i\rangle\langle g_i| + V_e(q_i)|e_i\rangle\langle e_i|,$$
$$\hat{H}_{cav} = \omega_c \hat{a}^\dagger \hat{a}, \qquad \hat{H}_I^{(i)} = g\left(|e_i\rangle\langle g_i|\hat{a} + |g_i\rangle\langle e_i|\hat{a}^\dagger\right),$$

are the Hamiltonians for the ith molecule, the cavity mode, and the interaction between them. Here, μ is the reduced mass of the nuclei, $|g_i\rangle$ and $|e_i\rangle$ are the molecular ground and excited electronic states, $V_{g/e}(q_i)$ are the ground and excited Potential Energy Surfaces (PES), $\hat{a}$ is the photon annihilation operator, and q_i is the vector of all molecular vibrations of molecule i (see Figure 3.1). When the PESs are harmonic, the model above reduces to the Holstein-Tavis Cummings model, which has been subject of recent studies [132, 145]. For the time being, we assume there is no disorder, neglect intermolecular interactions, and use the rotating wave approximation by considering the single-molecule coupling strength g to be much smaller than the bare photon frequency ω_c. Finally, we also ignore (non-radiative) couplings between the molecular ground and excited states whose PESs can form conical intersections [147–149]. Under these hypotheses, the excitation number [sum of electronic excitations (Frenkel excitons) and photon number] is conserved.

In this article we shall focus on the so-called first-excitation manifold, which describes processes in which the cavity triggers excited state dynamics of one

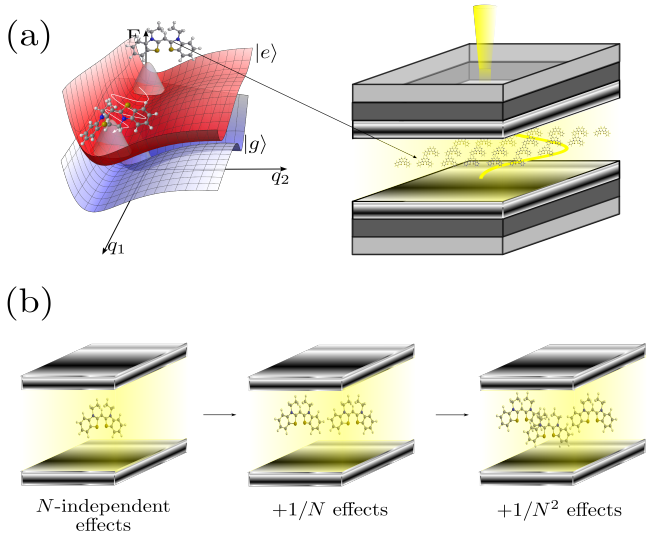

Figure 3.1: a) Molecular polaritons in the collective strong-coupling regime. Molecules are not well described by structureless two-level systems, and the interplay between their internal (e.g., vibrational) degrees of freedom and the collective interaction of their optical (e.g., electronic) transitions with the optical mode cannot be described using simple models such as the standard Tavis-Cummings Hamiltonian. b) Pictorial representation of the Collective dynamics Using Truncated Equations (CUT-E) method. Processes with $\mathcal{O}(N^{-k})$ rates can be described by a model of $k+1$ effective molecules coupled to a cavity mode.

molecule at a time. The position-representation ansatz takes the form

$$|\Psi(t)\rangle = \psi^{(0)}(\vec{q},t)|1\rangle + \sum_{i}^{N} \psi^{(i)}(\vec{q},t)|e_i\rangle, \tag{3.2}$$

with the states $|e_i\rangle = |g_1, g_2, ..., e_i, ..., g_N, 0_{ph}\rangle$ and $|1\rangle = |g_1, g_2, ..., g_N, 1_{ph}\rangle$, and the vibrational wavefunctions

$$\begin{aligned}
\psi^{(0)}(\vec{q},t) &= \sum_{j_1}^{m}\sum_{j_2}^{m}\cdots\sum_{j_N}^{m} A^{(0)}_{j_1 j_2 ... j_N}(t) \prod_{k=1}^{N} \varphi_{j_k}(q_k), \\
\psi^{(i)}(\vec{q},t) &= \sum_{j_1}^{m}\sum_{j_2}^{m}\cdots\sum_{j_N}^{m} A^{(i)}_{j_1 j_2 ... j_N}(t)\phi_{j_i}(q_i) \prod_{k\neq i}^{N} \varphi_{j_k}(q_k).
\end{aligned} \tag{3.3}$$

In this expansion, multiconfigurational vibrational wavefunctions ψ are built with sets of m single particle orthonormal functions $\varphi_{j_i}(q_i)$ and $\phi_{j_i}(q_i)$, respectively, that are equal for identical molecules. We choose such functions to be the eigenstates of the molecular Hamiltonian $\hat{H}^{(i)}_m$. The total wavefunction becomes exact as $m \to \infty$.

3.3 Results

3.3.1 Exploiting Permutational Symmetries

Since the Hamiltonian is invariant under the permutation of any pair of molecules α and κ, having an initial state such that $P_{\alpha\kappa}|\Psi(0)\rangle = |\Psi(0)\rangle$, implies permutation relations between the coefficients of the wavefunction. For the photonic and excitonic wavefunctions $\psi^{(0)}$ and $\psi^{(i)}$ we have,

$$\begin{aligned} A^{(0)}_{j_1 j_2 \ldots j_\kappa \ldots j_\nu \ldots j_N}(t) &= A^{(0)}_{j_1 j_2 \ldots j_\nu \ldots j_\kappa \ldots j_N}(t), \\ A^{(i)}_{j_1 j_2 \ldots j_\kappa \ldots j_i \ldots j_\nu \ldots j_N}(t) &= A^{(i)}_{j_1 j_2 \ldots j_\nu \ldots j_i \ldots j_\kappa \ldots j_N}(t). \end{aligned} \tag{3.4}$$

Additionally, there are permutations between coefficients of different excitons, given the interaction of the molecules with the cavity is assumed identical,

$$A^{(i)}_{j_1 j_2 \ldots j_i \ldots j_{i'} \ldots j_N}(t) = A^{(i')}_{j_1 j_2 \ldots j_{i'} \ldots j_i \ldots j_N}(t). \tag{3.5}$$

This means that every coefficient of the electronic state i' can be obtained directly from those in the electronic state i. In other words, Eqs. 3.4 and 3.5 yield the crucial observation that it is enough to calculate the dynamics of a single excitonic state to know the evolution of all of them. Moreover, the vibrational states of the ensemble of molecules can be completely characterized by specifying the number of molecules in each vibrational state; therefore the number of vibrational degrees of freedom also reduces drastically. The ground and excited state coefficients can be written in terms of permutationally-symmetric states,

$$\begin{aligned} A^{(0)}_{j_1 j_2 j_3 \cdots j_N} &\to A^{(0)}_{N_1 N_2 \cdots N_m} \\ A^{(i)}_{j_1 j_2 j_3 \cdots j_N} &\to A^{(1)}_{j_1 N_1 N_2 \cdots N_m}, \end{aligned} \tag{3.6}$$

where N_k is the number of ground state molecules in the vibrational state k. This new notation removes the information about the state of each specific molecule ($A^{(1)}_{j_1 N_1 N_2 \cdots N_m}$ represents a state where one molecule is in the electronic excited state in the vibrational state j_1, while the other $N-1$ molecules are distributed among all the vibrational states via $\{N_k\}$, $\sum_k N_k = N-1$). For the photonic coefficients $A^{(0)}_{N_1 N_2 \cdots N_m}$, the restriction is $\sum_k N_k = N$. For the vibrational wavefunction

$\psi^{(0)}$ not all m^N configurations are unique but only $\binom{N+m-1}{N}$. Using similar analysis we conclude a reduction of the total wavefunction in Eq. 3.2 from $(N+1)m^N$ to $\binom{N+m-1}{N}+m\binom{N+m-2}{N-1}$ configurations. This corresponds to reducing the complexity from an exponential scaling to a polynomic one, as has been shown in previous work that also exploit permutational symmetries for studying ensembles of identical systems [144, 150]. We will make use of these simplifications to redefine the EoM and subsequently the Hamiltonians. Such analysis is general and can also be done for higher excitation manifolds. In that case, the number of coefficients increases with the number of excitations due to permutations between electronically excited molecules; however after the number of excitations is half of the number of molecules this trend reverses. The EoM for the coefficients can be obtained by using the Dirac-Frenkel variational principle, or simply by inserting the ansatz wavefuntion into the Time-Dependent Schrödinger Equation.

Writing the ansatz as $|\Psi(t)\rangle = \sum_J^{m^N} A_J^{(0)}(t)\Phi_J^{(0)}|1\rangle + \sum_i \sum_J^{m^N} A_J^{(i)}(t)\Phi_J^{(i)}|e_i\rangle$, the EoM become [115]

$$i\dot{A}_J^{(i)}(t) = \sum_{i'}\sum_L \langle e_i, \Phi_J^{(i)}|\hat{H}|\Phi_L^{(i')}, e_{i'}\rangle A_L^{(i')}(t). \tag{3.7}$$

Since Eq. 3.1 ignores couplings between the molecules in the absence of the photon mode, $\langle\Phi_J^{(i)}|\hat{H}_I|\Phi_L^{(i')}\rangle = 0$ for $i, i' \neq 0$. Furthermore,

$$\langle e_i, \Phi_J^{(i)}|\hat{H}_I|\Phi_L^{(0)}, 1\rangle = g\langle\phi_{j_i}|\varphi_{l_i}\rangle \prod_{k\neq i}^{N} \delta_{j_k l_k}. \tag{3.8}$$

With these considerations, Eq. 3.7 becomes,

$$\begin{aligned}
i\dot{A}^{(i)}_{j_1 j_2 \ldots j_i \ldots j_N}(t) &= \left(\sum_{i'\neq i}^{N} E_{g,j_{i'}} + E_{e,j_i}\right) A^{(i)}_{j_1 j_2 \ldots j_i \ldots j_N}(t) \\
&\quad + g\sum_{l_i}\langle\phi_{j_i}|\varphi_{l_i}\rangle A^{(0)}_{j_1 j_2 \ldots l_i \ldots j_N}(t) \\
i\dot{A}^{(0)}_{j_1 j_2 \ldots j_N}(t) &= \left(\sum_{i'}^{N} E_{g,j_{i'}} + \omega_c\right) A^{(0)}_{j_1 j_2 \ldots j_N}(t) \\
&\quad + g\sum_{i=1}^{N}\sum_{l_i}\langle\varphi_{j_i}|\phi_{l_i}\rangle A^{(i)}_{j_1 j_2 \ldots l_i \ldots j_N}(t).
\end{aligned} \tag{3.9}$$

The last equation can be simplified using Eqs. 3.6 to write the dynamics in terms of permutationally-symmetric states:

$$
\begin{aligned}
i\dot{A}^{(1)}_{lN_1N_2\cdots N_m}(t) &= \left(\sum_{k=1}^{m} N_k E_{g,k} + E_{e,l}\right) A^{(1)}_{lN_1N_2\cdots N_m}(t) \\
&+ g\sum_k \langle\phi_l|\varphi_k\rangle A^{(0)}_{N_1N_2\cdots N_k+1\cdots N_m}(t) \\
i\dot{A}^{(0)}_{N_1N_2\cdots N_m}(t) &= \left(\sum_{k=1}^{m} N_k E_{g,k} + \omega_c\right) A^{(0)}_{N_1N_2\cdots N_m}(t) \\
&+ \sum_{k=1}^{m} N_k g \sum_{l=1}^{m} \langle\varphi_k|\phi_l\rangle A^{(1)}_{lN_1\cdots N_k-1\cdots N_m}(t).
\end{aligned} \tag{3.10}
$$

The first equation represents the absorption of the photon that takes a molecule from the state $\varphi_k|g\rangle$ into the state $\phi_l|e\rangle$. The second equation describes the conjugate process.

3.3.2 Structure of the Wavefunction

Even though Eqs. 3.10 are exact and represent a significant improvement over Eqs. 3.9, they also allow us to systematically introduce approximations by virtue of the factors N_k, which represent the number of ground state molecules in the vibrational state k. For initial states in which one of the values N_k is exceptionally large, the dynamics is such that N_k is almost conserved, as discussed below. As an example, assume we start with all the molecules in their ground vibrational state and 1 photon in the cavity mode, i.e., $A^{(0)}_{N00\cdots0}(0) = 1$. Thus, we can simplify even more our notation by only reporting the number of such vibrational excitations. By renormalizing the coefficients with N-dependent factors that indicate the number of states that correspond to the same amplitude, we can recover the basis originally introduced by Spano for harmonic modes [63], but which we now use for arbitrary PESs:

$$
\begin{aligned}
\tilde{A}^{(0)}_{0}(t) &= A^{(0)}_{N00\cdots0}(t),\\
\tilde{A}^{(1)}_{l0}(t) &= \sqrt{N}A^{(1)}_{l(N-1)0\cdots0}(t),\\
\tilde{A}^{(0)}_{k}(t) &= \sqrt{N}A^{(0)}_{(N-1)\cdots1_k\cdots0}(t),\\
\tilde{A}^{(1)}_{lk}(t) &= \sqrt{N(N-1)}A^{(1)}_{l(N-2)\cdots1_k\cdots0}(t),\\
\tilde{A}^{(0)}_{k\neq k'}(t) &= \sqrt{N(N-1)}A^{(0)}_{(N-2)\cdots1_k\cdots1_{k'}\cdots0}(t),\\
\tilde{A}^{(0)}_{kk}(t) &= \sqrt{\frac{N(N-1)}{2}}A^{(0)}_{(N-2)\cdots2_k\cdots0}(t),
\end{aligned}
\tag{3.11}
$$

With this final notation, the EoM are written in Eq. 3.12, where we have removed a constant $NE_{g,1}$ and defined $\omega_{eg,l} = E_{e,l} - E_{g,1}$ and $\omega_{g,k} = E_{g,k} - E_{g,1}$. In Figure 3.2 we provide a pictorial representation of the states associated with these coefficients.

$$
\begin{aligned}
i\dot{\tilde{A}}^{(0)}_{0}(t) &= \omega_c\tilde{A}^{(0)}_{0}(t) + g\sqrt{N}\sum_{l=1}^{m}\langle\varphi_1|\phi_l\rangle\tilde{A}^{(1)}_{l0}(t)\\
i\dot{\tilde{A}}^{(1)}_{l0}(t) &= \omega_{eg,l}\tilde{A}^{(1)}_{l0}(t) + g\sqrt{N}\langle\phi_l|\varphi_1\rangle\tilde{A}^{(0)}_{0}(t) + g\sum_{k=2}^{m}\langle\phi_l|\varphi_k\rangle\tilde{A}^{(0)}_{k}(t)\\
i\dot{\tilde{A}}^{(0)}_{k}(t) &= (\omega_{g,k}+\omega_c)\,\tilde{A}^{(0)}_{k}(t) + g\sqrt{N-1}\sum_{l=1}^{m}\langle\varphi_1|\phi_l\rangle\tilde{A}^{(1)}_{lk}(t) + g\sum_{l=1}^{m}\langle\varphi_k|\phi_l\rangle\tilde{A}^{(1)}_{l0}(t)\\
i\dot{\tilde{A}}^{(1)}_{lk}(t) &= (\omega_{eg,l}+\omega_{g,k})\,\tilde{A}^{(1)}_{lk}(t) + g\sqrt{N-1}\langle\phi_l|\varphi_1\rangle A^{(0)}_{k}(t) + g\sum_{k'\neq k}\langle\phi_l|\varphi_{k'}\rangle\tilde{A}^{(0)}_{kk'}(t)\\
&+ \sqrt{2}g\langle\phi_l|\varphi_k\rangle\tilde{A}^{(0)}_{kk}(t)\\
&\vdots
\end{aligned}
\tag{3.12}
$$

The first line of Eq. 3.12 reveals that the initial photonic state $\tilde{A}^{(0)}_{0}(t)$ is strongly coupled to states in which one molecule is electronically excited while the rest remain in their ground electronic and vibrational states $\tilde{A}^{(1)}_{l0}(t)$. However, the second equation reveals that such excited state can either emit back into the initial state (with no phonons), or can create states in which there is a vibrational excitation in one of the ground state molecules $\tilde{A}^{(0)}_{k}(t)$ upon emission. The first of these two processes depends on the collective light-matter coupling $\sqrt{N}g$, while the

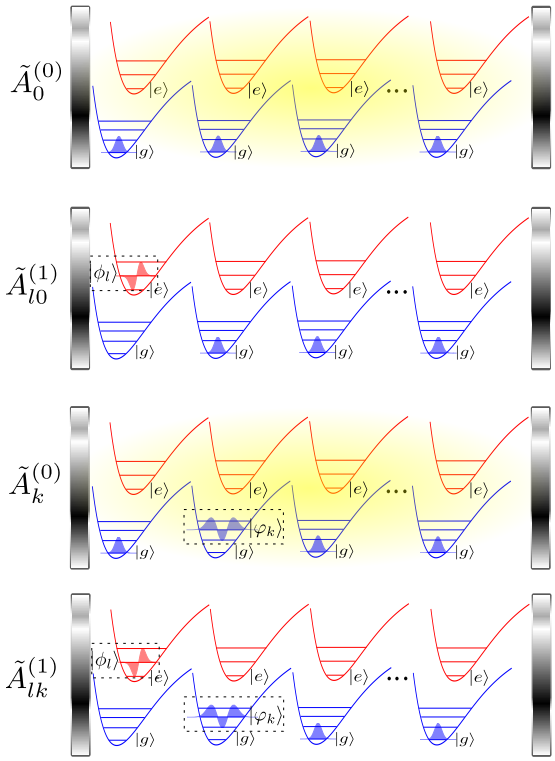

Figure 3.2: Permutationally symmetric basis in the first excitation manifold, originally introduced by Spano [63]. $\tilde{A}_0^{(0)}$: a photon in the cavity and N molecules in the global ground state. $\tilde{A}_{l0}^{(1)}$: 1 exciton in the vibrational state l and $N-1$ molecules are in the global ground state. $\tilde{A}_k^{(0)}$: a photon in the cavity, a ground state molecule in the vibrational state k, and $N-1$ molecules in the global ground state. $\tilde{A}_{lk}^{(1)}$: 1 exciton in the vibrational state l, 1 ground state molecule in the vibrational state k, and $N-2$ molecules in the global ground state.

second one depends on the single-molecule light-matter coupling g. This structure is repeated throughout the system of equations: coupling between states conserving the number of molecules with phonons is collective, while processes that increase the number of such molecules are proportional to the single-molecule coupling. It is interesting to note that this phenomenon is well-known in the literature of molecular aggregates. In particular, for J-aggregates, Spano and Yamagata [137] have noted that the ratio of the photoluminescence into the electronic ground state with no phonons versus that into the electronic ground state with one phonon is proportional to the coherence length N of the aggregate. While this phenomenon is routinely used as a spectroscopic probe for N, we use it in our case to drastically simplify the simulations of molecular polaritons, as explained below.

Assuming we have a large number of molecules we can treat the mixing of states with differing number of ground state molecules with phonons perturbatively, with the *single*-molecule light-matter coupling g as the perturbation. This is schematically represented in Figure 3.3.

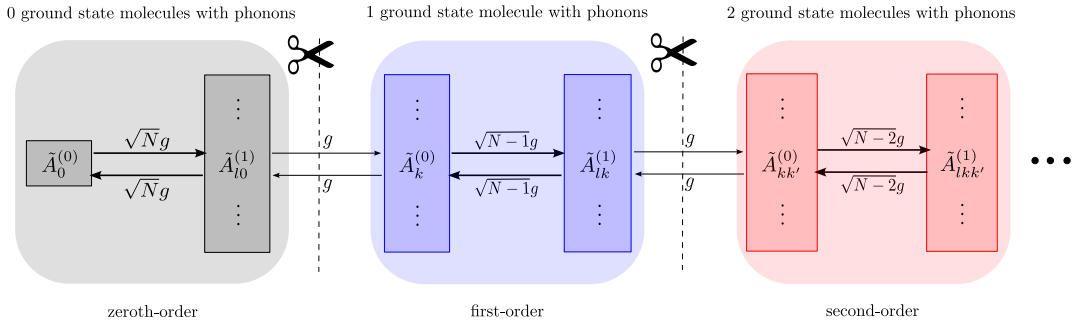

Figure 3.3: Hierarchical structure of the Equations of Motion (EoM) that gives rise to the Collective dynamics Using Truncated Equations (CUT-E) method. Notice that fast dynamics in each order of approximation conserves the number of electronic ground state molecules with phonons (due to collective $\sqrt{N}g$ couplings). These fast dynamics are linked by bottlenecks (due to single-molecule g couplings) which slowly change the number of molecules featuring such ground-state phonons. Zeroth-order approximation in g corresponds to restricting the dynamics to states with a fixed number of ground state molecules with phonons, while adding the first-order correction allows the dynamics to create (or annihilate) phonons in (from) 1 additional molecule.

In the limit where $g \to 0$ or $N \to \infty$ (while keeping $\sqrt{N}g$ constant), which is the regime that interests us, the number of ground state molecules that support vibrational excitations is conserved during the dynamics. For our initial state, the zeroth-order approximation implies that the wavefunction is described only by the basis states of the left most block of Figure 3.3. Adding the first-order correction allows states in the immediate next block (featuring only one ground state molecule with phonons) to contribute to the wavefunction. The timescale at which the first-order terms contribute is much longer than the ultrafast vibrational dynamics on each excited molecule. The exact wavefunction is recovered as one spans the entire Hilbert space from left to right in Figure 3.3, but as can be appreciated, there are only a few molecules with phonons in the electronic ground state for large N, even

for long times of interest, justifying the convenience of the shorthand notation in Eq. 3.11.

Although the fact that there is only one molecular specie in the system is central for the permutational symmetries of Eqs. 3.4 and 3.5 to hold, addition of different molecular species can be done without dramatically increasing the computational cost since permutational symmetries still apply for each type. The renormalization of the coefficients associated to each species as in Eq. 3.11 will depend on their concentration. Similarly, disorder due to inhomogeneous broadening or spacial variation of the coupling to the photon mode in multimode cavities, which has been shown to play a central role in molecular polaritonics systems [77,80,151], can be included by adding new molecular species for each value that is sampled according to the corresponding distribution of excitonic frequencies or interaction strength. The number of molecular species (disorder bins N_{bins}) required to simulate a disordered ensemble with frequency width W can be roughly estimated as $N_{bins} \approx W/(2\pi/T)$, where T is the total simulation time that allows to capture the physical phenomena of interest. We believe that this estimate is an upper-bound, as it does not take into account efficient ways to simulate disorder (see for instance, Ref. [78]), but future work will aim to study these subtleties.

3.3.3 Zeroth-Order Approximation

Let us assume that temperature $T = 0$, meaning our initial state in the original notation is given by $A^{(0)}_{111\ldots1}(0) = 1$. The time-dependent wavefunction (see Eq. 3.2) at the zeroth-order approximation is given by the following vibrational wavefunctions

$$\psi^{(0)}(\vec{q},t) = A^{(0)}_{11\cdots1}(t)\prod_{k}^{N}\varphi_1(q_k) \quad \text{and}$$
$$\psi^{(i)}(\vec{q},t) = \sum_{j_i}^{m} A^{(1)}_{j_i1\cdots1}(t)\phi_{j_i}(q_i)\prod_{k\neq i}^{N}\varphi_1(q_k). \tag{3.13}$$

By using the renormalized permutationally-symmetric coefficients, the EoM in Eq. 3.12 transform into those of an *effective* single molecule strongly coupled to the

cavity mode (see Eq. 3.14).

$$i\begin{pmatrix}\dot{\tilde{A}}_0^{(0)}(t)\\ \dot{\tilde{A}}_{10}^{(1)}(t)\\ \dot{\tilde{A}}_{20}^{(1)}(t)\\ \vdots\\ \dot{\tilde{A}}_{m0}^{(1)}(t)\end{pmatrix}=\begin{pmatrix}\omega_c & g\sqrt{N}\langle\varphi_1|\phi_1\rangle & g\sqrt{N}\langle\varphi_1|\phi_2\rangle & \cdots & g\sqrt{N}\langle\varphi_1|\phi_m\rangle\\ g\sqrt{N}\langle\phi_1|\varphi_1\rangle & \omega_{eg,1} & 0 & \cdots & 0\\ g\sqrt{N}\langle\phi_2|\varphi_1\rangle & 0 & \omega_{eg,2} & \cdots & 0\\ \vdots & \vdots & \vdots & \ddots & \vdots\\ g\sqrt{N}\langle\phi_m|\varphi_1\rangle & 0 & 0 & \cdots & \omega_{eg,m}\end{pmatrix}\begin{pmatrix}\tilde{A}_0^{(0)}(t)\\ \tilde{A}_{10}^{(1)}(t)\\ \tilde{A}_{20}^{(1)}(t)\\ \vdots\\ \tilde{A}_{m0}^{(1)}(t)\end{pmatrix} \tag{3.14}$$

Eq. 3.14 is consistent with previous results where an impurity (in this case the optical mode) coupled to a large environment can be simplified into an impurity interacting with an effective harmonic bath that includes the relevant frequencies of the environment [152]; in this case the optical transitions of an individual molecule. Alternatively, it is also consistent with the classical optics treatments of polaritons arising as the result of a photonic oscillator coupling to a set of effective oscillators representing the molecular transitions (e.g., transfer matrix methods) [153, 154]. This has also been justified by Keeling and co-workers within a quantum mechanical framework [145, 146]. We can rewrite Eq. 3.14 in a form that is better suited for implementation in quantum dynamics packages such as the Multiconfiguration Time-Dependent Hartree (MCTDH) method [115, 155, 156],

$$i\begin{pmatrix}\dot{\psi}_{ph}(q,t)\\ \dot{\psi}_{exc}(q,t)\end{pmatrix}=\begin{pmatrix}\mathbb{P}\hat{H}_g\mathbb{P}+\omega_c & g\sqrt{N}\\ g\sqrt{N} & \hat{H}_e\end{pmatrix}\begin{pmatrix}\psi_{ph}(q,t)\\ \psi_{exc}(q,t)\end{pmatrix}, \tag{3.15}$$

with the projector over the ground vibrational state $\mathbb{P}=|\varphi_1\rangle\langle\varphi_1|$ and the photonic and excitonic wavefunctions

$$\psi_{ph}(q,t)=\tilde{A}_0^{(0)}(t)\varphi_1(q),\quad \psi_{exc}(q,t)=\sum_j^m \tilde{A}_{j0}^{(1)}(t)\phi_j(q). \tag{3.16}$$

Here, we readily identify the zeroth-order Hamiltonian in Eq. 3.15 as

$$\begin{aligned}\hat{\tilde{H}}^{(0)}=&\left(\mathbb{P}\hat{H}_g\mathbb{P}+\omega_c\right)|1\rangle\langle 1|+\hat{H}_e|e\rangle\langle e|\\ &+g\sqrt{N}\left(|e\rangle\langle 1|+|1\rangle\langle e|\right),\end{aligned} \tag{3.17}$$

with $\hat{H}_{g/e} = \frac{1}{2\mu}\hat{p}^2 + V_{g/e}(\hat{q})$. Eq. 3.15 can be used to recover the original time-dependent many-body wavefunctions in Eq. 3.13,

$$\psi^{(0)}(\vec{q},t) = \psi_{ph}(q_1,t)\prod_{k=2}^{N}\varphi_1(q_k),$$
$$\psi^{(i)}(\vec{q},t) = \frac{1}{\sqrt{N}}\psi_{exc}(q_i,t)\prod_{k\neq i}^{N}\varphi_1(q_k). \tag{3.18}$$

As far as we are aware, the separation between collective and single-molecule emission processes was first pointed out by Spano when calculating vibrationally-dressed lower polariton states [62], although crucial ideas were introduced by the same author much earlier [137], as we shall discuss later. In a more recently article, the same author combined such ideas with the permutationally symmetric basis to compute photoluminescent spectra starting from approximated vibro-polaritonic eigenstates [63]. Our work formalizes Spano's observations into the hierarchy summarized in Figure 3.3, and capitalizes it to compute dynamics in complex molecular polaritonic systems featuring arbitrary PESs.

Three important comments are in order concerning Eq. 3.17. First, the artificial effective molecule in the ground state is only allowed to be in its ground vibrational state (no phonons). The physical intuition for this is simple: imagine the molecules have been collectively excited at their Franck-Condon (FC) configurations by the cavity field; each of them can in principle re-emit such energy into the cavity creating any vibrational state of their ground electronic state. However, only when they go back to their *vibrational* ground state, the number of ground state molecules with phonons is conserved and the process becomes collective. This seemingly unremarkable observation has an important implication: it states that single-molecule polariton simulations are not applicable to the collective regime unless the light-matter coupling is restricted to the FC region, where the vibrational ground state $\varphi_1(q)$ has significant amplitude (see Figure 3.4). However, as Eq. 3.15 reveals, such simulations can be simply adjusted for the collective regime by the appropriate inclusion of the projector $\mathbb{P}$. This projector can be readily implemented in various ways (e.g., by restricting the vibrational basis in the ground state to $|\varphi_1\rangle$ or by projecting the light-matter coupling, among several options).

Notice that Eq. 3.17 does not formally lead to the definition of polaritonic PESs that govern the nuclear dynamics in the presence of polaritons as in Ref. [33]. However, the key message in the latter work is still consistent with ours: nuclei feel different forces due to collective effects only near the Franck-Condon configuration. Second, since our formalism explicitly considers the vibrational degrees of freedom, the simplification to a single effective molecule does not imply the elimination of the dark state manifold from the Hilbert space, as we will explain in detail in Section 2B.1. Third, the results of this section are exact in the thermodynamic ($N \to \infty$) limit because they imply $g \to 0$. We next add the first-order correction, where the wavefunction now has states with amplitude of the order of g.

3.3.4 First-Order Correction and Beyond

Proceeding analogously, the EoM *up to* first order are given by 3.19, where we considered the case $m = 1$ for illustration purposes.

$$i\begin{pmatrix} \dot{\tilde{A}}_0^{(0)}(t) \\ \dot{\tilde{A}}_{10}^{(1)}(t) \\ \dot{\tilde{A}}_{10}^{(0)}(t) \\ \dot{\tilde{A}}_{11}^{(1)}(t) \end{pmatrix} = \begin{pmatrix} \omega_c & g\sqrt{N}\langle\varphi_1|\phi_1\rangle & 0 & 0 \\ g\sqrt{N}\langle\phi_1|\varphi_1\rangle & \omega_{eg,1} & \boxed{g\langle\phi_1|\varphi_2\rangle} & 0 \\ 0 & \boxed{g\langle\varphi_2|\phi_1\rangle} & \omega_{g,2}+\omega_c & g\sqrt{N-1}\langle\varphi_1|\phi_1\rangle \\ 0 & 0 & g\sqrt{N-1}\langle\phi_1|\varphi_1\rangle & \omega_{g,2}+\omega_{eg,1} \end{pmatrix} \begin{pmatrix} \tilde{A}_0^{(0)}(t) \\ \tilde{A}_{10}^{(1)}(t) \\ \tilde{A}_{10}^{(0)}(t) \\ \tilde{A}_{11}^{(1)}(t) \end{pmatrix} \tag{3.19}$$

The general case can be written in a compact form using projection operators, where $\mathbb{Q}_i = \mathbb{1}_{vib,i} - \mathbb{P}_i$ (see Eq. 3.20). The first 2×2 block corresponds to the zeroth-order approximation and describes the aforementioned effective molecule (say, molecule 1) coupled to the cavity with amplitude $\sqrt{N}g$. The second 2×2 block corresponds to the states where molecule 1 has phonons while another one (say, molecule 2) interacts with the cavity with a slightly weaker coupling strength $\sqrt{N-1}g$. This effective light-matter interaction nonlinearity, which conditions the light-matter interaction of the second molecule on the presence of phonons in the first one, might look odd at first sight, but must be endorsed as the emergent physics resulting from the hierarchy. Eq. 3.20 is in a suitable form for implemen-

tation in wavepacket dynamics methods.

$$i \begin{pmatrix} \dot{\psi}^{(0)}_{ph}(q_1,q_2) \\ \dot{\psi}^{(0)}_{exc}(q_1,q_2) \\ \dot{\psi}^{(1)}_{ph}(q_1,q_2) \\ \dot{\psi}^{(1)}_{exc}(q_1,q_2) \end{pmatrix} = \hat{\boldsymbol{H}}^{(\mathbf{1})} \begin{pmatrix} \psi^{(0)}_{ph}(q_1,q_2) \\ \psi^{(0)}_{exc}(q_1,q_2) \\ \psi^{(1)}_{ph}(q_1,q_2) \\ \psi^{(1)}_{exc}(q_1,q_2) \end{pmatrix} \tag{3.20}$$

$$\hat{\boldsymbol{H}}^{(\mathbf{1})} = \begin{pmatrix} \mathbb{P}_1\hat{H}_{g,1}\mathbb{P}_1 + \mathbb{P}_2\hat{H}_{g,2}\mathbb{P}_2 + \omega_c & g\sqrt{N} & 0 & 0 \\ g\sqrt{N} & \hat{H}_{e,1} + \mathbb{P}_2\hat{H}_{g,2}\mathbb{P}_2 & \boxed{g} & 0 \\ 0 & \boxed{g} & \mathbb{Q}_1\hat{H}_{g,1}\mathbb{Q}_1 + \mathbb{P}_2\hat{H}_{g,2}\mathbb{P}_2 + \omega_c & g\sqrt{N-1} \\ 0 & 0 & g\sqrt{N-1} & \mathbb{Q}_1\hat{H}_{g,1}\mathbb{Q}_1 + \hat{H}_{e,2} \end{pmatrix}. \tag{3.21}$$

Notice that ignoring the matrix elements proportional to g (boxed) amounts to block-diagonalizing the Hamiltonian according to the number of electronic ground state molecules with phonons, reiterating the approximate symmetry featured in Figure 3.3. Eq. 3.20 can be interpreted as two effective molecules coupled to the cavity. Finally, the original many-body wavefunction in Eq. 3.3 can be rewritten in terms of the 2-molecule wavepackets as

$$\begin{aligned} \psi^{(0)}(\vec{q},t) &= \psi^{(0)}_{ph}(q_1,q_2,t)\prod_{k=3}^{N}\varphi_1(q_k) + \sum_{i}^{N}\frac{\psi^{(1)}_{ph}(q_i,q_{i'\neq i},t)}{\sqrt{N}}\prod_{k\neq i,i'}^{N}\varphi_1(q_k), \\ \psi^{(i)}(\vec{q},t) &= \frac{\psi^{(0)}_{exc}(q_i,q_{i'\neq i},t)}{\sqrt{N}}\prod_{k\neq i,i'}^{N}\varphi_1(q_k) + \sum_{j\neq i}^{N}\frac{\psi^{(1)}_{exc}(q_{j\neq i},q_i,t)}{\sqrt{N(N-1)}}\prod_{k\neq i,j}^{N}\varphi_1(q_k), \end{aligned} \tag{3.22}$$

with i' is an arbitrary molecule of the ensemble and

$$\begin{aligned} \psi^{(0)}_{ph}(q_1,q_2,t) &= \tilde{A}^{(0)}_0(t)\varphi_1(q_1)\varphi_1(q_2), \\ \psi^{(1)}_{ph}(q_1,q_2,t) &= \sum_{k>1}^{m}\tilde{A}^{(0)}_k(t)\varphi_k(q_1)\varphi_1(q_2), \\ \psi^{(0)}_{exc}(q_1,q_2,t) &= \sum_{l}^{m}\tilde{A}^{(1)}_{l0}(t)\phi_l(q_1)\varphi_1(q_2), \\ \psi^{(1)}_{exc}(q_1,q_2,t) &= \sum_{l,k>1}^{m}\tilde{A}^{(1)}_{lk}(t)\phi_l(q_2)\varphi_k(q_1). \end{aligned} \tag{3.23}$$

We make use of this Hamiltonian in Section 3.3.6 and show that adding the first-order correction describes collective processes, in addition to those whose rates

scale as $1/N$. Similarly, corrections of kth order require using a Hamiltonian of $k+1$ effective molecules interacting with a cavity mode, and would include information about phenomena with rates that scale up to $1/N^k$. Such decomposition of the many-molecules problem into a few-molecules problem is what we call Collective dynamics Using Truncated Equations (CUT-E) method.

Let us summarize the central results of the article. Application of the permutational symmetries in Eqs. 3.4 and 3.5 to the Time-Dependent Schrödinger Equation for N identical molecules in a cavity gives rise to the EoM in Eq. 3.12. These EoM are endowed with a convenient hierarchy of timescale separations, schematically illustrated by the scissors in Figure 3.3. For a fixed collective coupling $\sqrt{N}g$, processes with N-independent ($\mathcal{O}(N^{-1})$) rates are captured by a single (two) effective molecule(s) in a cavity, according to Eq. 3.15 (Eq. 3.20). This is schematically represented in Figure 3.1b. Although high order corrections might become relevant when a small number of molecules is considered, here we are interested in the case where a large number of molecules is used to reach collective strong light-matter coupling. Thus, we will defer the exploration of corrections beyond first order for future works.

3.3.5 Observables in the zeroth-order approximation

Observables of the real system must be calculated using the many-body wavefunction $|\Psi(t)\rangle$ and not directly using the effective single-molecule wavefunction $|\tilde{\Psi}(t)\rangle$. However, there are particular observables for which both wavefunctions provide the same answer. This will depend on whether the observable is local or collective. For pedagogical purposes, throughout this section, we assume the zeroth-order approximation.

Local Properties

Hereafter, we define local properties to be quantities that only depend on one single molecule (e.g. a chemical reaction) or the photon field alone.

Chemical Properties: Consider a local observable $\hat{\Omega}^{(i)}$ that depends only on degrees of freedom of molecule i. As an example, assume we are interested in

the nuclear dynamics in the excited state $\hat{\Omega}^{(i)} = \hat{q}_i|e_i\rangle\langle e_i|$. Using the zeroth-order wavefunction in Eq. 3.13 we obtain

$$\langle\Psi(t)|\hat{q}_i|e_i\rangle\langle e_i|\Psi(t)\rangle = \frac{1}{N}\langle\tilde{\Psi}(t)|\hat{q}|e\rangle\langle e|\tilde{\Psi}(t)\rangle. \tag{3.24}$$

This is a remarkable result because it demonstrates that the excited-state dynamics of N molecules collectively coupled to a cavity mode (described by $|\Psi(t)\rangle$) is identical to the dynamics of an effective single molecule strongly coupled to a cavity (described by $|\tilde{\Psi}(t)\rangle$), except for a constant $1/N$ dilution factor. This factor is just a consequence of using a single photon to alter the excited-state dynamics of N molecules. The probability of *any* molecule being at the configuration q is the same as that of the single effective molecule strongly coupled to the cavity. However, we emphasize that the effective molecule is not allowed to have phonons while it is in the ground state, a restriction which can introduce significant differences compared to standard single-molecule calculations.

An important corollary of the above analysis is that effects predicted using single-molecule models might actually occur in the collective regime if they rely on changes in the excited PES at the FC region, but not the ones relying on changes beyond. This was first pointed out by Galego and coworkers [33] by analyzing polaritonic PESs for an ensemble of molecules interacting with a cavity mode. This is also consistent with a recent work by Cui and Nitzan [157], who concluded that excited-state dynamics in polaritonic systems is dominated by states that are reachable from the ground electronic state. Yet, we propose that modifications of chemical dynamics that occur on a timescale longer than the decay of the initially prepared excitations can occur in an N-independent manner if they dramatically depend on the ultrafast polariton-modified dynamics at the FC region. In Section 3.3.8 we present such an example.

Optical properties: Another set of properties that are equivalent in the single molecule and $N \to \infty$ cases are those that can be extracted only from the dynamics of the field. For example, the linear transmission, absorption and reflection spectra can be calculated from the photon autocorrelation function $c(t)$. In the zeroth-order approximation, it can be shown that $c(t) = \langle\Psi(0)|\Psi(t)\rangle =$

$\langle\tilde{\Psi}(0)|\tilde{\Psi}(t)\rangle$, where $|\tilde{\Psi}(0)\rangle = \varphi_0(q)|1\rangle$ is the photonic state. This is consistent with previous work by the Keeling group [145, 146].

Non-Local Properties

Another set of observables consists of operators that are delocalized across several molecules or depend on both molecular and optical degrees of freedom. Some of the most common observables of this kind are the populations of the polariton and dark-states. Such observables can be obtained with the effective single-molecule model but not from its reduced electronic-photonic density matrix, as we will show next.

Polariton and Dark-States Populations: Let us write the expectation value of an arbitrary electronic-photonic operator $\langle\hat{\Omega}\rangle = \mathrm{Tr}\left[\hat{\rho}\hat{\Omega}\right]$ in terms of the reduced density matrix of the effective single-molecule system $\hat{\tilde{\rho}}$,

$$\begin{aligned}\langle\hat{\Omega}\rangle = \mathrm{Tr}\left[\hat{\rho}\hat{\Omega}\right] = \sum_{ij}\rho_{ij}\Omega_{ji} = \tilde{\rho}_{11}\Omega_{11} + \tilde{\rho}_{1e}\sum_{i=1}^{N}\frac{1}{\sqrt{N}}\Omega_{1e_i} \\ + \tilde{\rho}_{e1}\sum_{i=1}^{N}\frac{1}{\sqrt{N}}\Omega_{e_i1} + \tilde{\rho}_{ee}\frac{1}{N}\sum_{i=1}^{N}\Omega_{e_ie_i} \\ + \frac{1}{N}\langle\tilde{\Psi}(t)|\tilde{\Psi}_{FC}\rangle\langle\tilde{\Psi}_{FC}|\tilde{\Psi}(t)\rangle\left(\sum_{i,i'\neq i}\Omega_{e_ie_{i'}}\right),\end{aligned} \tag{3.25}$$

where we have identified $|\tilde{\Psi}_{FC}\rangle = \varphi_1(q)|e\rangle$ as the FC wavepacket. The above equation implies that the reduced density matrix $\tilde{\rho}$ of the effective single molecule is, in general, not enough to calculate any delocalized molecular observables since the last term of Eq. 3.25 refers to the projection of the wavefunction onto the FC wavepacket, which corresponds to the inter-exciton coherences:

$$\langle e_i|\hat{\rho}(t)|e_{i'}\rangle = \frac{1}{N}\langle\tilde{\Psi}(t)|\tilde{\Psi}_{FC}\rangle\langle\tilde{\Psi}_{FC}|\tilde{\Psi}(t)\rangle. \tag{3.26}$$

An example, let $\hat{\Omega} = |P\rangle\langle P|$, with $|P\rangle = c_0|1\rangle + c_1|B\rangle$ (where $|B\rangle = \frac{1}{\sqrt{N}}\sum_{i=1}^{N}|e_i\rangle$ is the totally-symmetric excitonic state) being one of the polariton states. Using Eq. 3.25, population of this state is calculated to be

$$\begin{aligned}\langle\Psi(t)|P\rangle\langle P|\Psi(t)\rangle \approx |c_0|^2\tilde{\rho}_{11}(t) + c_0^*c_1\tilde{\rho}_{1e} + c_1^*c_0\tilde{\rho}_{e1} \\ + |c_1|^2\langle\tilde{\Psi}(t)|\tilde{\Psi}_{FC}\rangle\langle\tilde{\Psi}_{FC}|\tilde{\Psi}(t)\rangle.\end{aligned} \tag{3.27}$$

Similarly, dark states can be written as $|D\rangle = \sum_i c_i|e_i\rangle$, with $|c_1| = |c_2| = \cdots = |c_N| = 1/\sqrt{N}$, $\sum_{i=1}^{N} c_i = 0$, and $\Omega_{e_i e_j} = \langle e_i|D\rangle\langle D|e_j\rangle = c_i c_j^*$ (i.e., they are chosen orthogonal to the $|P\rangle$ states, so here we take them to be the Fourier combinations of excitons that are orthogonal to $|B\rangle$; see for instance [27]). This leads to

$$\langle\Psi(t)|D\rangle\langle D|\Psi(t)\rangle = \frac{1}{N}\langle\tilde{\Psi}(t)|e\rangle\mathbb{Q}\langle e|\tilde{\Psi}(t)\rangle. \tag{3.28}$$

Notice that this calculation is identical for every dark state in the chosen basis, therefore the population in the dark-state manifold yields

$$\begin{aligned}\sum_{k}^{N-1}\langle|D\rangle\langle D|\rangle \approx 1 &- \langle\tilde{\Psi}(t)|1\rangle\langle 1|\tilde{\Psi}(t)\rangle \\ &- \langle\tilde{\Psi}(t)|\tilde{\Psi}_{FC}\rangle\langle\tilde{\Psi}_{FC}|\tilde{\Psi}(t)\rangle,\end{aligned} \tag{3.29}$$

where we have made $\frac{N-1}{N} \approx 1$ since the zeroth-order approximation becomes exact for $N \to \infty$. From this result, we can extract the intuitive interpretation that the bright state $|B\rangle$ in the N-molecule system corresponds to a FC wavepacket in the excited state of the effective single molecule, while the dark states correspond to the rest of the wavefunction whose nuclear configurations lie outside of the FC region (See Figure 3.4).

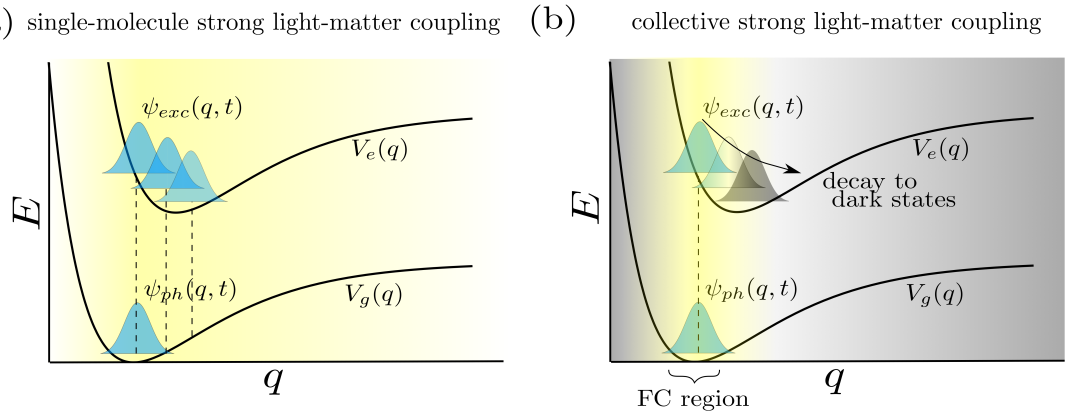

Figure 3.4: (a) For a cavity containing a single molecule, light-matter coupling (denoted in yellow) has the ability to modify nuclear dynamics throughout all configurations q. (b) This situation contrasts with a cavity containing an infinite number of molecules (zeroth-order approximation), where collective light-matter coupling is localized at the Franck Condon (FC) region. Nuclear displacement away from this region is equivalent to decay of polaritons into dark states.

For cases where the chemically relevant excited-state dynamics involves fast changes of the nuclear configurations away from the FC point, excited state reactivity is essentially relaxation to dark-states. The question is whether the relaxation occurs along the reactive coordinate of interest (e.g., particular reactive dark-modes), or whether it occurs along orthogonal modes to it. Thus, we have derived a powerful design principle for polariton chemistry which has so far unjustifiably gathered little attention: the strategy is not to avoid decay into dark states, which seems inexorable in most cases, but to use SC to control which dark states to target. In fact, using the zeroth-order approximation, we will illustrate some mechanisms to manipulate ratios for these relaxation pathways in Section 3.3.8.

3.3.6 Polariton Vibrational Relaxation

Previous work by del Pino and coworkers [158] addressed the relaxation dynamics of molecular polaritons using the Hamiltonian in Eq. 3.1 for a vibrational harmonic bath and linear vibronic coupling,

$$\begin{aligned}\hat{H}_m^{(i)} = &\sum_k \omega_{\nu,k} \hat{b}_k^{(i)\dagger} \hat{b}_k^{(i)} \\ &+ \left[\omega_{eg,1} + \sum_k \omega_{\nu,k} \sqrt{s_k} (\hat{b}_k^{(i)\dagger} + \hat{b}_k^{(i)}) \right] |e_i\rangle\langle e_i|. \end{aligned} \tag{3.30}$$

This model of relaxation is the single-photon mode simplification of a previous model by Litinskaya and Agranovich [159]. In the limit where vibronic coupling is much smaller than the collective light-matter coupling and there is an energy-dense set of vibrational modes k, we can use our formalism to analytically derive relaxation rates by including a collection of local vibrational modes and using Fermi's Golden Rule with the vibronic couplings as the perturbation. Although such a result is already well known, it serves as a benchmark and illustration for our formalism. To unclutter the calculations we consider the case where the excitons and the cavity are in resonance ($\omega_c = \omega_{eg,1} = \omega$).

Zeroth-Order Approximation: N-Independent Effects: Using Eqs. 3.17 and 3.30, the model of relaxation in the zeroth-order approximation is given

by the unperturbed and vibronic coupling Hamiltonians

$$\hat{\tilde{H}}^{(0)} = \hat{\tilde{H}}_0^{(0)} + \hat{\tilde{H}}_I^{(0)},$$

$$\begin{aligned}\hat{\tilde{H}}_0^{(0)} &= \omega|1,0\rangle\langle 1,0| + \left(\omega + \sum_k \omega_{\nu,k}\hat{b}_k^\dagger \hat{b}_k\right)|e\rangle\langle e| \\ &+ \sqrt{N}g\left(|e,0\rangle\langle 1,0| + |1,0\rangle\langle e,0|\right), \\ \hat{\tilde{H}}_1^{(0)} &= \sum_k \omega_{\nu,k}\sqrt{s_k}\left(\hat{b}_k^\dagger + \hat{b}_k\right)|e\rangle\langle e|, \end{aligned} \tag{3.31}$$

where we have used the Fock basis for the vibrational bath (the second index "0" means all vibrational modes k are empty). The eigenstates of $\hat{\tilde{H}}_0^{(0)}$ are trivial,

$$\begin{aligned}|\pm,0\rangle &= \frac{1}{\sqrt{2}}\left(|e,0\rangle \pm |1,0\rangle\right) \\ |D,m\rangle &= |e,m>0\rangle, \end{aligned} \tag{3.32}$$

where $m > 0$ denotes that at least one mode of the vibrational bath is not in the vacuum state. The eigenvalues are given by $\omega_{\pm,0} = \omega \pm g$ and $\omega_{D,m} = \omega + \sum_k \omega_{\nu,k} m_k$ respectively. Using Fermi's Golden Rule we can obtain the following relaxation rates:

$$\begin{aligned}\Gamma_{D\leftarrow +} &= 2\pi \sum_m |\langle D,m|\hat{\tilde{H}}_1^{(0)}|+,0\rangle|^2 \delta(\omega_{D,m} - \omega_{+,0}) \\ &= \frac{2\pi}{2}\sum_k \omega_{\nu,k}^2 s_k \delta(g - \omega_{\nu,k}), \end{aligned} \tag{3.33}$$

$$\Gamma_{-\leftarrow +} = 2\pi|\langle -,0|\hat{\tilde{H}}^{(1)}|+,0\rangle|^2\delta(2g) = 0, \tag{3.34}$$

$$\Gamma_{-\leftarrow D} = 2\pi|\langle -,0|\hat{\tilde{H}}^{(1)}|e,m\rangle|^2\delta(2g - \sum_k \omega_{\nu,k}m_k) = 0, \tag{3.35}$$

where the last two rates are equal to 0 because the resonance condition is not fulfilled. A schematic representation of the relaxation dynamics is shown in Figure 3.5.

First-Order Correction: $1/N$ Effects: By analogy with the previous section, we describe the vibrations using the eigenbasis of the electronic ground-state vibrational Hamiltonians for the two molecules. Here we first rewrite Eq. 3.19 in terms of projection operators. The second label corresponds to the number of ground state molecules with phonons.

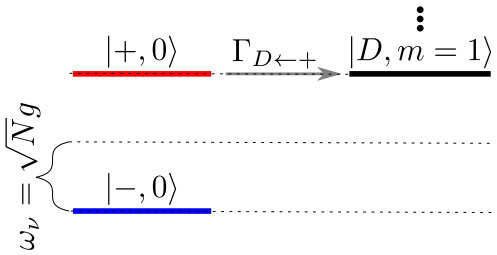

Figure 3.5: Relaxation from the upper polariton to the dark states as described by the zeroth-order approximation (blue: lower polariton, red: upper polariton, black: dark states). States $|+,0\rangle$ and $|D,m=1\rangle$ are resonantly coupled through vibronic coupling. $m=1$ means there is 1 phonon in one of the bath modes of the excited effective molecule.

$$\begin{aligned}\hat{\tilde{H}}^{(1)} = &\left(\mathbb{P}_1\hat{H}_{g,1}\mathbb{P}_1 + \mathbb{P}_2\hat{H}_{g,2}\mathbb{P}_2 + \omega_c\right)|1,0\rangle\langle 1,0| + \left(\hat{H}_{e,1} + \mathbb{P}_2\hat{H}_{g,2}\mathbb{P}_2\right)|e,0\rangle\langle e,0| \\ &+ \left(\mathbb{Q}_1\hat{H}_{g,1}\mathbb{Q}_1 + \mathbb{P}_2\hat{H}_{g,2}\mathbb{P}_2 + \omega_c\right)|1,1\rangle\langle 1,1| + \left(\mathbb{Q}_1\hat{H}_{g,1}\mathbb{Q}_1 + \hat{H}_{e,2}\right)|e,1\rangle\langle e,1| \\ &+ g\sqrt{N}\left(|e,0\rangle\langle 1,0| + |1,0\rangle\langle e,0|\right) + g\sqrt{N-1}\left(|e,1\rangle\langle 1,1| + |1,1\rangle\langle e,1|\right) \\ &+ g\left(|e,0\rangle\langle 1,1| + |1,1\rangle\langle e,0|\right). \end{aligned} \tag{3.36}$$

Using Eqs. 3.36, the relaxation model is described by the Hamiltonians in Eqs. 3.37.

$$
\begin{aligned}
\hat{\tilde{H}}^{(1)} &= \hat{\tilde{H}}_0^{(1)} + \hat{\tilde{H}}_1^{(1)}, \\
\hat{\tilde{H}}_0^{(1)} &= \omega|1,0,0,0\rangle\langle 1,0,0,0| + \sum_m \left(\omega + \sum_k \omega_{\nu,k} m_k\right) |e,0,m,0\rangle\langle e,0,m,0| \\
&+ \sum_{m>0} \left(\omega + \sum_k \omega_{\nu,k} m_k\right) |1,1,m,0\rangle\langle 1,1,m,0| \\
&+ \sum_{m>0,n} \left(\omega + \sum_k \omega_{\nu,k} m_k + \sum_k \omega_{\nu,k} n_k\right) |e,1,m,n\rangle\langle e,1,m,n| \\
&+ g\sqrt{N}\left(|1,0,0,0\rangle\langle e,0,0,0| + |e,0,0,0\rangle\langle 1,0,0,0|\right) \\
&+ g\sqrt{N-1}\sum_{m>0}\left(|1,1,m,0\rangle\langle e,1,m,0| + |e,1,m,0\rangle\langle 1,1,m,0|\right) \\
&+ g\sum_{m>0}\left(|e,0,m,0\rangle\langle 1,1,m,0| + |1,1,m,0\rangle\langle e,0,m,0|\right), \\
\hat{\tilde{H}}_1^{(1)} &= \sum_k \omega_{\nu,k}\sqrt{s_k}\left(\hat{b}_{1,k}^\dagger + \hat{b}_{1,k}\right)|e,0\rangle\langle e,0| + \sum_k \omega_{\nu,k}\sqrt{s_k}\left(\hat{b}_{2,k}^\dagger + \hat{b}_{2,k}\right)|e,1\rangle\langle e,1|.
\end{aligned}
\tag{3.37}
$$

The last two labels represent the vibrational states of molecules 1 and 2 in the Fock basis, $\hat{b}_{i,k}$ is the annihilation operator for the vibrational excitations of molecule i, and $m > 0$ means $m_k > 0$ for at least one mode k. The eigenstates of $\hat{\tilde{H}}_0^{(1)}$ are given by

$$
\begin{aligned}
|\pm,0,0\rangle &= \frac{1}{\sqrt{2}}\left(|1,0,0,0\rangle \pm |e,0,0,0\rangle\right), \\
|\pm,m>0,0\rangle &= \frac{1}{\sqrt{2}}|1,1,m>0,0\rangle \\
&\pm \frac{1}{\sqrt{2}}\left(\sqrt{\frac{N-1}{N}}|e,1,m>0,0\rangle + \frac{1}{\sqrt{N}}|e,0,m>0,0\rangle\right), \\
|D,m>0,0\rangle &= \frac{1}{\sqrt{N}}|e,1,m>0,0\rangle + \sqrt{\frac{N-1}{N}}|e,0,m>0,0\rangle, \\
|D,m>0,n\rangle &= |e,1,m>0,n>0\rangle,
\end{aligned}
$$

with eigenvalues $\omega_{\pm,0,0} = \omega \pm g\sqrt{N}$, $\omega_{\pm,m,0} = \omega + \sum_k \omega_{\nu,k} n_k \pm g\sqrt{N}$, and $\omega_{D,m,n} = \omega + \sum_k \omega_{\nu,k} m_k + \sum_k \omega_{\nu,k} n_k$ respectively. We can use these states to calculate the rate from the upper polariton to the lower polariton using Fermi's Golden Rule to get

$$\Gamma_{-\leftarrow+} = 2\pi \sum_m |\langle -,0,0|\hat{\tilde{H}}_1^{(1)}|+,0,0\rangle|^2 \delta\left(\omega_{-,0,0} - \omega_{+,0,0}\right)$$
$$= \frac{2\pi}{4N} \sum_k \omega_{\nu,k}^2 s_k \delta(2\sqrt{N}g - \omega_{\nu,k}). \tag{3.38}$$

Similarly, we can recalculate the decay rate from the upper polariton into the dark states,

$$\Gamma_{D\leftarrow+} = 2\pi \sum_m |\langle D,m,0|\hat{\tilde{H}}_1^{(1)}|+,0,0\rangle|^2 \delta(\omega_{+,0,0} - \omega_{D,m,0})$$
$$= \left(\frac{N-1}{N}\right) \pi \sum_k \omega_{\nu,k}^2 s_k \delta(\sqrt{N}g - \omega_{\nu,k}). \tag{3.39}$$

where we have recovered the $\frac{N-1}{N}$ factor missing from Eq. 3.33 in the zero-order approximation. The final state in the previous calculation can be used as initial state to describe the subsequent relaxation from the dark-states into the lower polariton,

$$\Gamma_{-\leftarrow D} = 2\pi \sum_{m'} |\langle -,m',0|\hat{\tilde{H}}_1^{(1)}|-,0,0\rangle|^2 \delta(\omega_{-,0,0} - \omega_{D,m=1,0})$$
$$= \left(\frac{N-1}{N^2}\right) \pi \sum_k \omega_{\nu,k}^2 s_k \delta(\sqrt{N}g - \omega_{\nu,k}). \tag{3.40}$$

The schematic representation of relaxation mechanisms is shown in Figs. 3.6 and 3.7.

The results of vibrational relaxation rates are summarized in Table 3.1.

Table 3.1: Polariton relaxation rates in the zeroth-order approximation and adding the first-order correction

	zeroth-order approximation	with first-order correction
$\Gamma_{-\leftarrow+}$	0	$\left(\frac{1}{4N}\right) 2\pi \sum_k \omega_{\nu,k}^2 s_k \delta(2\sqrt{N}g - \omega_{\nu,k})$
$\Gamma_{D\leftarrow+}$	$\pi \sum_k \omega_{\nu,k}^2 s_k \delta(\sqrt{N}g - \omega_{\nu,k})$	$\left(\frac{N-1}{N}\right) \pi \sum_k \omega_{\nu,k}^2 s_k \delta(\sqrt{N}g - \omega_{\nu,k})$
$\Gamma_{-\leftarrow D}$	0	$\left(\frac{N-1}{N^2}\right) \pi \sum_k \omega_{\nu,k}^2 s_k \delta(\sqrt{N}g - \omega_{\nu,k})$

Apart from missing a factor of $\frac{N-1}{N}$ in $\Gamma_{D\leftarrow+}$, the zeroth-order approximation correctly predicts the relaxation rate from upper polariton to dark states (which in this weak-vibronic coupling model in the effective single-molecule calculation, corresponds to the bare molecular exciton with a single phonon $|e,1\rangle$), but

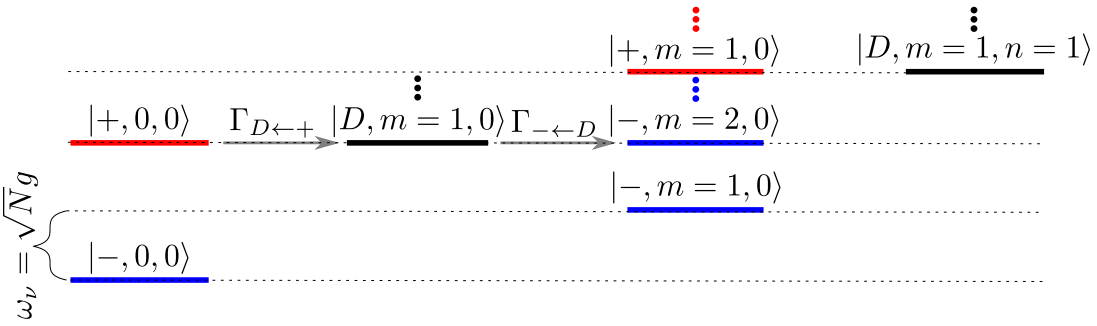

Figure 3.6: Relaxation from the upper polariton to the lower polariton passing through the dark states, as described by inclusion of the first-order correction (blue: lower polariton, red: upper polariton, black: dark states). States $|+, 0, 0\rangle$, $|D, m = 1, 0\rangle$, and $|-, m = 2, 0\rangle$ are resonantly coupled through vibronic coupling. $m = 2$ means there are 2 phonons of frequency $\omega_\nu = \sqrt{N}g$ in the bath modes of the effective molecule 1. In the derivation, we have assumed the second phonon is emitted into a different bath mode than the first one.

disregards both the upper to lower polariton, and dark state to lower polariton rates [158]. This makes sense since the latter two are known to be proportional to $1/N$, and the zeroth-order approximation is exact for $N \to \infty$. Thus, for this simple model, the only relaxation process of relevance at ultrafast timescales is the downhill one *into* dark states. Addition of the first-order correction recovers the decay rates $\Gamma_{-\leftarrow-}$ and $\Gamma_{-\leftarrow D}$, as well as the $\frac{N-1}{N}$ factor missing from $\Gamma_{D\leftarrow+}$ in the zero-order approximation. We suspect the factor $\frac{N-1}{N^2}$ in $\Gamma_{-\leftarrow D}$ will become exactly $1/N$ if the second-order correction is considered. It is unlikely that we would need to go to higher-order corrections for microcavity polaritons, or even for polaritons arising in plasmonic antennas, where $N = 100 - 1000$ [160], although if SC can be demonstrated with smaller N values, those corrections could start mattering. On the other hand, it would be of interest to compare the performance of our method with the standard one of explicitly simulating several molecules using an optimized algorithm such as multilayer MCTDH [68], and characterize the values of N after which our method can outcompete the latter.

3.3.7 Finite Temperature effects

In the previous sections we have only dealt with transitions from higher to lower lying polaritonic or dark states. To calculate rates such as $\Gamma_{D\leftarrow-}$ we need

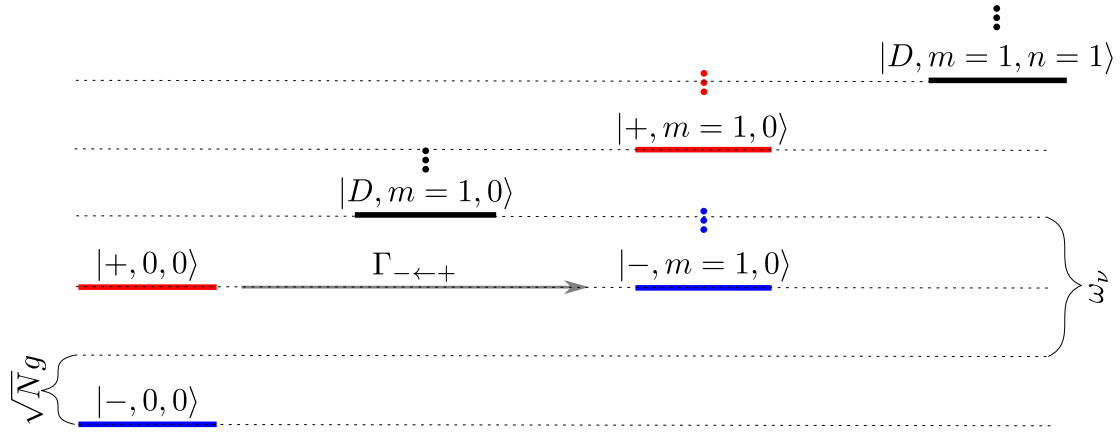

Figure 3.7: Direct relaxation from the upper polariton to the lower polariton as described until the first-order correction (blue: lower polariton, red: upper polariton, black: dark states). States $|+, 0, 0\rangle$ and $|-, m = 1, 0\rangle$ are resonantly coupled through vibronic coupling to modes of frequency $\omega_\nu = 2\sqrt{N}g$.

to consider all possible initial states allowed by thermal fluctuations. In general, such states involve breaking of the symmetry that is essential for the reduction of the dimensionality in Eqs. 3.10. Therefore, at the current stage, this formalism cannot be easily generalized to finite temperatures. Future works will focus on developing a density matrix approach in which permutational symmetries can be smoothly applied.

3.3.8 Non-statistical Excited-State Dynamics

In this section, we look at the mechanism whereby, given two molecular species strongly coupled to a cavity, excitation energy can be selectively funneled to one of the species. We will show that statistical yield estimates based on linear optical spectroscopy seem to be misleading at predicting these outcomes accurately.

For a system with N_A molecules of species A and N_B molecules of species B inside a cavity, The Hamiltonian in the zeroth-order approximation can be readily generalized from Eq. 3.14 to include two types of molecules A and B (see Supplementary Information in Ref. [87] for the Hamiltonian and parameters of the PESs of each molecule).

Example 1.- The excited PES of species A is a displaced harmonic oscillator

and that of species B is a dissociative potential. While the latter is mostly relevant for gas phase reactions, a completely analogous photochemical phenomenon in the condensed phases could be obtained with diabatically coupled harmonic surfaces. The cavity frequency is resonant with the FC transitions of both A and B (see Figure 3.8,1a).

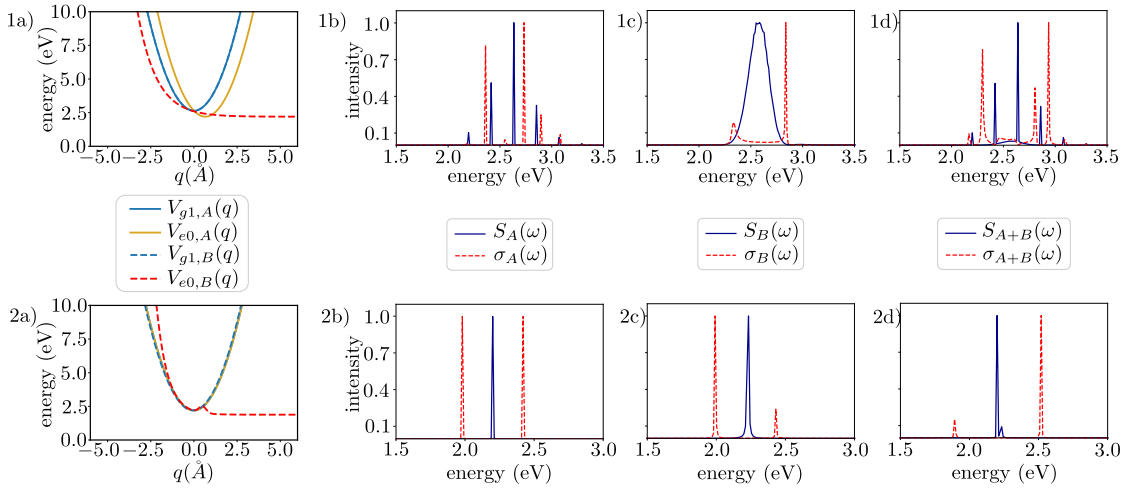

Figure 3.8: Summary of molecular features used in Section 3.3.8, Examples 1 and 2. The relevant Potential Energy Surfaces (PESs) (1a,2a); horizontal axis should read $q = q_i$, depending on whether the PES refers to $i = A$ or B. Linear absorption spectra outside (blue, $S(\omega)$) and inside (red, $\sigma(\omega)$) of cavity, corresponding to a (1b,2b) pure A, (1c,2c) pure B, and (1d,2d) A/B mixture at $1:1$ ratio. In both examples, A has a bound excited PES, while B has a dissociative one. This has an obvious effect in the outside-of-cavity absorption for Example 1 (1b,1c) but not for Example 2 (2b,2c). The underlying reason for this discrepancy is that the dissociative character of B is manifestly at the FC region in Example 1 (1a), while it is "hidden" from the FC region in Example 2 (2a).

Given the one-dimensional nature of the PESs, it is straightforward to explicitly construct the eigenstates and eigenenergies of the vibrational Hamiltonians and perform the short-time unitary dynamics; we use the standard Discrete Variable Representation method by Colbert and Miller [161]. This calculation was then used to compute spectra of the molecules outside and in the cavity using the formalism illustrated in [136, 145]. The parameters for calculation of the spectra are chosen such that the frequency resolution and total simulation time satisfy Fourier transform relations. The total simulation time of 2.5 ps determines the molecular and cavity linewidths as 0.002 eV (see Figure 3.8, 1b,c,d). The absorption spectra

of the bare molecules reveal the energy level structure accessed at the respective FC regions [162]. For molecules A, we see the strongest peak corresponding to the FC transition accompanied by the other peaks of the vibronic progression. On the other hand, for molecules B, we see a single broad feature due to the dissociative potential. When strongly coupled to a cavity, these peaks form a rich pattern of peak splittings which can be intuitively understood upon diagonalization of Eq. 3.14 (for instance, for molecule A, six sharp resonances become seven due to coupling to the cavity).

We build time-dependent wavefunctions by constructing the corresponding linear combinations of numerically computed eigenstates of the zeroth-order Hamiltonian. This procedure would obviously be impractical for realistic molecular species with many vibrational modes, in which case, an explicit time-dependent approach such as MCTDH would be preferred. This simulation illustrates a phenomenon where the energy initially given to the cavity is eventually channeled preferentially to one of the two molecules. The results of this simulation are consistent with the phenomenology originally theoretically proposed by Groenhof and Toppari, based on computational simulations with at most 1000 molecules of one of the species [163], and demonstrate the latter remains valid in the thermodynamic limit. For our simulation, we start with an excitation in the cavity, $|\Psi(0)\rangle = \varphi_1(q_A)\varphi_1(q_B)|1\rangle$, and calculate excited state populations for each of the effective molecules, which provides the excited state reactivity of a single molecule of type A/B in the entire molecular ensemble (because we are working in the first excitation manifold). At short times the cavity evenly distributes the energy into both types of molecules, exciting them at their respective FC regions. We monitor the excited-state populations as a function of time (see Figure 3.9a). We observe that at short times, the population is transferred equally to both species. However, as time progresses, the excitation is funneled selectively to species B via the cavity. The mechanism of the phenomenon is the following: at short times of the order of the Rabi oscillations, the cavity excites the bright modes of both species with equal populations at the respective FC regions due to the chosen equal collective light-matter couplings. However, as time progresses, excitations in species B decay

irreversibly into their dark states upon evolution away from the FC region (see Eq. 3.29) due to the dissociative character of $V_{e0,B}(q_B)$. Molecular species A does not undergo this fast dephasing due to the bound nature of $V_{e0,A}(q_A)$ and is the one that predominantly remains at its FC region and emits a photon to the cavity at the end of the Rabi cycle. The mechanism restarts with the re-excitation of both molecules by the photon. What results from this simulation is a net energy flow from molecular species A to species B mediated by the cavity, and which cannot be explained by the contribution of each molecule to the polariton states defined at the FC region. Notice that if the cavity decay is faster than the molecular dephasing, the excitation can leak out before energy transfer from A to B ensues. This issue can be overcome by having the cavity mode under continuous pumping.

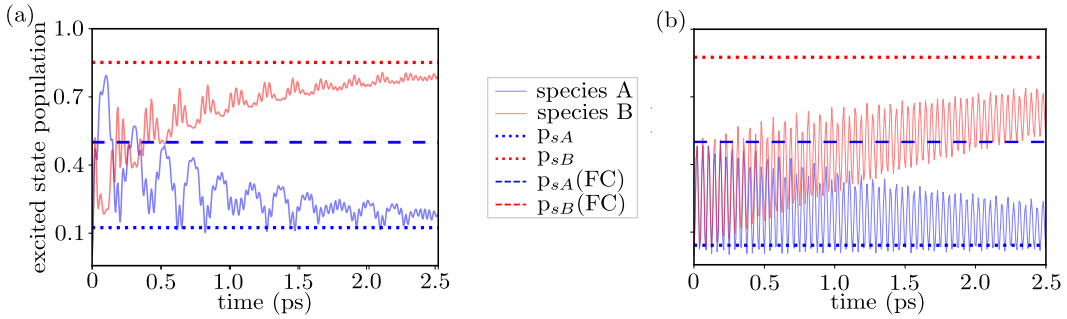

Figure 3.9: Excited state populations of molecular species A and B as a function of time for (a) Example 1 and (b) Example 2. Dotted (dashed) horizontal lines show the estimated populations p_{s_A}, p_{s_B} (p_{s_A}(FC),p_{s_B}(FC)) from the eigenstates ("short-time eigenstates" defined at the FC point). Energy funneling from species A into species B is observed in both cases, indicating that this phenomenon is not easily predicted from linear optical spectra alone, since at least for Example 2, the absorption spectra of bare molecules A and B are pretty much identical (see Figure 3.8, 2b,c).

Next, we compare the computed long-time populations accumulated in the excited states of molecules A and B to the infinite-time probabilities of molecules of the cavity exciting the different species (p_{s_j} for $j \in \{A, B\}$),

$$p_{s_j} = \sum_n |\langle n|e_j\rangle|^2 |\langle n|1\rangle|^2. \tag{3.41}$$

Here, $\{|n\rangle\}$ represent the eigenstates of $\hat{\tilde{H}}^{(0)}$. Eq. 3.41 computes the composition of probabilities of an eigenstate simultaneously having photonic and molecule

A(B) contribution. However, the entire set of eigenstates is not obtainable using linear absorption spectroscopy alone, given that the latter is a limited projection of information at the FC region [162]. As an extreme example, we consider "short-time-resolution eigenstates" consisting of the upper, middle, and lower polaritons computed at the FC region, and compute the analogous estimates p_{s_A}(FC) and p_{s_B}(FC). The infinite and short-time estimates are presented in Figure 3.9a. As expected, the plot suggests that the statistical estimate obtained from the full set of eigenvectors gives the right prediction of the yields at long times, while the FC estimate predicts the incorrect outcome of equal populations of A and B.

Example 2.- Example 1 highlights the danger of inferring excited-state dynamics relying solely on information obtained from linear optical spectroscopy. This issue becomes even more pertinent owing to some observations of Xiang et al. [28], where the authors observe selective cavity-mediated energy transfer into one of two molecules, despite the bare linear absorption spectral lineshapes being very similar outside the cavity. To highlight some of the described subtleties, we explore a second example where we consider a slightly different shape of the excited state PES for species B such that it resembles that of molecular species A in the FC region, while still being dissociative.

The computed spectra for the bare species and their corresponding spectra under SC to the cavity mode are shown in Figure 3.8, 2b,c,d. The resemblance of the excited state PESs at the FC region translates into very similar spectral lineshapes despite the dissociative *vs* bound nature away from the FC region. Regardless of the similarities in the absorption spectra, starting the dynamics with an excitation in the cavity mode still gives rise to the effective energy transfer from species A to B. Accordingly, the statistical ratio computed from the eigenstates at the FC point predicts equal populations of molecular species, while the full set of vibro-polaritonic eigenstates of the system (p_{s_A} and p_{s_B} in Figure3.9b) predicts the correct yields. Since such states are not easily accessible from linear absorption spectroscopy, we consider those measurements insufficient to predict the outcome of these photoproducts.

It is important to note that by virtue of our reliance on the zeroth-order

approximation, the cavity-mediated energy transfer mechanism studied in this section is N-independent, and thus differs from that put forward in Refs. [164, 165]. The latter relies on a bottleneck transfer of population from dark to polariton modes, whose rate scales as $1/N$.

In the future, it will be of great interest to ascertain whether the $\mathcal{O}(N^0)$ rate mechanism studied in the present work (originally put forward in [163]), or the mentioned $\mathcal{O}(N^{-1})$ rate mechanism is in order in the various experiments of cavity-mediated energy transfer [28, 43, 166, 167]. At least, for the last reference, it is clear that the latter mechanism cannot be operative, for it would yield rates of energy transfer that are much slower than those observed in the experiment.

Finally, we speculate that the mechanism highlighted in this section, where the cavity mediates energy transfer into the fastest dephasing molecular species, should be quite a generic phenomenon, and might be at play in the recent study in [168], which shows polariton enhanced photoconductivity of an organic film. However, a further consideration of this problem merit a careful inclusion of disorder and temperature effects, which will be the focus of future works.

3.4 Summary

The method of Collective dynamics Using Truncated Equations (CUT-E) exploits permutational symmetries of an ensemble of identical molecules and an emergent hierarchy of timescales, to elucidate the excited-state dynamics under collective strong light-matter interaction. Although previous works have used permutational symmetry arguments and have arrived at conclusions that are consistent with ours [63, 135, 136, 145, 157], elements of the present work uniquely provide opportunities for a systematic and intuitive treatment of molecular polariton dynamics.

It is important to note that, via quite a different formalism, another method that maps the dynamics of molecular polaritons to a single effective molecule in a cavity has already recently been reported before our work [136]. This method, based on density matrices, does not provide $\mathcal{O}(1/\sqrt{N})$ corrections to dynamics,

and considers a coherent state of the photon at all times, instead of the single-excitation manifold dynamics we have presented. We believe this method is quite complementary in its scope to ours. However, given the different formalisms, it is at present hard to assess the deeper conceptual connections between the methods; this will be subject of future work.

Let us conclude by highlighting some of the features of our approach. First, it allows for the systematic introduction of corrections to the thermodynamic limit. Second, our time-dependent approach generalizes some of the results found in previous work that also exploit permutational symmetries to compute optical properties [62, 63, 136, 137, 141, 145]; here we have generalized these concepts to chemical dynamics. Moreover, our work naturally provides an alternative interpretation of bright and dark-states based on permutationally-symmetric states, that is different from the one inherited from restrictive quantum optics models. These observations provide much needed physical intuition to design principles of polariton chemistry control, where rather than avoiding the decay into dark states, one embraces such phenomenon at one's advantage, such as with the examples provided in Section 3.3.8. Finally, the method enjoys numerical simplicity and is written in a language that makes it straightforward to modify existing codes for single-molecule strong light-matter calculations, and more generally, convenient for implementation in existing quantum molecular dynamics algorithms. At present, it is unclear whether the strategies here presented can be generalized to multimode cavities and finite temperature scenarios. These issues are the subject of present investigations.

3.5 Acknowledgments

Chapter 3, in full, is a reprint of the material as it appears in Proceedings of the National Academy of Sciences (PNAS). Pérez-Sánchez, Juan B.; Koner, Arghadip; Stern, Nathaniel P.; Yuen-Zhou, Joel. 120, 15, e2219223120, 2023. The dissertation author was the primary investigator and author of this paper. This work was supported as part of the Center for Molecular Quantum Transduction (CMQT), an Energy Frontier Research Center funded by the U.S. Department of

Energy, Office of Science, Basic Energy Sciences under Award No. DE-SC0021314. We also thank Kai Schwennicke and Matthew Du for useful discussions.

Chapter 4

Collective polaritonic effects on chemical dynamics suppressed by disorder

We present a powerful formalism, disordered collective dynamics using truncated equations (d-CUT-E), to simulate the ultrafast quantum dynamics of molecular polaritons in the collective SC regime, where a disordered ensemble of $N \gg 10^6$ molecules couples to a cavity mode. Notably, we can capture this dynamics with a cavity hosting a single *effective* molecule with $\sim N_{bins}$ electronic states, where $N_{bins} \ll N$ is the number of bins discretizing the disorder distribution. Using d-CUT-E we conclude that SC, as evaluated from linear optical spectra, can be a poor proxy for polariton chemistry. For highly disordered ensembles, total reaction yield upon broadband excitation is identical to that outside of the cavity, while narrowband excitation produces distinct reaction yields solely due to differences in the initial states prepared prior to the reaction.

4.1 Introduction

Disorder is an unavoidable feature that can impact polariton transport [50, 169–171], vibrational dynamics [77], superradiance [172], and polaron photoconductivity [168]. In this chapter, we generalize our recently developed Collective

dynamics Using Truncated Equations (CUT-E) method [87], that allows the efficient modeling of the quantum molecular dynamics of an arbitrarily large number of identical molecules, to study disordered ensembles. At the core of CUT-E lies the exploitation of permutational symmetries [63, 87, 141, 145, 157, 172–174], that scale the problem from an ensemble of $N \to \infty$ identical molecules down to a single *effective* molecule strongly interacting with the cavity mode. This effective molecule differs from an actual single-molecule in that its SC to the cavity occurs *solely* at the Franck-Condon (FC) region. We lift the constraint of identical molecules, coarse-grain the disorder distributions, and apply permutational symmetries among molecules that belong to the same disorder "bin". This approach is numerically exact for sufficiently short propagation times, where the number of disorder bins required to reach convergence (denoted as N_{bins}) is much smaller than N. This seemingly simple strategy has powerful consequences: the resulting d-CUT-E method maps a disordered molecular ensemble into a single effective molecule, with amplified number of electronic degrees of freedom (DoF) by N_{bins}. This is both conceptually insightful and computationally efficient compared to conventional methods that include every molecule of the ensemble explicitly. Although our method is general and can be applied to arbitrary disorder distributions of the parameters that shape the Potential Energy Surfaces (PESs), here we focus on Gaussian exciton-frequency disorder and study its impact on various ultrafast molecular and optical polaritonic properties.

Our study shows that: (a) broadband excitation can modify the reaction yield of the ensemble; however, in the large disorder regime, such changes can be explained just by changes in cavity leakage, despite the presence of the polariton bands in the absorption spectrum. (b) Narrowband excitation can modify the reaction yield even in the large disorder regime. In this case, external narrowband laser and strong light-matter coupling allows the selective excitation of high frequency vibrational states near the UP band, which are more reactive than the corresponding excitations of the LP band. Since the polariton processes involved in the preparation of these states vanish before the reaction ensues, this phenomenon should be interpreted as an optical effect and not as a chemical one.

4.2 Model

To illustrate the method, we assume a single-cavity mode, neglect intermolecular interactions, and restrict ourselves to the first excitation manifold. Our molecular model consists of a ground electronic state and two diabatically coupled excited electronic states, where only one of them can couple to the cavity mode. The molecular model is intentionally simplified to uncover the universal photochemical and photophysical behavior of molecular polaritons. In the CUT-E formalism, each disorder bin is represented by a single effective molecule with a collective coupling $g\sqrt{N}\sqrt{P_i}$, with P_i being the fraction of molecules in the i-th bin. Assuming that the molecules are initially in the global ground state, the CUT-E effective Hamiltonian in the large N limit is given by (see the Supplementary Information of Ref. [88] for details)

$$\begin{aligned}\hat{H}'_{eff} &= \omega_c|1\rangle\langle 1| + \sum_i^{N_{bins}} \left(-\frac{1}{2}\frac{\partial^2}{\partial q_i^2} + V_{e_1,i}(q_i)\right)|e_{1,i}\rangle\langle e_{1,i}| \\ &+ \sum_i^{N_{bins}} \left(-\frac{1}{2}\frac{\partial^2}{\partial q_i^2} + V_{e_2,i}(q_i)\right)|e_{2,i}\rangle\langle e_{2,i}| \\ &+ g\sqrt{N}\sum_i^{N_{bins}} \sqrt{P_i}\left(|e_{1,i}\rangle\langle 1| + |1\rangle\langle e_{1,i}|\right)\mathbb{P}_i + v_{12,i}|e_{1,i}\rangle\langle e_{2,i}| + \text{H.c.}. \end{aligned} \tag{4.1}$$

Here, q_i is the vector of mass-weighted coordinates of all vibrational degrees of freedom of molecule i; $|g_i\rangle$, $|e_{1,i}\rangle$, and $|e_{2,i}\rangle$ are the ground and excited electronic states; $V_{g/e_1/e_2}(q)$ are the PESs; $v_{12,i}$ is the diabatic coupling; ω_c is the cavity frequency; $\hat{a}$ is the photon annihilation operator; and $\mathbb{P}_i = |\varphi_{0,i}\rangle\langle\varphi_{0,i}|$ is the projector onto the FC state of the i-th effective molecule. Notice that the cavity mode only couples to the transition to the $|e_1\rangle$ electronic state of the molecules. This Hamiltonian incorporates the collective interaction between the molecules and the cavity mode, neglects all single-molecule coupling effects (which is valid for ultrafast processes if single-molecule coupling strength is sufficiently weak), and neglect finite temperature effects [87].

4.3 Results

4.3.1 Generalization of CUT-E for disordered ensembles

Although the CUT-E Hamiltonian is much simpler than conventional Hamiltonians granted $N_{bins} \ll N$, it still involves the vibrational and electronic degrees of freedom of all bins. Notably, $\hat{H}'_{eff}$ can be simplified even more by mapping it to another Hamiltonian $\hat{H}_{eff}$ [Eq. (4.2)] whose Hilbert space increases *linearly* with N_{bins} (see the Supplementary Information of Ref. [88]). This linear scaling is a consequence of the following considerations: first, restriction to the first excitation manifold implies that only one of the molecules is electronically excited at a time. Second, molecules in the ground electronic state do not exhibit vibrational dynamics, since the only mechanism by which they can acquire phonons is emission away from the FC region, which can be neglected in ultrafast dynamics according to CUT-E [87, 145]. These two features imply that the exact wavefunction of the system is a superposition of states in which only one effective molecule showcases vibrational dynamics, while the other $N_{bins} - 1$ are frozen.

We assume disorder only affects the excited state PESs $V_{e,1}(q)$ and $V_{e,2}(q)$. In this way, disorder bins only appear as additional "electronic" states. This dramatic reduction of the original system into a single effective molecule showcasing $2N_{bins}$ excited electronic states is the main computational contribution of this chapter. Its linear scaling with disorder represents a considerable improvement over methods that add an increasing number of molecules with parameters sampled from a disorder distribution, a computationally costly exercise that scales *exponentially* with N. A schematic representation of d-CUT-E is shown in Figure 4.1 using two disorder bins as an example, and the mathematical procedure is explained in detail in the Supplementary Information of Ref. [88].

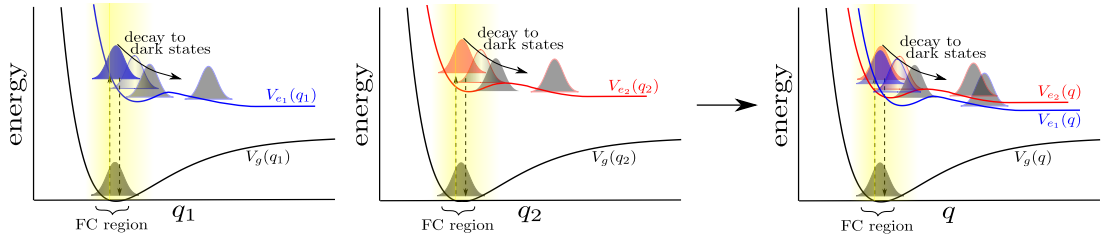

Figure 4.1: Linear scaling of the dynamics with the number of disorder bins. The first two panels depict cuts of the PESs along the reaction coordinate of two different bins, q_1 and q_2. d-CUT-E projects the two-dimensional vibrational dynamics of the two bins onto a single nuclear degree of freedom q (third panel).

The d-CUT-E Hamiltonian reads

$$\begin{aligned}\hat{H}_{eff} = \omega_c|1\rangle\langle 1| &+ \sum_i^{N_{bins}} \left(-\frac{1}{2}\frac{\partial^2}{\partial q^2} + V_{e_{1,i}}(q)\right)|e_{1,i}\rangle\langle e_{1,i}| \\ &+ \sum_i^{N_{bins}} \left(-\frac{1}{2}\frac{\partial^2}{\partial q^2} + V_{e_{2,i}}(q)\right)|e_{2,i}\rangle\langle e_{2,i}| \\ &+ g\sqrt{N}\sum_i^{N_{bins}} \sqrt{P_i}\left(|e_{1,i}\rangle\langle 1| + |1\rangle\langle e_{1,i}|\right)\mathbb{P} \\ &+ \sum_i^{N_{bins}} v_{12,i}|e_{1,i}\rangle\langle e_{2,i}| + \text{H.c.} \end{aligned} \tag{4.2}$$

Here, $\mathbb{P} = |\varphi_0\rangle\langle\varphi_0|$. The values for P_i and the parameters that define the PESs can be obtained from a disorder distribution $\rho(\omega)$.

As a proof of principle, and since we are interested in short-time processes that can be modified by strong-light matter interaction, we assume that short-time vibrational dynamics occurs only along the reaction coordinate and ignore vibrational degrees of freedom orthogonal to it [175, 176]. Hence, we use a single vibrational coordinate per molecule (see Figure 4.2).

The final Hamiltonian yields

$$\begin{aligned}\hat{H}_{eff} = (\omega_c - i\kappa/2)\,|1\rangle\langle 1| &+ \sum_i^{N_{bins}} \left(\omega_{0,i} + \omega_{\nu,i}\hat{D}(s_{1,i})\hat{b}^\dagger\hat{b}\hat{D}^\dagger(s_{1,i})\right) \otimes |e_{1,i}\rangle\langle e_{1,i}| \\ &+ \sum_i^{N_{bins}} \left(\omega_{0,i} + \omega_{\nu,i}\hat{D}(s_{2,i})\hat{b}^\dagger\hat{b}\hat{D}^\dagger(s_{2,i})\right) \otimes |e_{2,i}\rangle\langle e_{2,i}| \\ &+ g\sqrt{N}\sum_i^{N_{bins}} \sqrt{P_i}\left(|e_{1,i}\rangle\langle 1| + |1\rangle\langle e_{1,i}|\right)\mathbb{P} + \sum_i^{N_{bins}} v_{12,i}|e_{1,i}\rangle\langle e_{2,i}| + \text{H.c.}, \end{aligned} \tag{4.3}$$

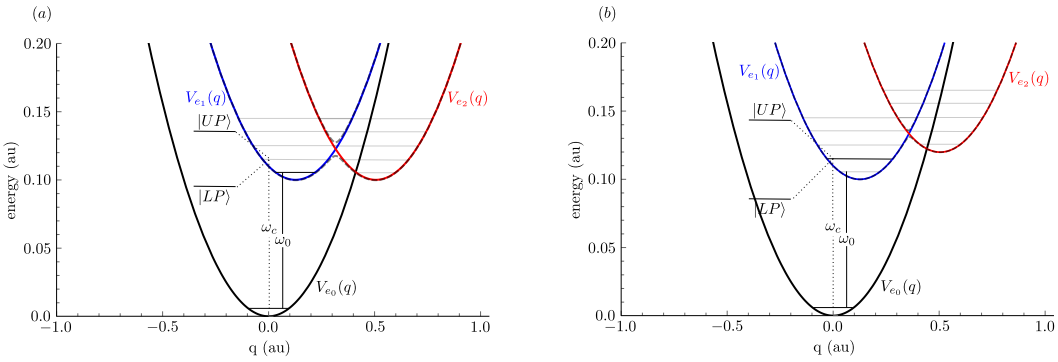

Figure 4.2: Potential energy curves for the molecular system. Each molecule in our model consists of two diabatically-coupled excited electronic states and one vibrational degree of freedom.

where $\hat{D}(s_{1,i}) = e^{\left(\hat{b}^\dagger - \hat{b}\right)s_{1,i}}$ is the displacement operator, and $\omega_{0,i}$, $\omega_{\nu,i}$, and $s_{1,i}$ are the exciton frequency, vibrational frequency, and Huang–Rhys factor for the $|e_{1,i}\rangle$ electronic state respectively. We incorporate cavity leakage by adding the imaginary term $i\kappa/2$ to the photon frequency, and the amount of energy that escapes the cavity by this mechanism can be quantified by calculating the norm of the wave function $\langle\Psi(t)|\Psi(t)\rangle$. For the rest of this work we will consider only exciton-frequency disorder. Here, disorder affects both $|e_1\rangle$ and $|e_2\rangle$ equivalently, thus the height of the barrier is the same for all bins.

4.3.2 Optical and Chemical Polariton Properties

To study optical effects, we calculate the linear absorption spectrum [145, 146, 177, 178],

$$A(\omega) = \kappa \,\mathrm{Re}\left[\tilde{C}(\omega)\right] - \frac{1}{2}\kappa^2|\tilde{C}(\omega)|^2, \tag{4.4}$$

with $\tilde{C}(\omega) = \int_0^{T_f} dt e^{i\omega t}\langle\Psi(0)|\Psi(t)\rangle$ and $|\Psi(0)\rangle = |\varphi_0\rangle \otimes |1\rangle$. To study chemical effects, we calculate populations of the electronic states $|e_1\rangle$ and $|e_2\rangle$, which can be thought of as the "reactant" and "product" states of a photochemical reaction, respectively. The reaction proceeds via tunneling of the vibrational wave packet from the $|e_1\rangle$ state. We calculate populations for each bin, and add them up to

obtain the total excited state population of reactant and product in the ensemble,

$$P_{e_1}(t) = \sum_{i}^{N_{bins}} P_{e_{1,i}}(t) = \sum_{i}^{N_{bins}} \langle \Psi(t)|e_{1,i}\rangle\langle e_{1,i}|\Psi(t)\rangle,$$
$$P_{e_2}(t) = \sum_{i}^{N_{bins}} P_{e_{2,i}}(t) = \sum_{i}^{N_{bins}} \langle \Psi(t)|e_{2,i}\rangle\langle e_{2,i}|\Psi(t)\rangle. \tag{4.5}$$

To capture the competition between cavity leakage and excited-state reactivity, we do not divide the expectation values by the norm.

Both optical and molecular properties are calculated for various values of exciton-frequency disorder σ and collective light-matter coupling $g\sqrt{N}$. We use the Gaussian exciton-frequency distribution $\rho(\omega) = \frac{1}{\sigma\sqrt{2\pi}} e^{-\frac{1}{2}\left(\frac{\omega-\omega_0}{\sigma}\right)^2}$, with the cavity frequency being resonant with the $\nu = 0 \rightarrow \nu' = 1$ transition $\omega_c = \omega_0 + \omega_\nu$. We discretize $\rho(\omega)$ by restricting its domain to $\omega_0 - 3\sigma < \omega < \omega_0 + 3\sigma$, and calculate the values of P_i and $\omega_{0,i}$ as

$$P_i = \int_{\omega_{i,min}}^{\omega_{i,max}} d\omega\rho(\omega) \qquad \omega_{0,i} = \int_{\omega_{i,min}}^{\omega_{i,max}} d\omega\omega\rho(\omega), \tag{4.6}$$

with $\omega_{i,min} = \omega_0 - 3\sigma + (i-1)(6\sigma/N_{bins})$ and $\omega_{i,max} = \omega_0 - 3\sigma + i(6\sigma/N_{bins})$. Ignoring the tails of the distribution is justified since molecules that fall at the ends of the energy distribution are off-resonant with the cavity mode and the polariton windows (see Figure 4.3).

4.3.3 Convergence analysis

In Figure 4.4 we analyze the convergence in cavity leakage $\Gamma(t) = 1 - \langle\Psi(t)|\Psi(t)\rangle$, photon population $|C(t)|^2$, linear absorption spectrum $A(\omega)$, and electronic populations $P_{e_1}(t)$ and $P_{e_2}(t)$, as a function of N_{bins}. We propagate the initially photonic wavepacket $|\Psi(0)\rangle = |\varphi_0\rangle \otimes |1\rangle$ for $T_f = 40$ fs.

We find that the width of the bins $\delta\omega$ required to reach convergence in optical and chemical observables obey a simple relation $\delta\omega \sim 2\pi/T_f$, where T_f is the final propagation time. This is not surprising since a finite propagation time implies a finite energy resolution. Thus, the number of bins required for convergence obeys $N_{bins} = 6\sigma T_f/2\pi$ (see the Supplementary Information of Ref. [88] for convergence analysis). Hence, the computational cost of disorder does not scale with N, and scales linearly with $N_{bins} \propto T_f$.

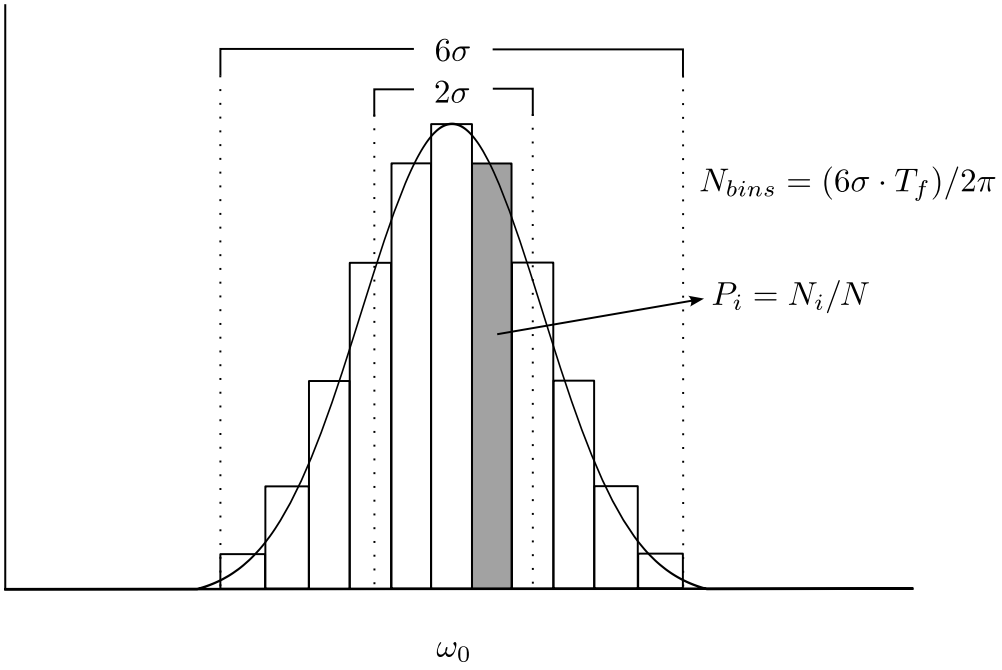

Figure 4.3: Discretization of exciton frequency disorder. The frequencies follow a Gaussian distribution and the number of bins required to reach convergence is proportional to the total disorder and final propagation time.

4.3.4 Broadband Excitation

Figure 4.5 shows optical and chemical effects of disorder for $T_f = 30$ fs, $N_{bins} = 40$, and an initially photonic wavepacket $|\Psi(0)\rangle = |\varphi_0\rangle \otimes |1\rangle$ (mimicking broadband excitation, $T_{pulse} \ll T_{Rabi}$). Final propagation time was chosen to avoid barrier recrossing due to the single-mode nature of our model.

Our calculations show that features that would be resolved at long timescales, such as vibronic progressions (small red peaks), vanish as disorder grows comparable to the collective light-matter coupling [Figure 4.5(1a)]. This is a consequence of damping of the coherent return of population between the bright state to the cavity mode [see Figure 4.5(1b)]. However, contrary to what intuition suggests, even if such dampening is significant within the timescale of the Rabi period $T_{Rabi} \sim 2.5$ fs, it does not imply that the UP and LP bands disappear. This is because only a small amplitude needs to return to the cavity (during the second half of the Rabi cycle) to create such an optical feature [162, 179]. The reduction in T_{Rabi} that fol-

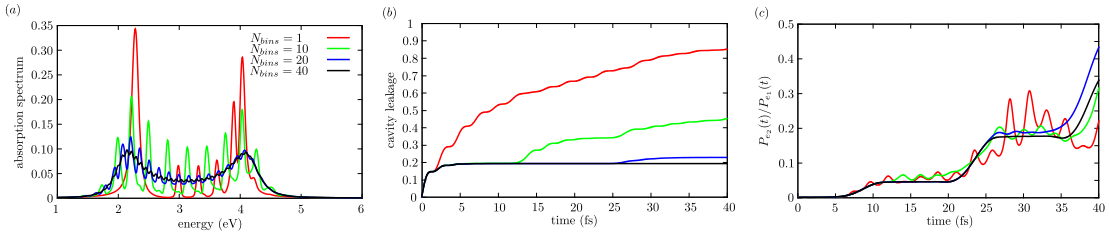

Figure 4.4: Convergence of the dynamics with the number of bins N_{bins}. (a) Linear absorption spectrum $A(\omega)$. (b) Cavity leakage $\Gamma(t)$, (c) Ratio of electronic excited state populations $P_{e_2}(t)/P_{e_1}(t)$. We find that the number of bins N_{bins} needed to reach convergence obeys $N_{bins} = 6\sigma \cdot T_f/2\pi$. Parameters: $\omega_0 = 0.11$ au, $\sigma = 0.02$ au, $\omega_\nu = 0.01$ au, $g\sqrt{N} = 0.03$ au, $\kappa = 0.006$ au, $v_{12} = 0.0025$ au, $s_1 = -1$, and $s_2 = -4$.

lows from the dampening of Rabi oscillations also leads to an increase in the Rabi splitting [80, 180]. Thus, for highly disordered polaritons, collective light-matter coupling strengths *cannot* be directly extracted from polariton Rabi splitting.

Figure 4.5(1c) shows changes in $P_{e_2}(T_f)$ that correspond to two regimes of disorder. The low disorder regime $2\sigma < g\sqrt{N}$, characterized by a strong dependence of the reaction yield with σ, and the large disorder regime $2\sigma > g\sqrt{N}$, where the reaction yield reaches a constant value. For low σ and low $g\sqrt{N}$ (red, green and blue lines), disorder leads to higher total reaction yields, but this effect vanishes for large $g\sqrt{N}$ (light blue and black lines) where "polaron decoupling" takes over [33, 181]. This behavior of the reaction yield in the low disorder regime arises as a consequence of interferences between the vibrational wavepackets of the electronic states for each bin $|e_{1,i}\rangle$, due to their common interaction with the photon state $|1\rangle$. These Rabi oscillations are significantly reduced at large disorder, causing the total reactivity of the ensemble to be independent of disorder. In this regime, changes of the total reaction yield upon broadband excitation for different collective coupling strengths can be explained by differences in cavity leakage (see normalized product populations in the Supplementary Information of Ref. [88]).

Figure 4.5(2a) shows that wave packet interferences in the large-disorder regime still cause differing reactivities on *individual* bins, despite them having the same PESs. By comparing the total excited state population $P_{e_1}(t) + P_{e_2}(t)$ with the product population $P_{e_2}(t)$, we conclude that this difference in product yields of

individual bins cannot be attributed to differences in their respective absorption. Additional calculations show that high-frequency bins become more reactive than those at low frequency as a consequence of vibronic coupling of the $|e_1\rangle$ electronic state (here, $s_1 = -1$), and that this effect is suppressed if $s_1 = 0$ (see the Supplementary Information of Ref. [88]). We will elaborate on the consequences of this effect when we consider narrowband excitation. Figure 4.5(2b) shows time-dependent total population dynamics for zero, intermediate, and large disorder. In the absence of disorder, strong light-matter coupling gives rise to large amplitude Rabi oscillations for $P_{e_1}(t)$ that last even after the reaction occurs, producing a low reaction yield. This polaritonic-induced reduction of reactivity (polaron decoupling) has been explained in previous theoretical works as a change in the PESs that prevents the nuclei from moving away from the FC region [33, 157, 181, 182]. However, for intermediate and large disorder, Rabi oscillations are damped before the reaction ensues, polaron decoupling disappears, and the reactivity reaches a constant value. This constant value corresponds to the reaction yield outside of the cavity, as shown in Figure 4.5(2c), where we have initiated the system in the bright state $|\Psi(0)\rangle = \sum_i^{N_{bins}} \sqrt{P_i}|\varphi_0\rangle \otimes |e_i\rangle$, for $g\sqrt{N} = 0$. From this we conclude that changes in the reaction yield upon broadband excitation are not possible if reactivity occurs on a timescale longer than that of Rabi oscillations, even if the linear absorption spectrum showcases two clear polariton bands [see Figure 4.5(a)].

Next, we systematically study how the large-disorder regime approaches the off-cavity limit by initiating the dynamics in the bright state, and calculating the total excited states populations for $g\sqrt{N} = 0.03$ au, increasing the disorder. This allows us to directly compare the ensuing dynamics with that outside of the cavity ($g\sqrt{N} = 0$). Importantly, the out-of-cavity population dynamics is independent of disorder for these initial conditions.

We find that broadband excitation in the large-disorder regime does not result in different photochemistry than outside of the cavity, although the linear absorption spectrum misleadingly suggests otherwise. As we discussed before, this occurs because, even for large disorder, the Rabi splitting in the absorption spectrum is a feature defined at short times ($T \sim 2.5$ fs), for which disorder has a

very minor effect. On the contrary, at the longer timescales of chemical reactivity, disorder has already caused decoherence of wavefunction in individual disorder bins. We also modified the PES of $|e_2\rangle$ so that it lies at higher energies with respect to $|e_1\rangle$. Contrary to the previous scenario, for low disorder, we observe a polariton-mediated increase in the total reaction yield if the target state $|e_2\rangle$ is 0.02 au blue detuned with respect to $|e_1\rangle$, thanks to the UP having high enough energy to allow the barrier crossing. Moreover, we observe that the behavior is not monotonic and population transfer is enhanced for low values of disorder, but eventually converges to the dynamics outside of the cavity [see Figure 4.6(c)].

4.3.5 Narrowband Excitation

We next examine selective excitation of either one of the polariton bands (narrowband excitation, $T_{pulse} > T_{Rabi}$). To this end, we initiate the dynamics in the states $|\Psi_{\pm}(0)\rangle = \frac{1}{\sqrt{2}}|\varphi_0\rangle \otimes \left(|1\rangle \pm \sum_i^{N_{bins}} \sqrt{P_i}|e_i\rangle\right)$, which allocate the same vibrational energy to all bins, and their average energy is that of the polaritons.

Figure 4.7 shows that selective pumping of polariton bands yields different excited-state reaction yields. As we might expect from Figure 4.5(2a), excitation of the UP results in a high reaction yield due to selective excitation of the bins with a higher reactivity, while excitation of the LP results in a low reaction yield. This can be explained as a cavity-assisted mixing of high-lying vibronic states of the low-energy bins with low-lying vibronic states of the high-frequency bins through Rabi oscillations, resulting in excitation of molecules near the UP with more vibrational energy, and molecules near the LP with lower vibrational energy. A scheme of this mechanism is shown in Figure 4.8, and numerical evidence is provided in the Supplementary Information of Ref. [88]. Notice that this mechanism is a consequence of the definition of the initial excited state. Since the laser pulse must be longer than the Rabi period to selectively excite a single polariton band, both the external laser and polariton dynamics simultaneously participate in the creation of the initial states with differing reactivities. Crucially, there is no reason to believe that these highly reactive states cannot be created without the cavity's presence using a *different* narrowband linear external laser that efficiently

targets high-energy vibronic progressions through the UP (LP) band. In fact, both strategies rely on non zero vibronic coupling to produce frequency-dependent photoreactivity. Therefore, whether collective SC in the large N limit provides any advantage to control chemical reactivity compared to conventional linear optical sources is not readily apparent, especially in light of recent experiments that suggest there are no polaritonic effects on chemical dynamics [183, 184].

4.4 Summary

We have successfully introduced the d-CUT-E method to efficiently simulate the ultrafast dynamics of disordered molecular ensembles under collective SC. Our findings challenge the notion that a Rabi splitting in the linear absorption spectrum inevitably implies changes in chemical reactivity. This is due to the disparity in timescales governing optical and chemical properties. Optical properties primarily manifest at short timescales when disorder has minimal impact, while chemical properties emerge at longer timescales. In the common scenario that disorder is comparable with the light-matter coupling strength, SC induces modifications in the reactivity of individual disorder bins, which can be selectively targeted by narrowband pulses. This phenomenon should be interpreted as a cavity-mediated initial state preparation effect.

4.5 Acknowledgements

Chapter 4, in full, is a reprint of the material as it appears in Physical Review Research. Pérez-Sánchez, Juan B.; Mellini, Federico; Giebink, Noel C.; Yuen-Zhou, Joel. PRR, 6, 013222, 2024. The dissertation author was the primary investigator and author of this paper. This work was supported by the Air Force Office of Scientific Research (AFOSR) through the Multi-University Research Initiative (MURI) Program No. FA9550-22-1-0317. We thank Gerrit Groenhof, Arghadip Koner, and Kai Schwennicke for useful discussions.

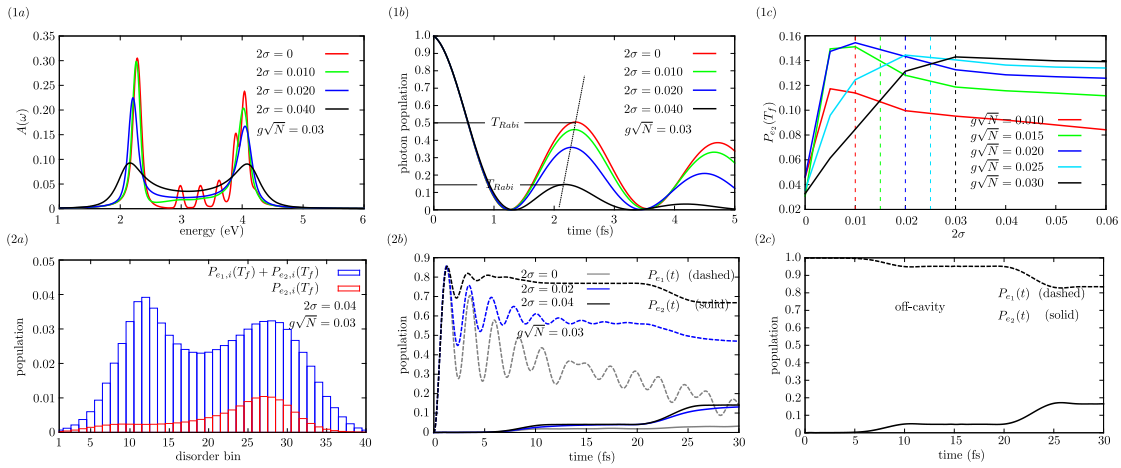

Figure 4.5: Effects of exciton-frequency disorder on optical and chemical properties of molecular polaritons. Parameters: $\omega_0 = 0.10$ au, $\omega_c = 0.11$ au, $\omega_\nu = 0.01$ au, $\kappa = 0.006$ au, $v_{12} = 0.0025$ au, $s_1 = -1$, and $s_2 = -4$. (1a) Linear absorption spectrum for different values of disorder. Disorder suppresses vibronic features and increases the polariton Rabi splitting. (1b) Time-dependent interpretation of Rabi splitting increase caused by disorder. (1c) Final population of the electronic state $|e_2\rangle$ [$P_{e_2}(T_f)$, $T_f = 30$ fs] for different values of disorder and collective light-matter coupling strength. Vertical lines on the disorder axis correspond to $2\sigma = g\sqrt{N}$. As expected, polaritonic effects become immune to disorder for large $g\sqrt{N}$. (2a) Final excited-state populations of each disorder bin show their reaction yield (red) is different even at large disorder, and not just due to polariton modified absorption (blue). Bins are ordered from low to high exciton frequency. (2b) Population dynamics of excited electronic states $P_{e_1}(t)$ (dashed) and $P_{e_2}(t)$ (solid) for $2\sigma = 0$ (gray), $2\sigma < g\sqrt{N}$ (blue), and $2\sigma > g\sqrt{N}$ (black). (2c) Population dynamics of excited electronic states $P_{e_1}(t)$ (dashed) and $P_{e_2}(t)$ (solid) outside of the cavity. The step-like behavior in $P_{e_2}(t)$ is attributed to the reaction proceeding via tunneling of the oscillating vibrational wavepacket from the $|e_1\rangle$ state. Notice the resemblance between the dynamics in (2c) and (2b) for $2\sigma/g\sqrt{N} = 2/3, 4/3$, indicating no polaritonic changes in the PESs in the presence of disorder.

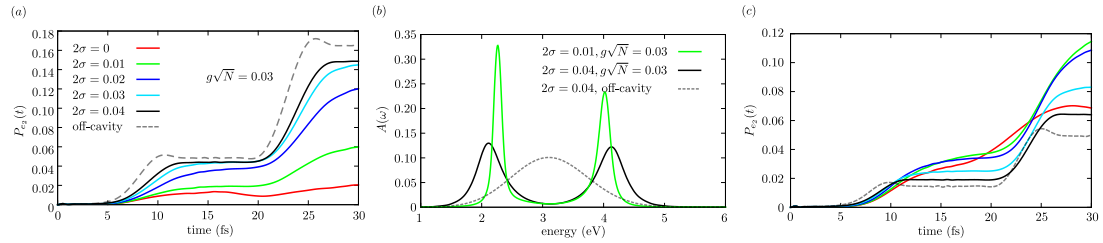

Figure 4.6: Reaction yield in the strong-coupling regime as a function of disorder upon broadband excitation (bright initial state). (a) Reaction is suppressed with SC; however, as disorder becomes comparable to the Rabi splitting, $P_{e_2}(t)$ resembles the behavior outside of the cavity. (b) Absorption spectrum $A(\omega)$ for the dynamics in (a): SC low disorder (green), SC-large disorder (black), and outside of the cavity (dashed). Notably, despite well-defined polariton bands for large disorder, the corresponding reactivity in (a) is similar to the off-cavity case. (c) Same as (a) but shifting the PES of $|e_2\rangle$ upwards by two vibrational quanta. In this case, SC enhances the reaction for weak disorder.

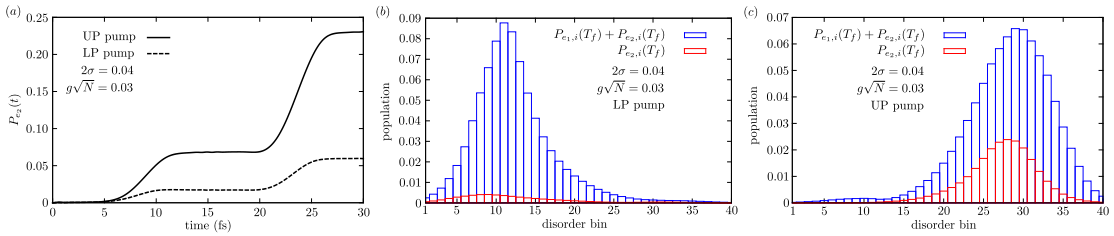

Figure 4.7: Reaction yield upon narrowband excitation in the strong-coupling and large-disorder regime (parameters: $g\sqrt{N} = 0.03$ au and $2\sigma = 0.04$ au). (a) Total product state population after pumping the UP (solid) and the LP (dashed). (b and c) Excited-state populations of each disorder bin showing their reaction yield (red) and absorption (blue), after LP pumping and UP pumping. Larger ratios $P_{e_{2,i}}(T_f)/[P_{e_{1,i}}(T_f) + P_{e_{2,i}}(T_f)]$ imply higher reactivity. (b) and (c) indicate that the higher reactivity of the UP bins cannot be explained simply by polariton absorption, which slightly favors the LP bins.

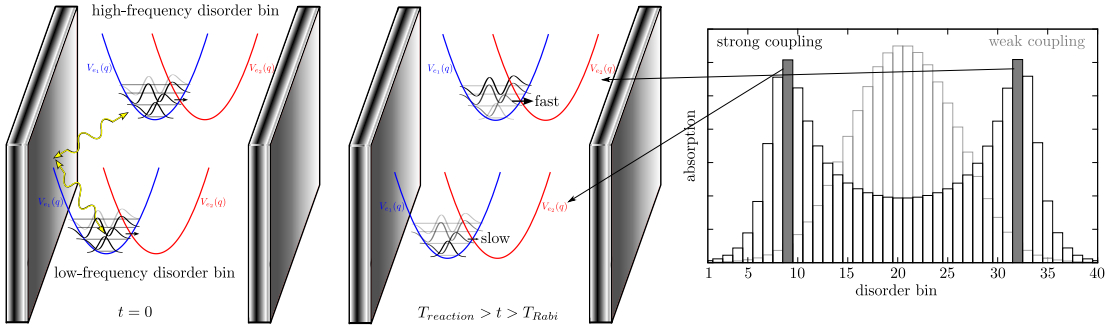

Figure 4.8: Mechanism of frequency-dependent photoreactivity in disordered molecular polaritons. Interplay of narrowband excitation and cavity-mediated interactions between disorder bins results in the preparation of states with different reactivities after damping of Rabi oscillations and before the chemical reaction. These highly (slightly) reactive bins can be excited at the UP (LP) frequency, leading to an increase (decrease) of the total reactivity upon narrowband excitation.

Chapter 5

Optical filtering effect in molecular polaritons and the $N \to \infty$ limit

5.1 Introduction

In the previous chapter we have concluded that, in the $N \to \infty$, changes in the excited state molecular dynamics under strong light-matter coupling must be understood as an optical effect rather than a chemical one: polaritons allows for the preparation of excited states that have more or less access to desired final states. A natural question that emerges from that is whether the initial states created with strong light-matter coupling offer any advantage when compared to more conventional excited state preparation effects outside of the cavity using pulse-shaped lasers. Using a theory of polaritonic linear response [145, 178, 185], Schwennicke and coworkers [89] demonstrated that, in the $N \to \infty$, the linear polariton absorption is proportional to the product of the bare molecular absorption $\mathrm{Im}[\chi^{(1)}(\omega)]$ and the polariton transmission spectrum $T(\omega)$ (here we assumed $\kappa_R = \kappa_L = \kappa/2$),

$$A(\omega) = 2\mathcal{Q}\mathrm{Im}[\chi^{(1)}(\omega)]T(\omega), \tag{5.1}$$

where $\mathcal{Q} = \frac{\omega_c}{\kappa}$ is the cavity-quality factor that accounts for an cavity-enhancement of the absorption.

Besides cavity-enhancement of the field, Eq. 5.1 suggests that polaritons act merely as "optical filters" that allow frequencies near the polariton transmission peaks to pass through, and interact weakly with the molecules inside the cavity. Therefore, the same polariton-modified chemical reactivity could be obtained by shining with a laser whose frequency profile looks like the polariton transmission spectrum. In this chapter we numerically show this to be the case, and explain this phenomenon based on our CUT-E formalism. Interestingly, this result holds even in the absence of disorder.

5.2 Model

In the previous chapter, we compared the excited state molecular dynamics inside and outside of the cavity under the same excitation conditions (broadband and narrowband excitations). However, Eq. 5.1 suggests that a more appropriate comparison involves pumping outside of the cavity with a weak laser whose intensity profile has been "shaped" to mimic the polariton transmission spectrum. Here, we consider explicitly the "filtered" pulse acting on the bare molecules $E(t) = E_0 C(t)$, where $C(t) = \langle \Psi(0) | \Psi(t) \rangle$, $|\Psi(0)\rangle = \varphi_0(q)|1\rangle$, is the photon-photon correlation function, and E_0 is a constant amplitude which is small enough to ensure we remain in the linear regime. We re-run the simulations for the system described in the previous chapter using the aforementioned laser pulses and the d-CUT-E method.

5.3 Results

5.3.1 Numerical evidence of linear optics

Our results in Figure 5.1 confirm that the photoreactivity of the bare molecules triggered by $E(t)$ is, up to a constant, *identical* to that observed inside the cavity.

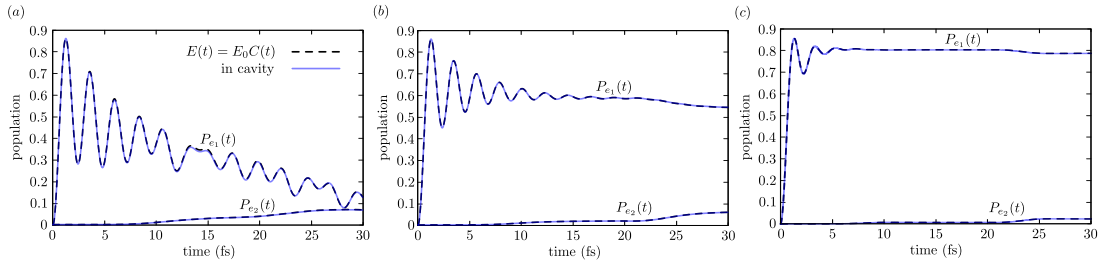

Figure 5.1: *Coherent dynamics in the large-N limit.*– Population dynamics of the first, $P_{e_1}(t)$, and second, $P_{e_2}(t)$, excited state populations inside the cavity versus when the system outside of the cavity is driven with a time-dependent pulse $E(t) = E_0 C(t)$. Since the polariton transmission spectrum $T(\omega)$ is proportional to $|\tilde{C}(\omega)|^2$ [173, 178, 185], this pulse is guaranteed to have the same intensity profile as the polariton transmission spectrum [note that the populations are normalized to the maximum value of $P_{e_1}(t)$]. The dynamics are identical up to a constant, particularly in the Rabi oscillations observed under SC.

5.3.2 Understanding the $N \to \infty$ limit

We now try to understand why the $N \to \infty$ implies that the molecular dynamics can be reproduced in linear regime. We can do so using out CUT-E method given that it is exact, systematic, and incorporates the $N \to \infty$ limit as a special limit [87] (we know what we ignore when we take such limit). The most important conclusion from CUT-E is that the collective light-matter coupling operates for optical transitions that do not create phonons in the ground state, while the single-molecule coupling operates for processes that do. Therefore, Rabi oscillations are dominated by Rayleigh-like molecular processes, while Raman and fluorescence rates (all processes that create phonons in the ground electronic state, see Fig. 5.2) are of $\mathcal{O}(1/N)$. In CUT-E we Keep the collective coupling $g\sqrt{N}$ constant and finite (since it is an experimental observable), and take the limit $N \to \infty$. This is equivalent to taking $g \to 0$, which leads to the dismissal of the aforementioned $\mathcal{O}(1/N)$ non-linearities. Even though several instances of Rayleigh scattering can take place due to collective SC, only the molecular linear susceptibility $\chi^{(1)}(\omega)$ contributes to the polaritonic response. In other words, non-trivial polaritonic effects (beyond optical filtering) rely on the single-molecule light-matter coupling terms g.

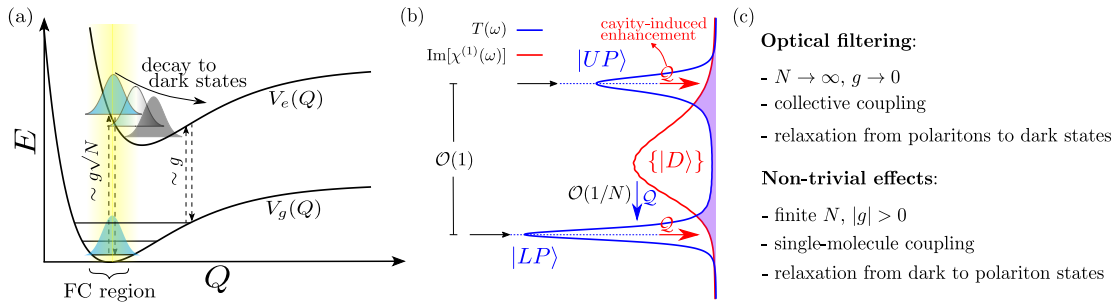

Figure 5.2: Collective vs single-molecule coupling effects. (a) Light-matter coupling is collectively enhanced with the Franck-Condon (FC) region for optical transitions that do not create phonons in the ground state, *i.e.*, inter-exciton coherence is preserved. This implies that only Rayleigh-like processes are relevant in the large-N limit. On the other hand, light-matter coupling is single-molecule-like for processes that create phonons in the ground state, *e.g.*, Raman and fluorescence. (b) Collective coupling creates upper and lower polaritons. Decay from polaritons to dark states is described by absorption through the polariton windows. Decay from dark states back to polariton states relies on single-molecule light-matter coupling g, hence $\mathcal{O}(1/N)$. These processes are enhanced by the cavity-quality factor $\mathcal{Q}$. (c) Listed are examples of processes that are interpretable as optical filtering versus examples of non-trivial polaritonic effects.

5.3.3 Connection with one-photon phase control

It is commonly believed that time-domain Rabi oscillations, which give rise to the frequency-domain Rabi splitting in the linear polaritonic response, imply the existence of nonlinear optical processes. Here, we show that these oscillations can be reproduced in the *linear* regime simply via constructive and destructive interference between the excited state amplitudes promoted by the two main frequencies of the filtered pulse at different times. This phenomenon is well-known in the field of ultrafast spectroscopy as linear wavepacket interferometry [179,186]; in fact, nonlinear wavepacket interferometry has been suggested as an alternative to provide real "pump-dump" control and detection of molecular dynamics beyond the FC region [2,3]. Our results are consistent with those found by Groenhof and coworkers using ab-initio quantum dynamics simulations [184]. Further analysis shows that this simple optical filtering description explains several theoretical and experimental works on molecular polaritons in the collective regime [89]. It is important to clarify that using an optically filtered linear source to excite the bare

molecules will not reproduce the ultrafast polariton dynamics unless the resulting light is coherent and has the same frequency-dependent phase as $D^{(R)}(\omega)$ [187,188]. If the control pulse is defined so that only its frequency *intensity* profile $|E(\omega)|^2$ agrees with transmission spectrum $T(\omega)$, the ultrafast dynamics for both free-space and intracavity molecules can be different to that under strong coupling before the steady-state is reached (one-photon phase control experiments) [187–189]. Moreover, if the steady-state is not reached before $1/N$ corrections start to matter (e.g., decay from dark states back to polaritons), the strong coupling dynamics and the dynamics with the pulse *may never be the same* (see Figure 5.2).

5.4 Summary

We showed that, in the $N \to \infty$ limit, excited state molecular dynamics under strong light-matter coupling can be reproduced using a weak laser pulse acting on the bare molecules. Since $1/N$ effects are crucial to obtain non-trivial polaritonic effects in the collective regime, it is clear that we must go beyond zeroth-order CUT-E. Although higher-order approximations are possible within CUT-E, it is still constraint to the first-excitation manifold. In the next chapter we develop a bosonic formalism that generalizes CUT-E to include an arbitrary number of excitations. We use this bosonic mapping to study the two most important $1/N$ mechanisms in the molecular polaritons field: vibrational relaxation and radiative pumping.

5.5 Acknowledgements

Chapter 5 is part of a review in preparation for publication whose authors are Kai Schwennicke, Arghadip Koner, Juan B. Pérez-Sánchez, Wei Xiong, Noel C. Giebink, Marissa L. Weichman and Joel Yuen-Zhou. The dissertation author was a co-author of this paper. This work was supported by the Air Force Office of Scientific Research (AFOSR) through the Multi-University Research Initiative (MURI) Program No. FA9550-22-1-0317. The authors acknowledge discussions

with Abraham Nitzan, who pointed out the analogies of collective and single-molecule couplings with Rayleigh and Raman scattering amplitudes, respectively.

Chapter 6

Radiative pumping vs vibrational relaxation of molecular polaritons: a bosonic mapping approach

We present a formalism to study molecular polaritons based on the bosonization of molecular vibronic states. This formalism accommodates an arbitrary number of molecules N, excitations and internal vibronic structures, making it ideal for investigating molecular polariton processes accounting for finite N effects. We employ this formalism to rigorously derive radiative pumping and vibrational relaxation rates. We show that radiative pumping is the emission from incoherent excitons and divide its rate into transmitted and re-absorbed components. On the other hand, the vibrational relaxation rate in the weak linear vibronic coupling regime is composed of a $\mathcal{O}(1/N)$ contribution already accounted for by radiative pumping, and a $\mathcal{O}(1/N^2)$ contribution from a second-order process in the *single*-molecule light-matter coupling that we identify as a polariton-assisted Raman scattering. This scattering is enhanced when the energy difference between the emission and the lower polariton transition corresponds to the vibrational excitations created in the Raman process.

6.1 Introduction

Molecular exciton polaritons are hybrid light-matter quasiparticles that emerge when the interaction strength between electronic matter excitations and confined electromagnetic fields is large enough to make Rabi oscillations faster than the molecular and cavity losses. A large variety of polaritonic architectures have been developed to reach this strong coupling regime over the last three decades, and several modifications of optical and molecular behavior have been reported [10, 11, 13–21]. While single molecules can strongly couple to confined fields of plasmonic nanocavities, a more common scenario requires an ensemble of matter excitations collectively coupled to optical modes in microcavities, leading to the emergence of polariton states and a dense manifold of so-called dark states [27]. Organic exciton polaritons are particularly interesting systems since strong coupling between electronic and vibrational degrees of freedom (DoF) gives rise to intricate relaxation processes that allow for population transfer between dark and polariton states, a feature which plays a central role in polariton-assisted remote energy transfer [43–45], polariton transport [46–49, 51, 52], and polariton condensation [53–61].

Seminal works contributed to the phenomenological understanding of relaxation processes by establishing semiclassical relaxation rates valid when molecules can be treated as two-level systems weakly coupled to a vibrational bath [190–192]. Based on these works, two different mechanisms have been proposed: radiative pumping, consisting of emission from incoherent excitations directly into a polariton mode, and vibrational relaxation, where the transfer into the polariton mode is accompanied by the release of a high-frequency phonon. Despite the formal derivation of vibrational relaxation from a weak vibronic coupling model [190] and the development of theories that numerically reproduce radiative pumping [193], a rigorous derivation of vibrational relaxation and an analytical derivation of radiative pumping for molecules with complex vibrational structures within a unified framework are missing until now.

First-principle Hamiltonians that go beyond the Holstein-Tavis-Cummings (HTC) model have been put forward with the aim of understanding polariton

modified chemical reactivity [194, 195], and recent theoretical works suggests that relaxation from polaritons to dark states in the $N \to \infty$ limit can be understood simply as an optical filtering effect: polaritons act as windows through which vibronic states can be optically excited [196]. The converse, dark state to polariton relaxation processes vanish when $N \to \infty$ (K. Schwennicke et al., in preparation). This striking finding has made understanding molecular polariton dynamics in the finite N limit more crucial than ever for achieving non-trivial polaritonic effects in the collective strong coupling regime, particularly the relaxation from dark states back to polariton states.

The aim of this work is twofold: first, we develop an exact bosonic picture of organic molecular polaritons from first principles to study molecular dynamics under collective light-matter coupling for arbitrary number of molecules N, excitations N_{exc}, and internal vibrational structure of the molecules. This mapping is ideal for numerical simulations using Meyer-Miller mappings [197–200], Quantum Cumulant Expansions [201], quantum computing with bosonic devices [202], and other quantum mechanical methods suited for bosonic systems [203]. Second, we focus on the large (yet finite) N case and the first excitation manifold to rigorously derive radiative pumping and vibrational relaxation rates. We achieve this by partitioning the bosonic Hamiltonian into "fast" and "slow" components, treating the slow components perturbatively. This allows us to identify two regimes, arising from the competition between *weak* vibronic couplings (W) and *single*-molecule light-matter coupling (g). Next, we unambiguously establish the fundamental differences between the polariton relaxation mechanisms. Radiative pumping is the emission from incoherent excitons that populate the polaritons, which can either leak out of the cavity or be reabsorbed by the material (polariton-assisted photon recycling). On the contrary, vibrational relaxation includes radiative pumping and higher-order processes in g such as polariton-assisted Raman scattering. We provide a simple analytical formula for radiative pumping based on simple spectroscopic observables, and lay out efficient numerical tools to calculate Raman scattering rates. In Figure 6.1 we provide an intuitive picture of the molecular polariton photophysics discussed in this chapter.

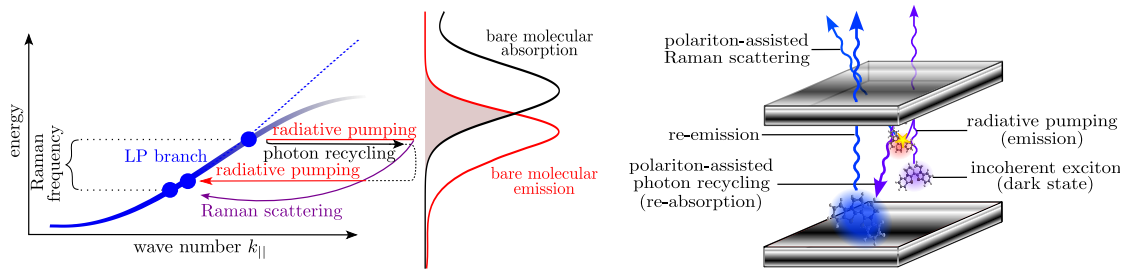

Figure 6.1: Schematic representation of the relaxation mechanisms classified in this work. Radiative pumping is the emission from dark states through the polaritons, while vibrational relaxation also includes higher-order processes such as Raman scattering. Polariton-assisted Raman scattering occurs when light emitted by dark states scatters off the vibrations of a second molecule. We also identify Polariton-assisted photon recycling as the re-absorption of the dark-state emission, which can be subsequently re-emitted.

6.2 Model

Consider a system of N non-interacting molecules collectively coupled to a single cavity mode. The generalized Tavis-Cummings Hamiltonian, extended to include internal vibrational degrees of freedom missing from original models, can be written as (hereafter $\hbar = 1$)

$$\hat{H} = \sum_{i}^{N} \left(\hat{H}_m^{(i)} + \hat{H}_I^{(i)} \right) + \hat{H}_{cav}, \tag{6.1}$$

where

$$\begin{aligned} \hat{H}_{mol}^{(i)} &= \left(\hat{T} + V_g(q_i) \right) |g_i\rangle\langle g_i| + \left(\hat{T} + V_e(q_i) \right) |e_i\rangle\langle e_i|, \\ \hat{H}_{cav} &= \omega_c \hat{a}^\dagger \hat{a}, \qquad \hat{H}_I^{(i)} = g \left(|e_i\rangle\langle g_i| \hat{a} + |g_i\rangle\langle e_i| \hat{a}^\dagger \right), \end{aligned} \tag{6.2}$$

are the Hamiltonians for the ith molecule, the cavity mode, and the interaction between them, respectively. Here, $\hat{T}$ is the kinetic energy operator, $|g_i\rangle$ and $|e_i\rangle$ are the molecular ground and excited electronic states, $V_{g/e}(q_i)$ are the ground and excited Potential Energy Surfaces (PES), $\hat{a}$ is the photon annihilation operator, and q_i is the vector of all vibrational degrees of freedom of molecule i. Here we consider only two electronic states per molecule and use the rotating wave, the Born-Oppenheimer, and the Condon approximations for convenience.

6.3 Bosonic mapping

In our previous work we have derived Collective Dynamics Using Truncated-Equations (CUT-E), a formalism that, by exploiting the permutational symmetries of the exact time-dependent many-body (many-molecule and cavity) wavefunction, yields a hierarchy of timescales that renders the simulation efficient for large N [87]. Here, we recognize that this formalism can be easily derived using second quantization. Starting from a permutationally symmetric wavefunction at an initial time, Eq. 6.1 preserves this symmetry for all times, thus allowing us to focus only on the bosonic (permutationally symmetric) subspace. The bosonic mapping of identical-noninteracting particles is well known [197, 198, 204], and it has been applied to ensembles of d-level systems strongly interacting with light [141, 205–208] (also see Ref. 174 for a fermionic mapping). We carry out this mapping by transforming all single-molecule operators, say $\hat{\Omega}$, according to the standard recipe,

$$\hat{\Omega} \to \sum_{i,j} \langle i|\hat{\Omega}|j\rangle \hat{\mathcal{B}}_i^\dagger \hat{\mathcal{B}}_j, \tag{6.3}$$

where $\hat{\mathcal{B}}_i$ are bosonic operators that annihilate a molecule (not an exciton) in a *vibronic* state $|i\rangle$. For convenience, we use the vibrational eigenstates of the ground electronic state, $|\varphi_i^{(g)}\rangle$, as a basis for the excited electronic state. This yields (see Supplementary Information in Ref. 90 Section 1 for a step-by-step derivation of the bosonic Hamiltonian)

$$\begin{aligned}\hat{H} =& \omega_c \hat{a}^\dagger \hat{a} + \sum_i^m \omega_{g,i} \hat{b}_i^\dagger \hat{b}_i + \sum_i^m \omega_{e,i} \hat{B}_i^\dagger \hat{B}_i + \sum_{i\neq j}^m \langle \varphi_i^{(g)}|\hat{V}_{eg}|\varphi_j^{(g)}\rangle \hat{B}_i^\dagger \hat{B}_j \\ &+ g \sum_i^m \left(\hat{B}_i^\dagger \hat{b}_i \hat{a} + \hat{B}_i \hat{b}_i^\dagger \hat{a}^\dagger \right),\end{aligned} \tag{6.4}$$

where $\hat{a}$, $\hat{b}_i$, and $\hat{B}_i$ annihilate a photon, a molecule in the vibronic state $|g, \varphi_i^{(g)}\rangle$, and a molecule in the vibronic state $|e, \varphi_i^{(g)}\rangle$, respectively. Moreover, $\hat{V}_{eg} = \hat{V}_e - \hat{V}_g$, $\omega_{e,i} = \langle \varphi_i^{(g)}|\hat{T} + \hat{V}_e(q_i)|\varphi_i^{(g)}\rangle$, and m is the size of the vibrational basis. The corresponding many-body basis states, $|n_1 n_2 \cdots n_m, n_1' n_2' \cdots n_m', N_{ph}\rangle$, are eigenstates of the non-interacting Hamiltonian (i.e., when $V_{eg,ij} = 0$ and $g = 0$), with $\sum_i^m n_i = N_g$ and $\sum_i^m n_i' = N_e$, and with N_g and N_e being the number of ground and excited molecules, respectively.

In this framework, absorption is seen as the destruction of a photon and a molecule in the initial vibronic state, to create a molecule in an excited vibronic state; each vibronic state corresponds to a harmonic oscillator "bucket" carrying a number of excitations equal to the number of molecules in such state (see Figure 6.2). This bosonization is exact for any values of N and N_{exc}, and can be easily applied beyond the approximations to the molecular Hamiltonian mentioned above. Finally, it is easy to check that the number of excitations and the number of molecules are conserved, since $\left[\hat{N}_{exc}, \hat{H}\right] = \left[\hat{N}, \hat{H}\right] = 0$, for $\hat{N}_{exc} = \hat{a}^\dagger\hat{a} + \sum_i^m \hat{B}_i^\dagger \hat{B}_i$ and $\hat{N} = \sum_i^m \hat{b}_i^\dagger \hat{b}_i + \sum_i^m \hat{B}_i^\dagger \hat{B}_i$.

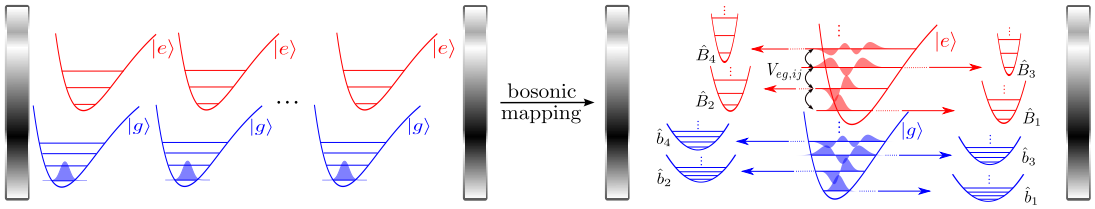

Figure 6.2: Bosonic mapping of molecular polaritons. A permutationally symmetric wavefunction (first-quantization) of the entire molecular ensemble and cavity remains in the permutationally symmetric subspace throughout its evolution generated by $\hat{H}$. Hence, a dramatic simplification of the simulation can be afforded by working in the bosonic subspace of second quantization, simply by tracking the number of molecules that occupy each of the vibronic states. We use the vibronic states $|g, \varphi_i^{(g)}\rangle$ and $|e, \varphi_i^{(g)}\rangle$ as the basis, with $|\varphi_i^{(g)}\rangle$ being the ith eigenstate of the electronic ground state molecular Hamiltonian $\hat{T} + \hat{V}_g$.

6.4 Partitioning the molecular polariton Hamiltonian

We start by partitioning the total bosonic Hamiltonian of Eq. 6.4 in terms of a zeroth-order Hamiltonian ($\hat{H}_0$), a *weak* vibronic coupling Hamiltonian ($\hat{H}_{vc}$),

and a single-molecule light-matter coupling Hamiltonian ($\hat{H}_{sm}$):

$$\begin{aligned}
\hat{H} &= \hat{H}_0 + \hat{H}_{vc} + \hat{H}_{sm} \\
\hat{H}_0 &= \omega_c \hat{a}^\dagger \hat{a} + \sum_{i=1}^{m} \omega_{g,i} \hat{b}_i^\dagger \hat{b}_i + \sum_{i=1}^{m} \omega_{e,i} \hat{B}_i^\dagger \hat{B}_i + \sum_{i,j=1}^{m'} V_{eg,ij} \hat{B}_i^\dagger \hat{B}_j + g \left(\hat{B}_1^\dagger \hat{b}_1 \hat{a} + \hat{B}_1 \hat{b}_1^\dagger \hat{a}^\dagger \right) \\
\hat{H}_{vc} &= \sum_{i=1}^{m'} \sum_{j>m'}^{m} \left(V_{eg,ij} \hat{B}_i^\dagger \hat{B}_j + V_{eg,ji}^* \hat{B}_i \hat{B}_j^\dagger \right) + \sum_{i,j>m'}^{m} V_{eg,ij} \hat{B}_i^\dagger \hat{B}_j \\
\hat{H}_{sm} &= g \sum_{i>1}^{m} \left(\hat{B}_i^\dagger \hat{b}_i \hat{a} + \hat{B}_i \hat{b}_i^\dagger \hat{a}^\dagger \right).
\end{aligned} \tag{6.5}$$

This partitioning is based on an important observation: at zero-temperature, all ground-state molecules are in the $\hat{b}_1$ mode, and light-matter coupling is collectively enhanced at the FC configuration via bosonic stimulation. Therefore, the term $g(\hat{B}_1^\dagger \hat{b}_1 \hat{a} + \hat{B}_1 \hat{b}_1^\dagger \hat{a}^\dagger)$ must be included in $\hat{H}_0$, while single-molecule light-matter coupling terms ($\langle \hat{H}_{sm} \rangle \sim g$) can be considered perturbatively (see Supplementary Information in Ref. 90 Section 2 for details). Similarly, vibronic coupling terms that can lead to vibronic features in the linear response are included in $\hat{H}_0$, while weak vibronic couplings away from the FC region ($\langle \hat{H}_{vc} \rangle \sim W$) can be treated perturbatively. This can be done formally using effective-mode theory [143, 209, 210] or chain mappings [211, 212]. The partitioning of the excited vibronic modes given by m' is to some degree arbitrary and dependent on the spectral (time) resolution that one wants to account for. In quantum optics models, the absorption spectrum showcases two clear polariton peaks, hence all vibronic couplings are considered small ($m' = 1$). However, if the polariton absorption spectrum showcases vibronic peaks [54], vibronic states strongly coupled to the FC state must be included in $\hat{H}_0$, and $m' > 1$.

Similar works that rely on a partitioning of the Hamiltonian into fast and slow components include the study of polariton-assisted triplet harvesting using the variational polaron transformation [213], and the study of spontaneous emission of atoms near hybrid metal-dielectric nanostructures [214]. Moreover, our use of permutationally-symmetric vibro-polaritonic wavefunctions instead of the eigenstates of the TC model shares deep connections with previous works by Herrera and Spano [215, 216]. For example, their work considers so-called one- and two-particle

states (exciton and exciton+phonon states, respectively) that are either permutationally or non-permutationally symmetric. Our formalism generalizes this picture by including states with arbitrary number of electronic and vibrational excitations, but leaves out non-permutationally symmetric states (see Supplementary Information in Ref. 90 Section 8 for details). We argue that those states cannot be populated if the interaction with the external laser that initially pumps the system is permutationally symmetric. Inclusion of intermolecular interactions and other couplings to the total Hamiltonian in Eq. 6.1 may break this symmetry.

In the rest of the chapter we restrict ourselves to the first excitation manifold, i.e., $N_{ph} + \sum_i^m n_i' = 1$. We also simplify the notation of the many-body states so that they showcase only essential information. This is done by using the multi-particle states introduced by Philpott [217], which has been applied to the polariton system by Herrera and Spano [193], and in our CUT-E formalism [87]:

$$
\begin{aligned}
|1\rangle &= |N00\cdots0, 00\cdots0, 1\rangle \\
|e_k\rangle &= |(N-1)00\cdots0, \cdots1_k\cdots, 0\rangle \\
|g_k1\rangle &= |(N-1)\cdots1_k\cdots, 00\cdots0, 1\rangle \\
|g_ke_{k'}\rangle &= |(N-2)\cdots1_k\cdots, \cdots1_{k'}\cdots, 0\rangle \\
|g_kg_{k'}1\rangle &= |(N-2)\cdots1_k\cdots1_{k'}\cdots, 00\cdots0, 1\rangle \\
|g_kg_{k'}e_1\rangle &= |(N-2)\cdots1_k\cdots1_{k'}\cdots, 10\cdots0, 0\rangle.
\end{aligned} \tag{6.6}
$$

We show that the competition between W and g gives rise to two regimes described by vibrational relaxation ($W \ll g$) and radiative pumping ($W \gg g$). We interpret each of these relaxation mechanisms into well-known photophysical processes using perturbation theory. The cavity leakage is assumed to be much faster than each of the aforementioned relaxation rates.

6.5 Radiative pumping

Consider the case where the slowest timescale of the system is the single-molecule light-matter coupling ($W \gg g$). We can derive the radiative pumping

rate by applying Fermi's Golden Rule (FGR) with $\hat{V}_{rp} = \hat{H}_{sm}$ being a perturbation that couples the eigenstates of the unperturbed Hamiltonian $\hat{H}_{rp}^{(0)} = \hat{H}_0 + \hat{H}_{vc}$. This treatment includes all-order processes in W and first-order processes in g.

6.5.1 Radiative pumping rate

We can write the eigenstates of $\hat{H}_{rp}^{(0)}$ in the first excitation manifold as (see Supplementary Information in Ref. 90 Section 3)

$$|\xi, \{n_j\}\rangle = a_{\{n_j\}}^{(\xi)} |n_1 n_2 \cdots n_m, 00\cdots 0, 1\rangle + \sum_i^m b_{\{n_j\}}^{(\xi,i)} |(n_1 - 1) n_2 \cdots n_m, \cdots 1_i \cdots, 0\rangle,$$

$$\hat{H}_{rp}^{(0)} |\xi, \{n_j\}\rangle = \omega_{\xi,\{n_j\}} |\xi, \{n_j\}\rangle \tag{6.7}$$

where $|\xi\rangle$ are polaritons and dark vibronic states, $\{n_j\}$ are the number of electronic ground-state molecules on each vibrational state, $a_{\{n_j\}}^{(\xi)}$ are photonic Hopfield coefficients, and $b_{\{n_j\}}^{(\xi,i)}$ are the matter Hopfield coefficients.

Although these eigenstates are dressed by *all* vibronic processes (including the slow ones given by W), we can define an initial dark state that corresponds to one excited molecule in a fully Stokes-shifted configuration with negligible overlap with the FC state (the lowest vibrational state of the molecular excited PES),

$$|ss\rangle = \sum_{i>1}^m c_{exc}^{(i)} |e_i\rangle, \quad \hat{H}_{rp}^{(0)} |ss\rangle \approx \omega_{ss} |ss\rangle. \tag{6.8}$$

This dark state is an incoherent exciton that can couple to the cavity mode via single-molecule light-matter coupling $\hat{H}_{sm}$ (despite the oxymoron of an "emissive dark state", we will continue using this terminology since it is widespread in the molecular polaritonics literature), and therefore differs from the dark states of the TC model whose couplings to the cavity mode vanish exactly [154,159,218,219] (see Supplementary Information in Ref. 90 Section 4 for a detailed comparison).

The FGR rate from $|ss\rangle$ to *all* possible eigenstates $|\xi, \{n_j\}\rangle$ yields (see Supplementary Information in Ref. 90 Section 5 for details)

$$\Gamma_{rp} = 2\pi g^2 \sum_\xi \sum_{j>1}^m |a_{1_j}^{(\xi)}|^2 |c_{exc}^{(j)}|^2 \frac{\gamma_\xi / \pi}{(\omega_\xi - (\omega_{ss} - \omega_{g,j}))^2 + \gamma_\xi^2}, \tag{6.9}$$

where we have used $\omega_{\xi,\{1_j\}} = \omega_\xi + \omega_{g,j}$, with $\omega_{g,j}$ being the frequency of the phonon created during the emission. In the derivation we have also summed over all final

eigenstates of $\hat{H}_{rp}^{(0)}$, which have a finite resolution γ_ξ due to finite cavity lifetime κ (molecular dissipation is not needed because every molecular interaction is in principle accounted for by Eq. 6.1). Finally, the coefficients $|c_{exc}^{(j)}|^2$ are FC factors associated with the bare molecular emission profile [179]

$$\sigma_{em}^{(out)}(\omega) = \sum_{j>1}^{m} |c_{exc}^{(j)}|^2 \delta(\omega - (\omega_{ss} - \omega_{g,j})), \tag{6.10}$$

which assumes that the same Stokes-shifted state is reached inside and outside the cavity [154, 159, 218, 219]. This is a good approximation given the separation of timescales between processes generated by $\hat{H}_{rp}^{(0)}$ and those generated by $\hat{V}_{rp}$.

From this analysis, it is clear that the radiative pumping rate in Eq. 6.9 is proportional to the fluorescence of a bare molecule at frequencies $\omega_{ss} - \omega_{g,j}$ into *all* final states $|\xi\rangle$ weighted by their Hopfield coefficient, as expected according to phenomenological and experimental works [43, 159, 190, 191, 220]. Although we cannot explicitly show it here due to the single-mode description of the cavity, radiative pumping can pump any polariton mode that is resonant with the molecular emission in multimode cavities.

6.5.2 Radiative pumping as an overlap between spectroscopic observables

A more intuitive understanding of Γ_{rp} is obtained by writing Eq. 6.9 in terms of the polaritonic linear spectroscopic observables in Refs. 145, 178, 185 (see Supplementary Information in Ref. 90 Section 3.1):

$$\Gamma_{rp} = \int d\omega \Gamma_{rp}(\omega) = \frac{2g^2}{\kappa} \int d\omega \sigma_{em}(\omega) \left[A(\omega) + 2T(\omega)\right], \tag{6.11}$$

with $A(\omega)$, and $T(\omega)$ being the polariton absorption and transmission spectra in the $N \to \infty$ limit (in the absence of single-molecule coupling effects), and the prefactor $g^2/\kappa \propto \mathcal{Q}/\mathcal{V}_c$ encodes cavity-enhancement of the molecular emission, where $\mathcal{Q}$ is the cavity-quality factor and $\mathcal{V}_c$ is the cavity mode volume. This linear optics description provides the rate of radiative decay of $|ss\rangle$ into all $|\xi\rangle$ states regardless of their photonic character, and divides it into transmitted and re-absorbed components. In other words, it accounts for the rate from $|ss\rangle$ to

polariton states and also the subsequent rates from polaritons back to dark states or out of the cavity.

6.5.3 Radiative pumping: numerical simulations

We consider a chromophore described by a two-mode linear vibronic coupling Hamiltonian [221],

$$\hat{H}_m = \sum_{i=1}^{2} \omega_{\nu,i} \hat{\beta}_i^\dagger \hat{\beta}_i + \sum_{i=1}^{2} \left[\omega_0 + \omega_{\nu,i} \sqrt{s_i} \left(\hat{\beta}_i^\dagger + \hat{\beta}_i \right) \right] |e\rangle\langle e|, \tag{6.12}$$

where $\hat{\beta}_i$ annihilates a *phonon* in the vibrational mode ith, with frequency $\omega_{\nu,i}$, and vibronic coupling determined by the Huang-Rhys (HR) factor s_i. These operators must not be confused with the operators $\hat{b}_i$ and $\hat{B}_i$ used in Section 6.3, which annihilate *molecules* instead of excitations (see Supplementary Information in Ref. 90 Section 6 for PESs).

We choose the molecule to have strong vibronic coupling to a high and a low frequency modes with parameters $\omega_{\nu,1} = 12.5\omega_{\nu,2} = 0.01$ a.u. In Figure 6.3 we calculate the radiative pumping rate for $\sqrt{s_1} = 1$, $\omega_c = \omega_0 + \omega_{\nu,1}s_1 + \omega_{\nu,2}s_2$ (cavity resonant with the molecular vertical transition), $g\sqrt{N} = 0.04$ a.u., $N = 10^5$ molecules, $\gamma_\xi = \gamma = 0.0015$ a.u., and different values of $\sqrt{s_2}$. Notice that the computational cost of our calculations does not scale with the number of molecules. We show how radiative pumping increases when Stokes shift causes a significant overlap between the bare molecular emission and the lower polariton band.

Due to the large Stokes shift s_2, the lower polariton branch does not significantly overlap with the bare molecular absorption. As we show in the next section, this implies that most of the light emitted from dark states is transmitted out of the cavity, and $\Gamma_{rp}(\omega)$ essentially yields the polariton photoluminescence spectrum.

6.5.4 Polariton-assisted photon recycling

Using Equation 34 from Ref. 178 relating the linear spectroscopy of polaritons to the molecular susceptibilities, we can obtain an expression for the ratio of

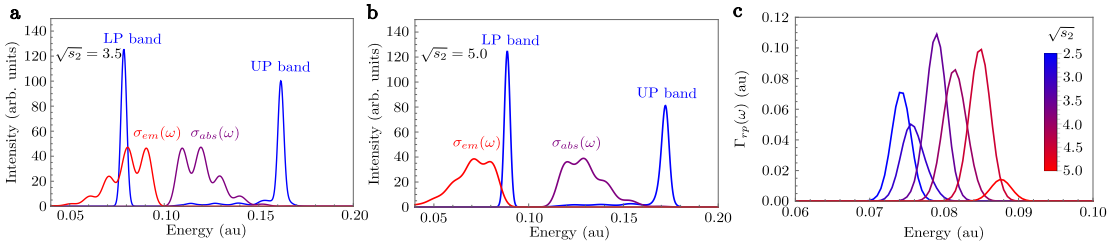

Figure 6.3: Radiative pumping for different values of Stokes shift ($\propto s_2$). a,b) Polariton bands from the polariton absorption and transmission spectra $A(\omega) + 2T(\omega)$, bare molecular absorption profile $\sigma_{abs}(\omega)$, and bare molecular emission profile $\sigma_{em}(\omega)$, for $\sqrt{s_2} = 3.5$ (a) and $\sqrt{s_2} = 5.0$ (b). c) The frequency-resolved radiative pumping $\Gamma_{rp}(\omega)$ is proportional to the overlap between the polariton bands and the bare molecular emission. The total radiative pumping rate Γ_{rp} is the integral of $\Gamma_{rp}(\omega)$.

the light emitted by dark states that is re-absorbed and transmitted [89],

$$\frac{A(\omega)}{2T(\omega)} = \mathcal{Q}\mathrm{Im}\left[\chi^{(1)}(\omega)\right], \tag{6.13}$$

where $\chi^{(1)}(\omega)$ is the bare absorption spectrum of the ensemble ($\propto Ng^2$). This demonstrates that the light emitted by incoherent excitons can be re-absorbed by other molecules inside the cavity, a phenomenon which is enhanced by the collective coupling and the cavity-quality factor. This process has recently been characterized as polariton-assisted photon recycling [222], and has also been discussed in several previous works [43–45, 223]. It can significantly impact photoluminescence of polaritonic systems due to re-emission of the absorbed light (see Figure 6.4).

6.6 Vibrational relaxation

We obtain the vibrational relaxation rate by considering $\hat{V}_{vr} = \hat{H}_{vc}$ as a perturbation that causes transitions between eigenstates of $\hat{H}_{vr}^{(0)} = \hat{H}_0 + \hat{H}_{sm}$. This treatment includes first-order processes in W and all-order processes in g. This is a natural description when collective light-matter coupling is reached with a few tens of molecules or less, or when the molecular process of interest is much slower than radiative decay (e.g., reverse intersystem crossing in organic molecules [213, 224]). We show that this strategy generalizes the vibrational relaxation rate in the linear

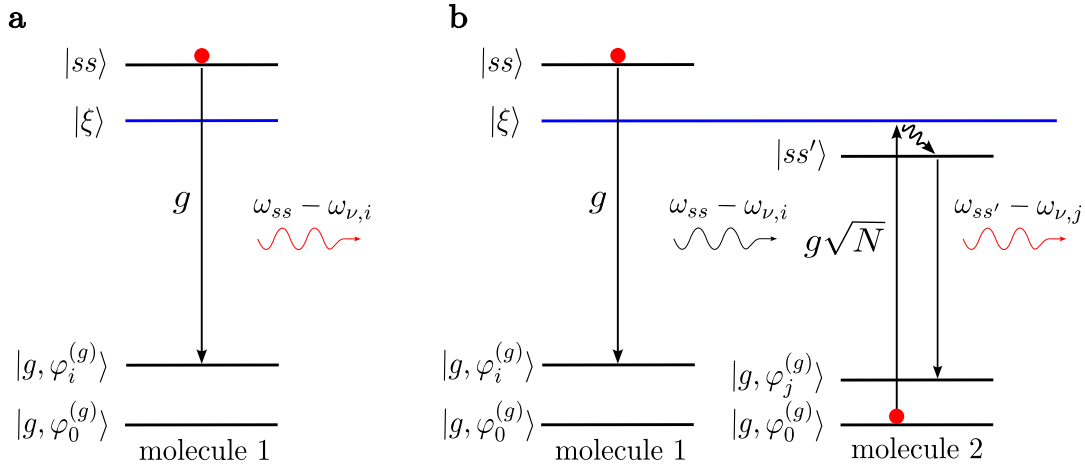

Figure 6.4: Radiative pumping and polariton-assisted photon recycling mechanisms. a) Radiative pumping: emission from a Stokes-shifted molecule $|ss\rangle$ through a polariton state $|\xi\rangle$ (typically the LP). b) polariton-assisted photon recycling: light emitted from dark states is re-absorbed before it leaks out of the cavity via collective strong light-matter coupling ($g\sqrt{N} > \kappa$). This excitation creates a new Stokes-shifted molecule $|ss'\rangle$ that can subsequently re-emit. This occurs if the bare emission and absorption spectra of the material overlap.

vibronic coupling limit originally studied by Litinskaia et al. [159], and compare it with the radiative pumping rate derived in the last section.

6.6.1 Vibrational relaxation in the weak vibronic coupling limit

The Hamiltonian $\hat{H}_{vr}^{(0)}$ can be diagonalized exactly to obtain polaritons and dark states (see Supplementary Information in Ref. 90 Section 5). We calculate the FGR rate from a dark initial eigenstate with a single phonon in the vibrational state k

$$|D_k\rangle = \sqrt{\frac{N-1}{N}}|e_k\rangle - \sqrt{\frac{1}{N}}|g_k e_1\rangle. \tag{6.14}$$

Notice that this dark state differs from the incoherent excitons considered by Litinskaia and coworkers (see Eq. 6.8) [159], mainly in the $1/\sqrt{N}$ correction that arises due to the single-molecule coupling g. We will show that this $1/\sqrt{N}$ correction is crucial since it gives rise to a non-trivial Raman scattering process (A. Koner et al., in preparation) that contributes to the vibrational relaxation rate, and is not

taken into account in previous works [158, 159].

Assuming no detuning between cavity and exciton frequencies, the vibrational relaxation rate yields

$$\Gamma_{\xi_\pm \leftarrow D_k} = 2\pi \left(\frac{N-1}{2N^2}\right) \sum_{i>1\neq k}^{m} |V_{eg,ik}|^2 \frac{\gamma_{\xi_\pm}/\pi}{(\omega_{g,i} - \omega_{g,k} \pm g\sqrt{N})^2 + \gamma_{\xi_\pm}^2} + 2\pi \left(\frac{1}{2N^2}\right) \sum_{i>1\neq k}^{m} |V_{eg,i1}|^2 \frac{\gamma_{\xi_\pm}/\pi}{(\omega_{g,i} - \omega_{g,1} \pm g\sqrt{N})^2 + \gamma_{\xi_\pm}^2}. \tag{6.15}$$

Here, we have ignored terms that correspond to couplings from Stokes-shifted configurations directly into the FC region (excited state vibrational recurrences, which are unlikely after Stokes shift has ensued given that they involve the recoherence of a large number of vibrational modes back into the FC region), and processes in which a phonon is produced in the same vibrational mode k as the initial dark state. This is a good approximation in the vibrational bath limit (see Supplementary Information in Ref. 90 Section 5). Equation 6.15 is a generalization to the well-known vibrational relaxation rate by Litinskaia [158, 159, 190], and essentially reduces to it upon consideration of four additional assumptions. Two of them are: (a) removal of the second term (not really justified) and (b) in the *linear* vibronic coupling limit. This can be easily seen by noticing that the sum over vibronic *states* $i > 1$ can be changed for a sum over vibrational *modes*, given that each mode of the vibrational bath will contribute with a single state:

$$\Gamma_{\xi_\pm \leftarrow D_k} \approx 2\pi \left(\frac{N-1}{2N^2}\right) \sum_{i} \omega_{\nu,i}^2 s_i \frac{\gamma_{\xi_\pm}/\pi}{(\omega_{\nu,i} \pm g\sqrt{N})^2 + \gamma_{\xi_\pm}^2}. \tag{6.16}$$

The other two additional assumptions are: (c) $(N-1)/N^2 \approx 1/N$ when $N \gg 1$, (d) there are many photon modes in the cavity (given the single-mode assumption throughout this chapter, we do not attempt further comparison). Regardless, the main physics we are interested in is the second term in Eq. 6.15 which has been missing in the literature throughout.

6.6.2 Vibrational relaxation vs radiative pumping

We now interpret the mechanisms involved in the vibrational relaxation rate. We do so by looking at the initial and final states in the FGR rate that

generate each of the two terms in Eq. 6.15 (see Supplementary Information in Ref. 90 Section 7 for a more detailed analysis). We find that the first term ($\propto \frac{N-1}{N^2}$) is a first-order process in g, and can be interpreted as single phonon emission from an incoherent exciton followed by emission, i.e., the tails of the emission spectra: $|e_k\rangle \xrightarrow{W} |e_i\rangle \xrightarrow{g} |g_i 1\rangle$. On the other hand, the second term ($\propto \frac{1}{N^2}$) is a second-order process in g that consists of the *virtual* emission from an incoherent exciton, followed by polariton-assisted Raman scattering into a lower energy polariton (see Figure 6.5): $|e_k\rangle \xrightarrow{g} |g_k 1\rangle \xrightarrow{g\sqrt{N-1}} |g_k e_1\rangle \xrightarrow{W} |g_k e_i\rangle \xrightarrow{g} |g_k g_i 1\rangle$; the frequency of the actual photon emission (via the polariton) is equal to the emission frequency of the first molecule minus the energy of the phonons created in the second molecule. Notice that this is just the coherent version of polariton-assisted photon recycling. From this we conclude that the first term in Eq. 6.15 is already contained in the radiative pumping rate. A more interesting scenario arises when strong vibronic coupling is present, since it is the more realistic scenario with most molecular systems, and it allows vibrational relaxation to include third and higher order processes in g (see Supplementary Information in Ref. 90 Section 8). However, based on the analysis detailed in the Supplementary Information of Ref. 90 Section 8 and in Chapter 3, each of these scattering processes would be penalized by a $1/N$ factor *in the rate*, rendering those processes relevant only for small N, long-time dynamics, or large number of excitations.

Based on the analysis above, we can characterize each mechanism that contributes to the vibrational relaxation rate by taking the single-molecule coupling g as a perturbation (see Sec. 6.5), granted that all orders of perturbation theory are considered (fluorescence, Raman, and hyper-Raman processes [225]). In the next section we study the polariton-assisted scattering mechanism of Figure 6.5 in the strong vibronic coupling regime using the aforementioned approach.

6.6.3 Polariton-assisted Raman scattering

To calculate the polariton-assisted Raman scattering rate in the strong vibronic coupling regime, we partition the Hamiltonian as $\hat{H} = \hat{H}_{rp}^{(0)} + \hat{V}_{rp}$. As in Section 6.5, the Stokes-shifted state $|ss\rangle$ is chosen as the initial dark state.

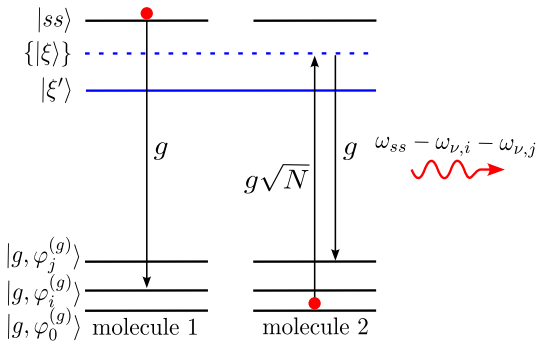

Figure 6.5: Polariton-assisted Raman scattering mechanism. Second-order process in the single-molecule light-matter coupling g that results in the creation of a polariton $|\xi'\rangle$ and vibrational excitations ω_{ν_i} and ω_{ν_j} in two different molecules. It is fundamentally different to radiative pumping and can be regarded as a coherent version of the polariton-assisted photon recycling mechanism in Figure 6.4b.

Second-order perturbation theory on $\hat{V}_{rp} = \hat{H}_{sm}$ yields the polariton-assisted Raman scattering rate when summing over all final states that have two additional ground-state molecules with phonons (the first molecule acquires phonons via virtual emission and the second molecule acquires phonons via Raman scattering),

$$\Gamma_{scatt} = 2\pi \sum_{\xi',\{n'_j\}} |A_{\xi',\{n'_j\}\leftarrow ss}|^2 \frac{\gamma_{\xi'}/\pi}{(\omega_{\xi',\{n'_j\}} - \omega_{ss})^2 + \gamma_{\xi'}^2}$$
$$A_{\xi',\{n'_j\}\leftarrow ss} = \sum_{\xi,\{n_j\}} \frac{\langle \xi', \{n'_j\}|\hat{H}_{sm}|\xi, \{n_j\}\rangle\langle \xi, \{n_j\}|\hat{H}_{sm}|ss\rangle}{\omega_{\xi,\{n_j\}} - \omega_{ss} + i\gamma_\xi}. \tag{6.17}$$

Here, $|\xi, \{n_j\}\rangle$ are the eigenstates of $\hat{H}_{rp}^{(0)}$. The scattering rate is fairly easy to calculate in the large N (yet finite) limit, even in the presence of strong vibronic coupling (see details in the Appendix I).

We compute Γ_{scatt} for the model system introduced in Section 6.5, with parameters $\omega_{\nu,1} = 10\omega_{\nu,2} = 0.01$ a.u., $\sqrt{s_1} = 0.3$, $\omega_c = \omega_0 + \omega_{\nu,1}s_1 + \omega_{\nu,2}s_2$, $g\sqrt{N} = 0.035$ a.u., $N = 10^5$ molecules, $\gamma_\xi = \gamma = 0.0015$ a.u., and different values of $\sqrt{s_2}$.

Besides the phonons released during the virtual emission $\omega_{\nu,i}$ from the incoherent dark state $|ss\rangle$, the scattering mechanism also creates phonons via Raman scattering on a second molecule $\omega_{\nu,j}$. As a consequence, the scattering relaxation rate does not rely on the overlap between the bare emission and the lower polari-

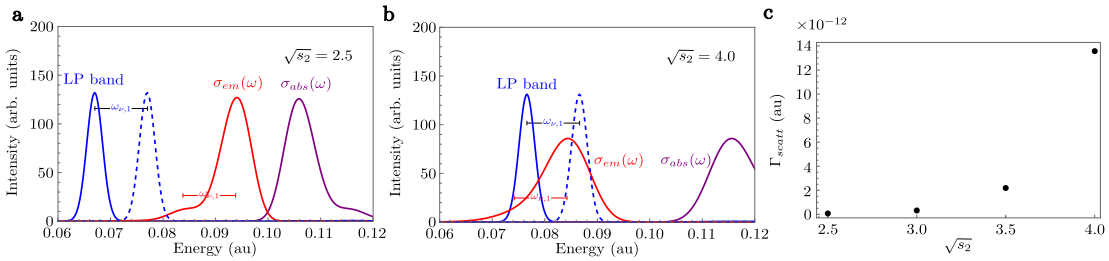

Figure 6.6: Polariton Raman-scattering rate for different values of Stokes shift ($\propto s_2$). a,b) Polariton bands from the polariton transmission spectra $T(\omega)$, bare molecular absorption profile $\sigma_{abs}(\omega)$, and bare molecular emission profile $\sigma_{em}(\omega)$, for $\sqrt{s_2} = 2.5$ (a) and $\sqrt{s_2} = 4.0$ (b). c) decay rate from dark to lower polariton via Raman scattering Γ_{scatt}. The rate increases when the energy difference between the emission and the lower polariton corresponds to the vibrational excitation created in the Raman process, e.g., $\omega_{\nu,1}$. Yet, Γ_{scatt} is quite low since the broadening γ is quite large, there are no polaritons to *resonantly* scatter from due to the single-mode nature of the model, and we do not include non-Condon effects.

ton band. Instead, it requires that the difference between the emission and the lower polariton is compensated by the vibrational excitation created in the Raman process, i.e., $\omega_{\xi'} + \omega_{\nu_j} - (\omega_{ss} - \omega_{\nu_i})$ (note that i is a vibrational *state* that can represent single or multiple phonons). We illustrate this phenomenon by shifting the lower polariton by $\omega_{\nu,1}$ in Figure 6.6b (blue-dashed band), although all vibrational states coupled to the FC region (including those with more than one phonon) contribute to the rate. Importantly, ω_{ν_i} also produces vibronic progressions in the bare molecular emission spectrum. This means that resonant conditions for radiative pumping and Raman scattering always coexist, making it challenging to identify which relaxation mechanism is in play. This explains why Tichauer and coworkers found that vibrational relaxation and radiative pumping are driven by similar vibrational modes [226].

Finally, we believe the scattering mechanism here shown corresponds to the vibrationally-assisted scattering (VAS) mechanism [226–230]. Yet, our calculations in Figure 6.6c show that Γ_{scatt} is quite weak due to its $1/N^2$ dependence. It may be the case that the low values we obtain are a consequence of considering only off-resonant Raman scattering (see Figure 6.6a), and ignoring non-Condon effects. We expect the rate to increase for multimode cavities since resonant scattering can be mediated by the entire lower polariton branch. Our future works will focus

on generalizing our formalism to account for the multi-mode nature of the optical cavity.

6.7 Summary

We have used an exact bosonic mapping of the generalized Holstein-Tavis-Cummings Hamiltonian based on its projection to a subspace of permutationally symmetric vibronic states. The resulting bosonic Hamiltonian describes molecular polaritons for arbitrary internal vibrational structure, number of molecules, and number of excitations [141, 205–208]. Here we show that this formalism is ideal to study molecular polaritons beyond the $N \to \infty$ limit numerically and analytically. In particular, we use it to the study vibrational relaxation and radiative pumping mechanisms. We find that the relaxation mechanism in play is determined by the competition between single-molecule light-matter coupling and weak vibronic couplings, and characterize each mechanism based on their underlying photophysical processes.

We show that radiative pumping is the emission from Stokes-shifted molecules into the polaritons, and can be divided into transmitted and re-absorbed components. The latter leads to a polariton-assisted photon recycling mechanism. On the other hand, we show that vibrational relaxation includes radiative pumping as well as higher-order processes in the single-molecule light-matter coupling g; up to second-order processes in the weak linear vibronic coupling regime. We find that each order in g is penalized by a $1/N$ factor in the rate, suggesting that the main contribution to the vibrational relaxation rate comes from radiative pumping. Finally, we classify the second-order processes in g as either polariton-assisted photon recycling or polariton-assisted Raman scattering. The latter occurs when the frequency difference between the bare emission and the polariton state coincides with the vibrational excitation created in the Raman process.

Our work constitutes a rigorous derivation and comparison between these polariton relaxation rates, offering a path forward to study molecular polaritons beyond the $N \to \infty$ limit. Finally, since the bosonic formalism already allows

arbitrary number of excitations, we believe it is ideal to study processes such as exciton-polariton condensation.

6.8 Acknowledgements

Chapter 6, in full, is a reprint of the material in preparation for publication whose authors are Juan B. Pérez-Sánchez and Joel Yuen-Zhou. The dissertation author was the primary investigator and author of this paper. This work was supported by the Air Force Office of Scientific Research (AFOSR) through the Multi-University Research Initiative (MURI) program no. FA9550-22-1-0317. We also thank Arghadip Koner, Kai Schwennicke, Stéphane Kéna-Cohen, Gerrit Groenhof, and Jonathan Keeling for useful discussions.

Chapter 7

Conclusions and outlook

We have conducted a series of works addressing some of the most important challenges and making significant contributions to the field of organic exciton polaritons. Our research demonstrates how single molecules under strong coupling can exhibit non-trivial chemical and optical properties. However, we show that these effects may disappear when strong coupling occurs in the collective regime, where the light-matter coupling per molecule can be treated perturbatively. This underscores the importance of considering the large number of molecules participating in the coupling.

To understand when non-trivial polaritonic effects can arise in the collective regime, we developed a formalism called Collective dynamics using Truncated Equations (CUT-E), which accounts for an arbitrary number of molecules and the internal vibrational degrees of freedom of each molecule. We have systematically improved our theory to incorporate realistic features such as inhomogeneous broadening and a large number of excitations. The picture that arises from our formalism is that of an ensemble of excitons that can collectively couple to the cavity mode only while they retain inter-exciton coherence (bright state). Conversely, excitons can only couple through single-molecule interactions upon excited state vibrational dynamics and decoherence (dark states). This implies that chemical applications depend on the dynamics of these dark states, while polaritons primarily assist in creating initial conditions that influence the reaction yield.

Although our theories align with several experimental and theoretical works,

they challenge the notion that collective strong coupling leads to non-trivial effects capable of modifying chemical reactivity. In the limit where the collective light-matter interaction is strong but the single-molecule contributions are negligible, the initial state preparation assisted by polaritons can be understood simply as an optical filtering effect. Consequently, chemical dynamics can be reproduced using weak-tailored laser pulses acting on the bare molecules. To achieve nonlinear polaritonic effects, the single-molecule coupling must be considered. Although this coupling is weaker than the collective one, it can be enhanced by increasing the cavity-$\mathcal{Q}$ factor, decreasing the volume of confinement, and appropriately modifying the photonic density of states via the collective component of the light-matter coupling. We demonstrate that well-known relaxation mechanisms in organic exciton polaritons, such as radiative pumping and vibrational relaxation, are examples of these non-trivial effects. They play a crucial role in most polaritonic applications, such as polariton transport and polariton condensation. We reinterpret these mechanisms from a molecular spectroscopy perspective: they correspond to photophysical processes like fluorescence, polariton-assisted Raman scattering, polariton-assisted photon recycling, and higher-order processes from incoherent excitons. These processes enable applications like long-range resonance energy transfer and modifications of matter processes occurring beyond photoluminescence timescales.

To date, several experimental observations remain unexplained by our theories. To continue progress in the field, it is crucial to identify the missing elements that could change the paradigm established in our works. These elements include multiple cavity modes and finite temperature effects. It is paramount to determine what polaritons can achieve and their advantages compared to analogous phenomena in the weak coupling regime.

Bibliography

[1] Nicolaas Bloembergen and Ahmed H Zewail. Energy redistribution in isolated molecules and the question of mode-selective laser chemistry revisited. *J. Phys. Chem.*, 88(23):5459–5465, 1984.

[2] Moshe Shapiro and Paul Brumer. The equivalence of unimolecular decay product yields in pulsed and cw laser excitation. *J. Chem. Phys.*, 84:540–541, 1986.

[3] David J. Tannor and Stuart A. Rice. Control of selectivity of chemical reaction via control of wave packet evolution. *J. Chem. Phys.*, 83:5013–5018, 1985.

[4] Richard S. Judson and Herschel Rabitz. Teaching lasers to control molecules. *Phys. Rev. Lett.*, 68:1500–1503, 1992.

[5] Ignacio R. Solá, Bo Y. Chang, Jesús Santamaría, Vladimir S. Malinovsky, and Jeffrey L. Krause. Selective excitation of vibrational states by shaping of light-induced potentials. *Phys. Rev. Lett.*, 85:4241–4244, 2000.

[6] Michael Reitz and Claudiu Genes. Floquet engineering of molecular dynamics via infrared coupling. *J. Chem. Phys.*, 153(23):234305, 2020.

[7] R.M. Bowman, M. Dantus, and A.H. Zewail. Femtosecond transition-state spectroscopy of iodine: From strongly bound to repulsive surface dynamics. *Chem. Phys. Lett.*, 161:297–302, 1989.

[8] Kerry J. Vahala. Optical microcavities. *Nature*, 424(6950):839–846, 2003.

[9] Parinda Vasa and Christoph Lienau. Strong light–matter interaction in quantum emitter/metal hybrid nanostructures. *ACS Photonics*, 5(1):2–23, 2018.

[10] D. N. Basov, M. M. Fogler, and F. J. García de Abajo. Polaritons in van der waals materials. *Science*, 354(6309):aag1992, 2016.

[11] Raphael F. Ribeiro, Luis A. Martínez-Martínez, Matthew Du, Jorge Campos-Gonzalez-Angulo, and Joel Yuen-Zhou. Polariton chemistry: controlling molecular dynamics with optical cavities. *Chem. Sci.*, 9:6325–6339, 2018.

[12] Anton Frisk Kockum, Adam Miranowicz, Simone De Liberato, Salvatore Savasta, and Franco Nori. Ultrastrong coupling between light and matter. *Nat. Rev. Phys.*, 1(1):19–40, 2019.

[13] Felipe Herrera and Jeffrey Owrutsky. Molecular polaritons for controlling chemistry with quantum optics. *J. Chem. Phys.*, 152(10):100902, 2020.

[14] Tao E. Li, Bingyu Cui, Joseph E. Subotnik, and Abraham Nitzan. Molecular polaritonics: Chemical dynamics under strong light–matter coupling. *Annu. Rev. Phys. Chem.*, 73(Volume 73, 2022):43–71, 2022.

[15] Kenji Hirai, James A. Hutchison, and Hiroshi Uji-i. Molecular chemistry in cavity strong coupling. *Chem. Rev.*, 123(13):8099–8126, 2023. PMID: 37390295.

[16] Thomas W. Ebbesen, Angel Rubio, and Gregory D. Scholes. Introduction: Polaritonic chemistry. *Chem. Rev.*, 123(21):12037–12038, 2023. PMID: 37936399.

[17] Wei Xiong. Molecular vibrational polariton dynamics: What can polaritons do? *Acc. Chem. Res.*, 56(7):776–786, 2023. PMID: 36930582.

[18] Rahul Bhuyan, Jürgen Mony, Oleg Kotov, Gabriel W. Castellanos, Jaime Gómez Rivas, Timur O. Shegai, and Karl Börjesson. The rise and current status of polaritonic photochemistry and photophysics. *Chem. Rev.*, 123(18):10877–10919, 2023. PMID: 37683254.

[19] Denis G. Baranov, Christian Schäfer, and Maxim V. Gorkunov. Toward molecular chiral polaritons. *ACS Photonics*, 10(8):2440–2455, 2023.

[20] Arkajit Mandal, Michael A.D. Taylor, Braden M. Weight, Eric R. Koessler, Xinyang Li, and Pengfei Huo. Theoretical advances in polariton chemistry and molecular cavity quantum electrodynamics. *Chem. Rev.*, 123(16):9786–9879, 2023. PMID: 37552606.

[21] Bo Xiang and Wei Xiong. Molecular polaritons for chemistry, photonics and quantum technologies. *Chem. Rev.*, 124(5):2512–2552, 2024. PMID: 38416701.

[22] Rohit Chikkaraddy, Bart de Nijs, Felix Benz, Steven J. Barrow, Oren A. Scherman, Edina Rosta, Angela Demetriadou, Peter Fox, Ortwin Hess, and Jeremy J. Baumberg. Single-molecule strong coupling at room temperature in plasmonic nanocavities. *Nature*, 535:127, 2016.

[23] James A. Hutchison, Tal Schwartz, Cyriaque Genet, Eloïse Devaux, and Thomas W. Ebbesen. Modifying chemical landscapes by coupling to vacuum fields. *Angew. Chem., Int. Ed. Engl.*, 51(7):1592–1596, 2012.

[24] Hongfei Zeng, Juan B. Pérez-Sánchez, Christopher T. Eckdahl, Pufan Liu, Woo Je Chang, Emily A. Weiss, Julia A. Kalow, Joel Yuen-Zhou, and Nathaniel P. Stern. Control of photoswitching kinetics with strong light–matter coupling in a cavity. *J. Am. Chem. Soc.*, 145(36):19655–19661, 2023. PMID: 37643086.

[25] Adam D. Dunkelberger, Blake S. Simpkins, Igor Vurgaftman, and Jeffrey C. Owrutsky. Vibration-cavity polariton chemistry and dynamics. *Annu. Rev. Phys. Chem.*, 73(1):429–451, 2022.

[26] Wonmi Ahn, Johan F. Triana, Felipe Recabal, Felipe Herrera, and Blake S. Simpkins. Modification of ground-state chemical reactivity via light-matter coherence in infrared cavities. *Science*, 380(6650):1165–1168, 2023.

[27] Raphael F. Ribeiro, Luis A. Martínez-Martínez, Matthew Du, Jorge Campos-Gonzalez-Angulo, and Joel Yuen-Zhou. Polariton chemistry: controlling molecular dynamics with optical cavities. *Chem. Sci.*, 9:6325–6339, 2018.

[28] Bo Xiang, Raphael F. Ribeiro, Matthew Du, Liying Chen, Zimo Yang, Jiaxi Wang, Joel Yuen-Zhou, and Wei Xiong. Intermolecular vibrational energy transfer enabled by microcavity strong light-matter coupling. *Science*, 368(6491):665–667, 2020.

[29] Teng-Teng Chen, Matthew Du, Zimo Yang, Joel Yuen-Zhou, and Wei Xiong. Cavity-enabled enhancement of ultrafast intramolecular vibrational redistribution over pseudorotation. *Science*, 378(6621):790–794, 2022.

[30] J. A. Campos-Gonzalez-Angulo, Y. R. Poh, M. Du, and J. Yuen-Zhou. Swinging between shine and shadow: Theoretical advances on thermally activated vibropolaritonic chemistry. *J. Chem. Phys.*, 158(23):230901, 2023.

[31] Arkajit Mandal, Michael A.D. Taylor, Braden M. Weight, Eric R. Koessler, Xinyang Li, and Pengfei Huo. Theoretical advances in polariton chemistry and molecular cavity quantum electrodynamics. *Chem. Rev.*, 123(16):9786–9879, 2023.

[32] Felipe Herrera and Jeffrey Owrutsky. Molecular polaritons for controlling chemistry with quantum optics. *J. Chem. Phys.*, 152(10):100902, 2020.

[33] Javier Galego, Francisco J Garcia-Vidal, and Johannes Feist. Suppressing photochemical reactions with quantized light fields. *Nat. Commun.*, 7:13841, 2016.

[34] Mónica Sánchez-Barquilla, Antonio I. Fernández-Domínguez, Johannes Feist, and Francisco J. García-Vidal. A theoretical perspective on molecular polaritonics. *ACS Photonics*, 9(6):1830–1841, 2022.

[35] Michael Reitz, Christian Sommer, and Claudiu Genes. Langevin approach to quantum optics with molecules. *Phys. Rev. Lett.*, 122:203602, 2019.

[36] Tomohiro Ishii, Fatima Bencheikh, Sébastien Forget, Sébastien Chénais, Benoît Heinrich, David Kreher, Lydia Sosa Vargas, Kiyoshi Miyata, Ken Onda, Takashi Fujihara, Stéphane Kéna-Cohen, Fabrice Mathevet, and Chihaya Adachi. Enhanced light–matter interaction and polariton relaxation by the control of molecular orientation. *Adv. Opt. Mater.*, 9(22):2101048, 2021.

[37] Christopher R. Gubbin, Stefan A. Maier, and Stéphane Kéna-Cohen. Low-voltage polariton electroluminescence from an ultrastrongly coupled organic light-emitting diode. *Appl. Phys. Lett.*, 104(23):233302, 2014.

[38] Tao E. Li and Sharon Hammes-Schiffer. Qm/mm modeling of vibrational polariton induced energy transfer and chemical dynamics. *J. Am. Chem. Soc.*, 145(1):377–384, 2023.

[39] Sindhana Pannir-Sivajothi, Jorge A. Campos-Gonzalez-Angulo, Luis A. Martínez-Martínez, Shubham Sinha, and Joel Yuen-Zhou. Driving chemical reactions with polariton condensates. *Nat. Commun.*, 13(1):1645, 2022.

[40] Markus Kowalewski, Kochise Bennett, and Shaul Mukamel. Cavity femtochemistry: Manipulating nonadiabatic dynamics at avoided crossings. *J. Phys. Chem. Lett.*, 7:2050–2054, 2016.

[41] Norah M. Hoffmann, Lionel Lacombe, Angel Rubio, and Neepa T. Maitra. Effect of many modes on self-polarization and photochemical suppression in cavities. *J. Chem. Phys.*, 153(10):104103, 2020.

[42] Hoi Ling Luk, Johannes Feist, J. Jussi Toppari, and Gerrit Groenhof. Multiscale molecular dynamics simulations of polaritonic chemistry. *J. Chem. Theory Comput.*, 13(9):4324–4335, 2017.

[43] David M. Coles, Niccolo Somaschi, Paolo Michetti, Caspar Clark, Pavlos G. Lagoudakis, Pavlos G. Savvidis, and David G. Lidzey. Polariton-mediated energy transfer between organic dyes in a strongly coupled optical microcavity. *Nat. Mater.*, 13(7):712–719, 2014.

[44] Rocío Sáez-Blázquez, Johannes Feist, Francisco J. García-Vidal, and Antonio I. Fernández-Domínguez. Theory of energy transfer in organic nanocrystals. *Adv. Opt. Mater.*, 8(23):2001447, 2020.

[45] Matthew Du, Luis A. Martínez-Martínez, Raphael F. Ribeiro, Zixuan Hu, Vinod M. Menon, and Joel Yuen-Zhou. Theory for polariton-assisted remote energy transfer. *Chem. Sci.*, 9:6659–6669, 2018.

[46] Johannes Schachenmayer, Claudiu Genes, Edoardo Tignone, and Guido Pupillo. Cavity-enhanced transport of excitons. *Phys. Rev. Lett.*, 114:196403, 2015.

[47] D. M. Myers, S. Mukherjee, J. Beaumariage, D. W. Snoke, M. Steger, L. N. Pfeiffer, and K. West. Polariton-enhanced exciton transport. *Phys. Rev. B*, 98:235302, 2018.

[48] Georgi Gary Rozenman, Katherine Akulov, Adina Golombek, and Tal Schwartz. Long-range transport of organic exciton-polaritons revealed by ultrafast microscopy. *ACS Photonics*, 5(1):105–110, 2018.

[49] Ding Xu, Arkajit Mandal, James M. Baxter, Shan-Wen Cheng, Inki Lee, Haowen Su, Song Liu, David R. Reichman, and Milan Delor. Ultrafast imaging of polariton propagation and interactions. *Nat. Commun.*, 14(1):3881, 2023.

[50] Enes Suyabatmaz and Raphael F. Ribeiro. Vibrational polariton transport in disordered media. *J. Chem. Phys.*, 159(3):034701, 2023.

[51] Ilia Sokolovskii and Gerrit Groenhof. Photochemical initiation of polariton-mediated exciton propagation. *Nanophotonics*, 2024.

[52] Jingyu Liu and Yao Yao. Exciton transport coherent with upper and lower polaritons, 2024.

[53] Hui Deng, Hartmut Haug, and Yoshihisa Yamamoto. Exciton-polariton bose-einstein condensation. *Rev. Mod. Phys.*, 82:1489–1537, 2010.

[54] S Kéna-Cohen and SR Forrest. Room-temperature polariton lasing in an organic single-crystal microcavity. *Nat. Photonics*, 4(6):371–375, 2010.

[55] Jonathan Keeling and Natalia G. Berloff. Exciton–polariton condensation. *Contemp. Phys.*, 52(2):131–151, 2011.

[56] KS Daskalakis, SA Maier, Ray Murray, and Stéphane Kéna-Cohen. Nonlinear interactions in an organic polariton condensate. *Nat. Mater.*, 13(3):271–278, 2014.

[57] Tim Byrnes, Na Young Kim, and Yoshihisa Yamamoto. Exciton–polariton condensates. *Nat. Phys.*, 10(11):803–813, 2014.

[58] David W. Snoke and Jonathan Keeling. The new era of polariton condensates. *Phys. Today*, 70(10):54–60, 2017.

[59] Giovanni Lerario, Antonio Fieramosca, Fábio Barachati, Dario Ballarini, Konstantinos S. Daskalakis, Lorenzo Dominici, Milena De Giorgi, Stefan A. Maier, Giuseppe Gigli, Stéphane Kéna-Cohen, and Daniele Sanvitto. Room-temperature superfluidity in a polariton condensate. *Nat. Phys.*, 13(9):837–841, 2017.

[60] Sindhana Pannir-Sivajothi, Jorge A. Campos-Gonzalez-Angulo, Luis A. Martínez-Martínez, Shubham Sinha, and Joel Yuen-Zhou. Driving chemical reactions with polariton condensates. *Nat. Commun.*, 13(1):1645, 2022.

[61] Ravindra Kumar Yadav, Sitakanta Satapathy, Prathmesh Deshmukh, Biswajit Datta, Addhyaya Sharma, Andrew H. Olsson, Junsheng Chen, Bo W. Laursen, Amar H. Flood, Matthew Y. Sfeir, and Vinod M. Menon. Direct writing of room temperature polariton condensate lattice. *Nano Lett.*, 24(16):4945–4950, 2024. PMID: 38598721.

[62] F. C. Spano. Optical microcavities enhance the exciton coherence length and eliminate vibronic coupling in j-aggregates. *J. Chem. Phys.*, 142(18):184707, 2015.

[63] Frank C. Spano. Exciton–phonon polaritons in organic microcavities: Testing a simple ansatz for treating a large number of chromophores. *J. Chem. Phys.*, 152(20):204113, 2020.

[64] Zhedong Zhang and Shaul Mukamel. Fluorescence spectroscopy of vibronic polaritons of molecular aggregates in optical microcavities. *Chem. Phys. Lett.*, 683:653–657, 2017.

[65] Raphael F. Ribeiro. Multimode polariton effects on molecular energy transport and spectral fluctuations. *Commun. Chem.*, 5(1):48, 2022.

[66] Ding Xu, Arkajit Mandal, James M. Baxter, Shan-Wen Cheng, Inki Lee, Haowen Su, Song Liu, David R. Reichman, and Milan Delor. Ultrafast imaging of polariton propagation and interactions. *Nat. Commun.*, 14(1):3881, 2023.

[67] Georg Engelhardt and Jianshu Cao. Unusual dynamical properties of disordered polaritons in microcavities. *Phys. Rev. B*, 105:064205, 2022.

[68] Oriol Vendrell and Hans-Dieter Meyer. Multilayer multiconfiguration time-dependent hartree method: Implementation and applications to a henon–heiles hamiltonian and to pyrazine. *J. Chem. Phys.*, 134(4):044135, 2011.

[69] Lionel Lacombe, Norah M. Hoffmann, and Neepa T. Maitra. Exact potential energy surface for molecules in cavities. *Phys. Rev. Lett.*, 123:083201, 2019.

[70] Ruth H. Tichauer, Johannes Feist, and Gerrit Groenhof. Multi-scale dynamics simulations of molecular polaritons: The effect of multiple cavity modes on polariton relaxation. *J. Chem. Phys.*, 154(10):104112, 2021.

[71] M. A. Sentef, M. Ruggenthaler, and A. Rubio. Cavity quantum-electrodynamical polaritonically enhanced electron-phonon coupling and its influence on superconductivity. *Sci. Adv.*, 4(11):eaau6969, 2018.

[72] Christian Schäfer, Michael Ruggenthaler, Heiko Appel, and Angel Rubio. Modification of excitation and charge transfer in cavity quantum-electrodynamical chemistry. *Proc. Natl. Acad. Sci. USA.*, 116(11):4883–4892, 2019.

[73] Dominik Sidler, Christian Schäfer, Michael Ruggenthaler, and Angel Rubio. Polaritonic chemistry: Collective strong coupling implies strong local modification of chemical properties. *J. Phys. Chem. Lett.*, 12(1):508–516, 2021.

[74] Maxim Sukharev, Joseph Subotnik, and Abraham Nitzan. Dissociation slowdown by collective optical response under strong coupling conditions. *J. Chem. Phys.*, 158(8):084104, 2023.

[75] Subhadip Mondal, Derek S. Wang, and Srihari Keshavamurthy. Dissociation dynamics of a diatomic molecule in an optical cavity. *J. Chem. Phys.*, 157(24):244109, 2022.

[76] R. Houdré, R. P. Stanley, and M. Ilegems. Vacuum-field rabi splitting in the presence of inhomogeneous broadening: Resolution of a homogeneous linewidth in an inhomogeneously broadened system. *Phys. Rev. A*, 53:2711–2715, 1996.

[77] David Wellnitz, Guido Pupillo, and Johannes Schachenmayer. Disorder enhanced vibrational entanglement and dynamics in polaritonic chemistry. *Commun. Phys.*, 5(1):120, 2022.

[78] Maxim F. Gelin, Amalia Velardo, and Raffaele Borrelli. Efficient quantum dynamics simulations of complex molecular systems: A unified treatment of dynamic and static disorder. *J. Chem. Phys.*, 155(13):134102, 2021.

[79] Kewei Sun, Cunzhi Dou, Maxim F. Gelin, and Yang Zhao. Dynamics of disordered tavis–cummings and holstein–tavis–cummings models. *J. Chem. Phys.*, 156(2):024102, 2022.

[80] Bar Cohn, Shmuel Sufrin, Arghyadeep Basu, and Lev Chuntonov. Vibrational polaritons in disordered molecular ensembles. *J. Phys. Chem. Lett.*, 13(35):8369–8375, 2022.

[81] Aleksandr G. Avramenko and Aaron S. Rury. Light emission from vibronic polaritons in coupled metalloporphyrin-multimode cavity systems. *J. Phys. Chem. Lett.*, 13(18):4036–4045, 2022.

[82] Mikhail Tokman, Alex Behne, Brandon Torres, Maria Erukhimova, Yongrui Wang, and Alexey Belyanin. Dissipation-driven formation of entangled dark states in strongly coupled inhomogeneous many-qubit systems in solid-state nanocavities. *Phys. Rev. A*, 107:013721, 2023.

[83] Georg Engelhardt and Jianshu Cao. Polariton localization and dispersion properties of disordered quantum emitters in multimode microcavities. *Phys. Rev. Lett.*, 130:213602, 2023.

[84] Antonios M. Alvertis, Raj Pandya, Claudio Quarti, Laurent Legrand, Thierry Barisien, Bartomeu Monserrat, Andrew J. Musser, Akshay Rao, Alex W. Chin, and David Beljonne. First principles modeling of exciton-polaritons in polydiacetylene chains. *J. Chem. Phys.*, 153(8):084103, 2020.

[85] Francesca Fassioli, Kyu Hyung Park, Sarah E. Bard, and Gregory D. Scholes. Femtosecond photophysics of molecular polaritons. *J. Phys. Chem. Lett.*, 12(46):11444–11459, 2021.

[86] Juan B. Pérez-Sánchez and Joel Yuen-Zhou. Polariton assisted down-conversion of photons via nonadiabatic molecular dynamics: A molecular dynamical casimir effect. *J. Phys. Chem. Lett.*, 11(1):152–159, 2020.

[87] Juan B. Pérez-Sánchez, Arghadip Koner, Nathaniel P. Stern, and Joel Yuen-Zhou. Simulating molecular polaritons in the collective regime using few-molecule models. *Proc. Natl. Acad. Sci. USA.*, 120(15):e2219223120, 2023.

[88] Juan B. Pérez-Sánchez, Federico Mellini, Joel Yuen-Zhou, and Noel C. Giebink. Collective polaritonic effects on chemical dynamics suppressed by disorder. *Phys. Rev. Res.*, 6:013222, 2024.

[89] Kai Schwennicke, Arghadip Koner, Juan B. Pérez-Sánchez, Wei Xiong, Noel C. Giebink, Marissa L. Weichman, and Joel Yuen-Zhou. When do molecular polaritons behave like optical filters?, 2024.

[90] Juan B. Pérez-Sánchez and Joel Yuen-Zhou. Radiative pumping vs vibrational relaxation of molecular polaritons: a bosonic mapping approach, 2024.

[91] Kotni Santhosh, Ora Bitton, Lev Chuntonov, and Gilad Haran. Vacuum rabi splitting in a plasmonic cavity at the single quantum emitter limit. *Nat. Commun.*, 7(1):11823, 2016.

[92] Johannes Flick and Prineha Narang. Cavity-correlated electron-nuclear dynamics from first principles. *Phys. Rev. Lett.*, 121:113002, 2018.

[93] Christian Schäfer, Michael Ruggenthaler, and Angel Rubio. Ab initio nonrelativistic quantum electrodynamics: Bridging quantum chemistry and quantum optics from weak to strong coupling. *Phys. Rev. A*, 98:043801, 2018.

[94] Javier Galego, Francisco J. Garcia-Vidal, and Johannes Feist. Cavity-induced modifications of molecular structure in the strong-coupling regime. *Phys. Rev. X*, 5:041022, 2015.

[95] Lionel Lacombe, Norah M. Hoffmann, and Neepa T. Maitra. Exact potential energy surface for molecules in cavities. *Phys. Rev. Lett.*, 123:083201, 2019.

[96] Nimrod Moiseyev, Milan Šindelka, and Lorenz S Cederbaum. Laser-induced conical intersections in molecular optical lattices. *J. Phys. B*, 41(22):221001, 2008.

[97] Markus Kowalewski, Kochise Bennett, and Shaul Mukamel. Non-adiabatic dynamics of molecules in optical cavities. *J. Chem. Phys.*, 144(5):054309, 2016.

[98] András Csehi, Gábor J. Halász, Lorenz S. Cederbaum, and Ágnes Vibók. Intrinsic and light-induced nonadiabatic phenomena in the nai molecule. *Phys. Chem. Chem. Phys.*, 19:19656–19664, 2017.

[99] Johan F. Triana, Daniel Peláez, and José Luis Sanz-Vicario. Entangled photonic-nuclear molecular dynamics of lif in quantum optical cavities. *J. Phys. Chem. A*, 122(8):2266–2278, 2018.

[100] Oriol Vendrell. Coherent dynamics in cavity femtochemistry: Application of the multi-configuration time-dependent hartree method. *Chem. Phys.*, 509:55–65, 2018. High-dimensional quantum dynamics (on the occasion of the 70th birthday of Hans-Dieter Meyer).

[101] Markus Kowalewski and Shaul Mukamel. Manipulating molecules with quantum light. *Proc. Natl. Acad. Sci. USA.*, 114(13):3278–3280, 2017.

[102] Arkajit Mandal and Pengfei Huo. Investigating new reactivities enabled by polariton photochemistry. *J. Phys. Chem. Lett.*, 10(18):5519–5529, 2019.

[103] Johannes Feist, Javier Galego, and Francisco J. Garcia-Vidal. Polaritonic chemistry with organic molecules. *ACS Photonics*, 5(1):205–216, 2018.

[104] Gerrit Groenhof and J. Jussi Toppari. Coherent light harvesting through strong coupling to confined light. *J. Phys. Chem. Lett.*, 9(17):4848–4851, 2018.

[105] J. Fregoni, G. Granucci, E. Coccia, M. Persico, and S. Corni. Manipulating azobenzene photoisomerization through strong light-molecule coupling. *Nat. Commun.*, 9(1):4688, 2018.

[106] Matthew Du, Luis A. Martínez-Martínez, Raphael F. Ribeiro, Zixuan Hu, Vinod M. Menon, and Joel Yuen-Zhou. Theory for polariton-assisted remote energy transfer. *Chem. Sci.*, 9:6659–6669, 2018.

[107] Helmut Ritsch, Peter Domokos, Ferdinand Brennecke, and Tilman Esslinger. Cold atoms in cavity-generated dynamical optical potentials. *Rev. Mod. Phys.*, 85:553–601, 2013.

[108] Sonia Fernández-Vidal, Stefano Zippilli, and Giovanna Morigi. Nonlinear optics with two trapped atoms. *Phys. Rev. A*, 76:053829, 2007.

[109] R. Stassi, A. Ridolfo, O. Di Stefano, M. J. Hartmann, and S. Savasta. Spontaneous conversion from virtual to real photons in the ultrastrong-coupling regime. *Phys. Rev. Lett.*, 110:243601, 2013.

[110] Roberto Stassi, Salvatore Savasta, Luigi Garziano, Bernardo Spagnolo, and Franco Nori. Output field-quadrature measurements and squeezing in ultrastrong cavity-QED. *NJP*, 18(12):123005, 2016.

[111] Kunihito Hoki and Paul Brumer. Mechanisms in adaptive feedback control: Photoisomerization in a liquid. *Phys. Rev. Lett.*, 95:168305, 2005.

[112] S. Ashhab and Franco Nori. Qubit-oscillator systems in the ultrastrong-coupling regime and their potential for preparing nonclassical states. *Phys. Rev. A*, 81:042311, 2010.

[113] I. Dobrovsky and R.D. Levine. Electronically non-adiabatic transitions in the evans-polanyi valence bond model. *Chem. Phys. Lett.*, 286(1):155 – 162, 1998.

[114] Johannes Flick, Heiko Appel, Michael Ruggenthaler, and Angel Rubio. Cavity born-oppenheimer approximation for correlated electron-nuclear-photon systems. *J. Chem. Theory Comput.*, 13(4):1616–1625, 2017.

[115] G. A. Worth, M. H. Beck, A. Jäckle, and Hans-Dieter Meyer. *The MCTDH Package, Version 8.2*, 2000.

[116] Oriol Vendrell. Coherent dynamics in cavity femtochemistry: Application of the multi-configuration time-dependent hartree method. *Chem. Phys.*, 509:55 – 65, 2018.

[117] Vasil Rokaj, Davis M Welakuh, Michael Ruggenthaler, and Angel Rubio. Light-matter interaction in the long-wavelength limit: No ground-state without dipole self-energy. *J. Phys. B*, 51(3):034005, 2018.

[118] Inga S. Ulusoy, Johana A. Gomez, and Oriol Vendrell. Modifying the nonradiative decay dynamics through conical intersections via collective coupling to a cavity mode. *J. Phys. Chem. A*, 123(41):8832–8844, 2019.

[119] J Pelal Reithmaier, G Sek, A Löffler, C Hofmann, S Kuhn, S Reitzenstein, LV Keldysh, VD Kulakovskii, TL Reinecke, and A Forchel. Strong coupling in a single quantum dot-semiconductor microcavity system. *Nature*, 432(7014):197, 2004.

[120] Oluwafemi S Ojambati, Rohit Chikkaraddy, William D Deacon, Matthew Horton, Dean Kos, Vladimir A Turek, Ulrich F Keyser, and Jeremy J Baumberg. Quantum electrodynamics at room temperature coupling a single vibrating molecule with a plasmonic nanocavity. *Nat. Commun.*, 10(1):1049, 2019.

[121] Kyoung-Duck Park, Molly A. May, Haixu Leng, Jiarong Wang, Jaron A. Kropp, Theodosia Gougousi, Matthew Pelton, and Markus B. Raschke. Tip-enhanced strong coupling spectroscopy, imaging, and control of a single quantum emitter. *Sci. Adv.*, 5(7), 2019.

[122] Rohit Chikkaraddy, VA Turek, Nuttawut Kongsuwan, Felix Benz, Cloudy Carnegie, Tim van de Goor, Bart de Nijs, Angela Demetriadou, Ortwin Hess, Ulrich F. Keyser, and Jeremy J. Baumberg. Mapping nanoscale hotspots with single-molecule emitters assembled into plasmonic nanocavities using dna origami. *Nano Lett.*, 18(1):405–411, 2017.

[123] Daqing Wang, Hrishikesh Kelkar, Diego Martin-Cano, Dominik Rattenbacher, Alexey Shkarin, Tobias Utikal, Stephan Götzinger, and Vahid Sandoghdar. Turning a molecule into a coherent two-level quantum system. *Nat. Phys.*, 15(5):483, 2019.

[124] Robert H Dicke. Coherence in spontaneous radiation processes. *Phys. Rev.*, 93(1):99, 1954.

[125] Javier Galego, Francisco J. Garcia-Vidal, and Johannes Feist. Many-molecule reaction triggered by a single photon in polaritonic chemistry. *Phys. Rev. Lett.*, 119:136001, 2017.

[126] Oriol Vendrell. Collective jahn-teller interactions through light-matter coupling in a cavity. *Phys. Rev. Lett.*, 121:253001, 2018.

[127] Michael Tavis and Frederick W. Cummings. Exact solution for an n-molecule-radiation-field hamiltonian. *Phys. Rev.*, 170:379–384, 1968.

[128] Jacopo Fregoni, Francisco J. Garcia-Vidal, and Johannes Feist. Theoretical challenges in polaritonic chemistry. *ACS Photonics*, 9(4):1096–1107, 2022.

[129] J. M. Fink, R. Bianchetti, M. Baur, M. Göppl, L. Steffen, S. Filipp, P. J. Leek, A. Blais, and A. Wallraff. Dressed collective qubit states and the tavis-cummings model in circuit QED. *Phys. Rev. Lett.*, 103:083601, 2009.

[130] Iacopo Carusotto and Cristiano Ciuti. Quantum fluids of light. *Rev. Mod. Phys.*, 85:299–366, 2013.

[131] Javier del Pino, Florian A. Y. N. Schröder, Alex W. Chin, Johannes Feist, and Francisco J. Garcia-Vidal. Tensor network simulation of non-markovian dynamics in organic polaritons. *Phys. Rev. Lett.*, 121:227401, 2018.

[132] Felipe Herrera and Frank C. Spano. Dark vibronic polaritons and the spectroscopy of organic microcavities. *Phys. Rev. Lett.*, 118:223601, 2017.

[133] Gerrit Groenhof, Clàudia Climent, Johannes Feist, Dmitry Morozov, and J. Jussi Toppari. Tracking polariton relaxation with multiscale molecular dynamics simulations. *J. Phys. Chem. Lett.*, 10(18):5476–5483, 2019.

[134] Dominik Sidler, Michael Ruggenthaler, Christian Schäfer, Enrico Ronca, and Angel Rubio. A perspective on ab initio modeling of polaritonic chemistry: The role of non-equilibrium effects and quantum collectivity. *J. Chem. Phys.*, 156(23):230901, 2022.

[135] Christian Schäfer. Polaritonic chemistry from first principles via embedding radiation reaction. *J. Phys. Chem. Lett.*, 13(30):6905–6911, 2022.

[136] Piper Fowler-Wright, Brendon W. Lovett, and Jonathan Keeling. Efficient many-body non-markovian dynamics of organic polaritons. *Phys. Rev. Lett.*, 129:173001, Oct 2022.

[137] Frank C. Spano and Hajime Yamagata. Vibronic coupling in j-aggregates and beyond: A direct means of determining the exciton coherence length from the photoluminescence spectrum. *J. Phys. Chem. B*, 115(18):5133–5143, 2011.

[138] Nathan Shammah, Shahnawaz Ahmed, Neill Lambert, Simone De Liberato, and Franco Nori. Open quantum systems with local and collective incoherent processes: Efficient numerical simulations using permutational invariance. *Phys. Rev. A*, 98:063815, 2018.

[139] Felipe Herrera and Frank C. Spano. Theory of nanoscale organic cavities: The essential role of vibration-photon dressed states. *ACS Photonics*, 5(1):65–79, 2018.

[140] Rui E. F. Silva and Johannes Feist. Permutational symmetry for identical multilevel systems: A second-quantized approach. *Phys. Rev. A*, 105:043704, 2022.

[141] M. Ahsan Zeb. Efficient linear scaling mapping for permutation symmetric fock spaces. *Comput. Phys. Commun.*, 276:108347, 2022.

[142] Jorge A. Campos-Gonzalez-Angulo and Joel Yuen-Zhou. Generalization of the tavis–cummings model for multi-level anharmonic systems: Insights on the second excitation manifold. *J. Chem. Phys.*, 156(19):194308, 2022.

[143] Lorenz S. Cederbaum. Cooperative molecular structure in polaritonic and dark states. *J. Chem. Phys.*, 156(18):184102, 2022.

[144] Michael Gegg and Marten Richter. Efficient and exact numerical approach for many multi-level systems in open system CQED. *NJP*, 18(4):043037, 2016.

[145] M. Ahsan Zeb, Peter G. Kirton, and Jonathan Keeling. Exact states and spectra of vibrationally dressed polaritons. *ACS Photonics*, 5(1):249–257, 2018.

[146] Justyna A. Ćwik, Peter Kirton, Simone De Liberato, and Jonathan Keeling. Excitonic spectral features in strongly coupled organic polaritons. *Phys. Rev. A*, 93:033840, 2016.

[147] Gábor J. Halász, Milan Šindelka, Nimrod Moiseyev, Lorenz S. Cederbaum, and Ágnes Vibók. Light-induced conical intersections: Topological phase, wave packet dynamics, and molecular alignment. *J. Phys. Chem. A*, 116(11):2636–2643, 2012.

[148] Oriol Vendrell. Collective jahn-teller interactions through light-matter coupling in a cavity. *Phys. Rev. Lett.*, 121(25), 2018.

[149] András Csehi, Oriol Vendrell, Gábor J Halász, and Ágnes Vibók. Competition between collective and individual conical intersection dynamics in an optical cavity. *NJP*, 24(7):073022, 2022.

[150] Michael Gegg and Marten Richter. Psiquasp–a library for efficient computation of symmetric open quantum systems. *Sci. Rep.*, 7(1):16304, 2017.

[151] Johannes Schachenmayer, Claudiu Genes, Edoardo Tignone, and Guido Pupillo. Cavity-enhanced transport of excitons. *Phys. Rev. Lett.*, 114:196403, 2015.

[152] Nancy Makri. The linear response approximation and its lowest order corrections: An influence functional approach. *J. Phys. Chem. B*, 103(15):2823–2829, 1999.

[153] Mathias Schubert. Polarization-dependent optical parameters of arbitrarily anisotropic homogeneous layered systems. *Phys. Rev. B*, 53:4265–4274, 1996.

[154] V. M. Agranovich, M. Litinskaia, and D. G. Lidzey. Cavity polaritons in microcavities containing disordered organic semiconductors. *Phys. Rev. B*, 67:085311, 2003.

[155] M.H. Beck, A. Jäckle, G.A. Worth, and H.-D. Meyer. The multiconfiguration time-dependent hartree (mctdh) method: a highly efficient algorithm for propagating wavepackets. *Phys. Rep.*, 324(1):1–105, 2000.

[156] Inga S. Ulusoy, Johana A. Gomez, and Oriol Vendrell. Modifying the nonradiative decay dynamics through conical intersections via collective coupling to a cavity mode. *J. Phys. Chem. A*, 123(41):8832–8844, 2019.

[157] Bingyu Cui and Abraham Nizan. Collective response in light–matter interactions: The interplay between strong coupling and local dynamics. *J. Chem. Phys.*, 157(11):114108, 2022.

[158] Javier del Pino, Johannes Feist, and Francisco J Garcia-Vidal. Quantum theory of collective strong coupling of molecular vibrations with a microcavity mode. *NJP*, 17:053040, 2015.

[159] M. Litinskaya, P. Reineker, and V.M. Agranovich. Fast polariton relaxation in strongly coupled organic microcavities. *J. Lumin.*, 110(4):364–372, 2004. 325th Wilhelm and Else Heraeus Workshop. Organic Molecular Solids : Excited Electronic States and Optical Properties.

[160] Battulga Munkhbat, Martin Wersäll, Denis G. Baranov, Tomasz J. Antosiewicz, and Timur Shegai. Suppression of photo-oxidation of organic chromophores by strong coupling to plasmonic nanoantennas. *Sci. Adv.*, 4(7):eaas9552, 2018.

[161] Daniel T. Colbert and William H. Miller. A novel discrete variable representation for quantum mechanical reactive scattering via the s-matrix kohn method. *J. Chem. Phys.*, 96(3):1982–1991, 1992.

[162] Eric J. Heller. The semiclassical way to molecular spectroscopy. *Acc. Chem. Res.*, 14(12):368–375, 1981.

[163] Gerrit Groenhof and J. Jussi Toppari. Coherent light harvesting through strong coupling to confined light. *J. Phys. Chem. Lett.*, 9(17):4848–4851, 2018.

[164] Matthew Du, Luis A. Martínez-Martínez, Raphael F. Ribeiro, Zixuan Hu, Vinod M. Menon, and Joel Yuen-Zhou. Theory for polariton-assisted remote energy transfer. *Chem. Sci.*, 9:6659–6669, 2018.

[165] R. Sáez-Blázquez, J. Feist, A. I. Fernández-Domínguez, and F. J. García-Vidal. Organic polaritons enable local vibrations to drive long-range energy transfer. *Phys. Rev. B*, 97:241407, 2018.

[166] Xiaolan Zhong, Thibault Chervy, Shaojun Wang, Jino George, Anoop Thomas, James A. Hutchison, Eloise Devaux, Cyriaque Genet, and Thomas W. Ebbesen. Non-radiative energy transfer mediated by hybrid light-matter states. *Angew. Chem., Int. Ed. Engl.*, 55(21):6202–6206, 2016.

[167] Xiaolan Zhong, Thibault Chervy, Lei Zhang, Anoop Thomas, Jino George, Cyriaque Genet, James A. Hutchison, and Thomas W. Ebbesen. Energy transfer between spatially separated entangled molecules. *Angew. Chem., Int. Ed. Engl.*, 56(31):9034–9038, 2017.

[168] Nina Krainova, Alex J. Grede, Demetra Tsokkou, Natalie Banerji, and Noel C. Giebink. Polaron photoconductivity in the weak and strong light-matter coupling regime. *Phys. Rev. Lett.*, 124:177401, 2020.

[169] Ding Xu, Arkajit Mandal, James M. Baxter, Shan-Wen Cheng, Inki Lee, Haowen Su, Song Liu, David R. Reichman, and Milan Delor. Ultrafast imaging of polariton propagation and interactions. *Nat. Commun.*, 14(1):3881, 2023.

[170] Thomas F. Allard and Guillaume Weick. Disorder-enhanced transport in a chain of lossy dipoles strongly coupled to cavity photons. *Phys. Rev. B*, 106:245424, 2022.

[171] Raj Pandya, Arjun Ashoka, Kyriacos Georgiou, Jooyoung Sung, Rahul Jayaprakash, Scott Renken, Lizhi Gai, Zhen Shen, Akshay Rao, and Andrew J. Musser. Tuning the coherent propagation of organic exciton-polaritons through dark state delocalization. *Adv. Sci.*, 9(18):2105569, 2022.

[172] Hsing-Ta Chen, Zeyu Zhou, Maxim Sukharev, Joseph E. Subotnik, and Abraham Nitzan. Interplay between disorder and collective coherent response: Superradiance and spectral motional narrowing in the time domain. *Phys. Rev. A*, 106:053703, 2022.

[173] M. Ahsan Zeb, Peter G. Kirton, and Jonathan Keeling. Incoherent charge transport in an organic polariton condensate. *Phys. Rev. B*, 106:195109, 2022.

[174] Bing Gu. Toward collective chemistry by strong light-matter coupling, 2023.

[175] Nicholas Anto-Sztrikacs and Dvira Segal. Capturing non-markovian dynamics with the reaction coordinate method. *Phys. Rev. A*, 104:052617, 2021.

[176] Lorenz S. Cederbaum, Etienne Gindensperger, and Irene Burghardt. Short-time dynamics through conical intersections in macrosystems. *Phys. Rev. Lett.*, 94:113003, 2005.

[177] Felipe Herrera and Frank C. Spano. Absorption and photoluminescence in organic cavity QED. *Phys. Rev. A*, 95:053867, 2017.

[178] Joel Yuen-Zhou and Arghadip Koner. Linear response of molecular polaritons. *J. Chem. Phys.*, 160(15):154107, 2024.

[179] D.J. Tannor. *Introduction to Quantum Mechanics: A time dependent perspective*. University Science Books, 2007.

[180] Tarun Gera and K. L. Sebastian. Effects of disorder on polaritonic and dark states in a cavity using the disordered Tavis–Cummings model. *J. Chem. Phys.*, 156(19), 2022. 194304.

[181] Felipe Herrera and Frank C. Spano. Cavity-controlled chemistry in molecular ensembles. *Phys. Rev. Lett.*, 116:238301, 2016.

[182] Joel Kuttruff, Marco Romanelli, Esteban Pedrueza-Villalmanzo, Jonas Allerbeck, Jacopo Fregoni, Valeria Saavedra-Becerril, Joakim Andréasson, Daniele Brida, Alexandre Dmitriev, Stefano Corni, and Nicolò Maccaferri. Sub-picosecond collapse of molecular polaritons to pure molecular transition in plasmonic photoswitch-nanoantennas. *Nat. Commun.*, 14(1):3875, 2023.

[183] Philip A. Thomas, Wai Jue Tan, Vasyl G. Kravets, Alexander N. Grigorenko, and William L. Barnes. Non-polaritonic effects in cavity-modified photochemistry. *Adv. Mater.*, 36(7):2309393, 2024.

[184] Arpan Dutta, Ville Tiainen, Luis Duarte, Nemanja Markesevic, Ilia Sokolovskii, Dmitry Morozov, Hassan A. Qureshi, Siim Pikker, Gerrit Groenhof, and J. Jussi Toppari. Ultra-fast photochemistry in the strong light-matter coupling regime. *ChemRxiv*, 2024.

[185] Justyna A. Ćwik, Peter Kirton, Simone De Liberato, and Jonathan Keeling. Excitonic spectral features in strongly coupled organic polaritons. *Phys. Rev. A*, 93:033840, 2016.

[186] Norbert F Scherer, Roger J Carlson, Alexander Matro, Mei Du, Anthony J Ruggiero, Victor Romero-Rochin, Jeffrey A Cina, Graham R Fleming, and Stuart A Rice. Fluorescence-detected wave packet interferometry: Time resolved molecular spectroscopy with sequences of femtosecond phase-locked pulses. *J. Chem. Phys.*, 95(3):1487–1511, 1991.

[187] Michael Spanner, Carlos A. Arango, and Paul Brumer. Communication: Conditions for one-photon coherent phase control in isolated and open quantum systems. *J. Chem. Phys.*, 133(15):151101, 2010.

[188] Carlos A. Arango and Paul Brumer. Communication: One-photon phase control of cis-trans isomerization in retinal. *J. Chem. Phys.*, 138(7):071104, 2013.

[189] Paul Brumer and Moshe Shapiro. One photon mode selective control of reactions by rapid or shaped laser pulses: An emperor without clothes? *Chem. Phys.*, 139(1):221–228, 1989.

[190] M. Litinskaya, P. Reineker, and V.M. Agranovich. Exciton–polaritons in organic microcavities. *J. Lumin.*, 119-120:277–282, 2006. Dynamical Processes in Excited States of Solids.

[191] Paolo Michetti and Giuseppe C. La Rocca. Simulation of j-aggregate microcavity photoluminescence. *Phys. Rev. B*, 77:195301, 2008.

[192] Paolo Michetti and Giuseppe C. La Rocca. Exciton-phonon scattering and photoexcitation dynamics in j-aggregate microcavities. *Phys. Rev. B*, 79:035325, 2009.

[193] Felipe Herrera and Frank C. Spano. Dark vibronic polaritons and the spectroscopy of organic microcavities. *Phys. Rev. Lett.*, 118:223601, 2017.

[194] Javier Galego, Francisco J. Garcia-Vidal, and Johannes Feist. Cavity-induced modifications of molecular structure in the strong-coupling regime. *Phys. Rev. X*, 5:041022, 2015.

[195] Dominik Sidler, Michael Ruggenthaler, Christian Schäfer, Enrico Ronca, and Angel Rubio. A perspective on ab initio modeling of polaritonic chemistry: The role of non-equilibrium effects and quantum collectivity. *J. Chem. Phys.*, 156(23):230901, 2022.

[196] Arpan Dutta, Ville Tiainen, Ilia Sokolovskii, Luís Duarte, Nemanja Markešević, Dmitry Morozov, Hassan A. Qureshi, Siim Pikker, Gerrit Groenhof, and J. Jussi Toppari. Thermal disorder prevents the suppression of ultra-fast photochemistry in the strong light-matter coupling regime. *Nat. Commun.*, 15(1):6600, 2024.

[197] Hans-Dieter Meyer and William H. Miller. Analysis and extension of some recently proposed classical models for electronic degrees of freedom. *J. Chem. Phys.*, 72(4):2272–2281, 2008.

[198] Gerhard Stock and Michael Thoss. Semiclassical description of nonadiabatic quantum dynamics. *Phys. Rev. Lett.*, 78:578–581, 1997.

[199] Jing Sun, Sudip Sasmal, and Oriol Vendrell. A bosonic perspective on the classical mapping of fermionic quantum dynamics. *J. Chem. Phys.*, 155(13):134110, 2021.

[200] Deping Hu, Arkajit Mandal, Braden M. Weight, and Pengfei Huo. Quasi-diabatic propagation scheme for simulating polariton chemistry. *J. Chem. Phys.*, 157(19):194109, 2022.

[201] Piper Fowler-Wright, Kristín B. Arnardóttir, Peter Kirton, Brendon W. Lovett, and Jonathan Keeling. Determining the validity of cumulant expansions for central spin models. *Phys. Rev. Res.*, 5:033148, 2023.

[202] Rishab Dutta, Delmar G. A. Cabral, Ningyi Lyu, Nam P. Vu, Yuchen Wang, Brandon Allen, Xiaohan Dan, Rodrigo G. Cortiñas, Pouya Khazaei, Max Schäfer, Alejandro C. C. d. Albornoz, Scott E. Smart, Scott Nie, Michel H. Devoret, David A. Mazziotti, Prineha Narang, Chen Wang, James D. Whitfield, Angela K. Wilson, Heidi P. Hendrickson, Daniel A. Lidar, Francisco Pérez-Bernal, Lea F. Santos, Sabre Kais, Eitan Geva, and Victor S. Batista. Simulating chemistry on bosonic quantum devices, 2024.

[203] Axel U. J. Lode. Multiconfigurational time-dependent hartree method for bosons with internal degrees of freedom: Theory and composite fragmentation of multicomponent bose-einstein condensates. *Phys. Rev. A*, 93:063601, 2016.

[204] L.C. Biedenharn and H. Van Dam. *Quantum Theory of Angular Momentum: A Collection of Reprints and Original Papers*. Perspectives in Physics: a Series of Reprint Collections. Academic Press, 1965.

[205] Nathan Shammah, Shahnawaz Ahmed, Neill Lambert, Simone De Liberato, and Franco Nori. Open quantum systems with local and collective incoherent processes: Efficient numerical simulations using permutational invariance. *Phys. Rev. A*, 98:063815, 2018.

[206] Rui E. F. Silva and Johannes Feist. Permutational symmetry for identical multilevel systems: A second-quantized approach. *Phys. Rev. A*, 105:043704, 2022.

[207] Andrea Pizzi, Alexey Gorlach, Nicholas Rivera, Andreas Nunnenkamp, and Ido Kaminer. Light emission from strongly driven many-body systems. *Nat. Phys.*, 19(4):551–561, 2023.

[208] Vladislav Sukharnikov, Stasis Chuchurka, Andrei Benediktovitch, and Nina Rohringer. Second quantization of open quantum systems in liouville space. *Phys. Rev. A*, 107:053707, 2023.

[209] Lee Tutt, David Tannor, Eric J. Heller, and Jeffrey I. Zink. The mime effect: absence of normal modes corresponding to vibronic spacings. *Inorg. Chem.*, 21(10):3858–3859, 1982.

[210] Keith H. Hughes, Clara D. Christ, and Irene Burghardt. Effective-mode representation of non-Markovian dynamics: A hierarchical approximation of the spectral density. I. Application to single surface dynamics. *J. Chem. Phys.*, 131(2):024109, 2009.

[211] Ralf Bulla, Theo A. Costi, and Thomas Pruschke. Numerical renormalization group method for quantum impurity systems. *Rev. Mod. Phys.*, 80:395–450, 2008.

[212] Javier Prior, Alex W. Chin, Susana F. Huelga, and Martin B. Plenio. Efficient simulation of strong system-environment interactions. *Phys. Rev. Lett.*, 105:050404, 2010.

[213] Luis A. Martínez-Martínez, Elad Eizner, Stéphane Kéna-Cohen, and Joel Yuen-Zhou. Triplet harvesting in the polaritonic regime: A variational polaron approach. *J. Chem. Phys.*, 151(5):054106, 2019.

[214] Carlos J. Sánchez Martínez, Johannes Feist, and Francisco J. García-Vidal. A mixed perturbative-nonperturbative treatment for strong light-matter interactions. *Nanophotonics*, 13(14):2669–2678, 2024.

[215] Felipe Herrera and Frank C. Spano. Theory of nanoscale organic cavities: The essential role of vibration-photon dressed states. *ACS Photonics*, 5(1):65–79, 2018.

[216] Frank C. Spano. Exciton–phonon polaritons in organic microcavities: Testing a simple ansatz for treating a large number of chromophores. *J. Chem. Phys.*, 152(20):204113, 2020.

[217] Michael R. Philpott. Theory of the Coupling of Electronic and Vibrational Excitations in Molecular Crystals and Helical Polymers. *J. Chem. Phys.*, 55(5):2039–2054, 09 1971.

[218] T. Virgili, D. Coles, A. M. Adawi, C. Clark, P. Michetti, S. K. Rajendran, D. Brida, D. Polli, G. Cerullo, and D. G. Lidzey. Ultrafast polariton relaxation dynamics in an organic semiconductor microcavity. *Phys. Rev. B*, 83:245309, 2011.

[219] Tal Schwartz, James A. Hutchison, Jérémie Léonard, Cyriaque Genet, Stefan Haacke, and Thomas W. Ebbesen. Polariton dynamics under strong light–molecule coupling. *ChemPhysChem*, 14(1):125–131, 2013.

[220] D. G. Lidzey, A. M. Fox, M. D. Rahn, M. S. Skolnick, V. M. Agranovich, and S. Walker. Experimental study of light emission from strongly coupled organic semiconductor microcavities following nonresonant laser excitation. *Phys. Rev. B*, 65:195312, 2002.

[221] F. C. Spano and Leonardo Silvestri. Multiple mode exciton-vibrational coupling in H-aggregates: Synergistic enhancement of the quantum yield. *J. Chem. Phys.*, 132(9):094704, 2010.

[222] Tomohiro Ishii, Juan B. Pérez-Sánchez, Joel Yuen-Zhou, Chihaya Adachi, Takuji Hatakeyama, and Stéphane Kéna-Cohen. Modified prompt and delayed kinetics in a strongly-coupled organic microcavity containing a multiresonance tadf emitter. *ACS photonics*.

[223] H. Benisty, H. De Neve, and C. Weisbuch. Impact of planar microcavity effects on light extraction-part ii: selected exact simulations and role of photon recycling. *IEEE J. Quantum Electron.*, 34(9):1632–1643, 1998.

[224] Yi Yu, Suman Mallick, Mao Wang, and Karl Börjesson. Barrier-free reverse-intersystem crossing in organic molecules by strong light-matter coupling. *Nat. Commun.*, 12(1):3255, 2021.

[225] Shaul Mukamel. *Principles of Nonlinear Optical Spectroscopy*. Oxford University Press, 1995.

[226] Ruth H. Tichauer, Dmitry Morozov, Ilia Sokolovskii, J. Jussi Toppari, and Gerrit Groenhof. Identifying vibrations that control non-adiabatic relaxation of polaritons in strongly coupled molecule–cavity systems. *J. Phys. Chem. Lett.*, 13(27):6259–6267, 2022. PMID: 35771724.

[227] J Chovan, IE Perakis, S Ceccarelli, and DG Lidzey. Controlling the interactions between polaritons and molecular vibrations in strongly coupled organic semiconductor microcavities. *Phys. Rev. B*, 78(4):045320, 2008.

[228] David M Coles, Paolo Michetti, Caspar Clark, Wing Chung Tsoi, Ali M Adawi, Ji-Seon Kim, and David G Lidzey. Vibrationally assisted polariton-relaxation processes in strongly coupled organic-semiconductor microcavities. *Adv. Funct. Mater.*, 21(19):3691–3696, 2011.

[229] N Somaschi, L Mouchliadis, D Coles, IE Perakis, DG Lidzey, PG Lagoudakis, and PG Savvidis. Ultrafast polariton population build-up mediated by molecular phonons in organic microcavities. *Appl. Phys. Lett.*, 99(14), 2011.

[230] L. Mazza, S. Kéna-Cohen, P. Michetti, and G. C. La Rocca. Microscopic theory of polariton lasing via vibronically assisted scattering. *Phys. Rev. B*, 88:075321, 2013.